PPPL--2609

DE89 012914

ON THE SELF-CONSISTENCY OF THE PRINCIPLE OF PROFILE CONSISTENCY RESULTS FOR SAWTOOTHING TOKAMAK DISCHARGES

V. Arunasalam, N.L. Bretz, P.C. Efthimion, R.J. Goldston, B. Grek,

D.W. Johnson, M. Murakami**, K. McGuire, D.A. Rasmussen**,

F.J. Stauffer*, and J. Wilgen**

Princeton University

Princeton Plasma Physics Laboratory,

Princeton, New Jersey 08543

*AT&T Microelectronics, Reading, PA 19612

**Oak Ridge National Laboratory, Oak Ridge, TN 37831

ABSTRACT

The principle of profile consistency states that for fixed limiter safety factor q_a, there exists unique natural equilibrium profile shapes for the current density $j(r)$ [and consequently $q(r)$], and the electron temperature $T_e(r)$ for any tokamak plasma independent of the shapes of the heating power deposition profiles. The mathematical statement of the three basic consequences of this principle for sawtoothing discharges [i.e., discharges with $q(0) \le 1$] are: (1) $(r_1/a) = F_1\ (1/q_a)$ [$\approx 1/q_a$, empirically], (2) $\langle T_e \rangle / T_{eo} = F_2(1/q_a)$, and (3) a unique scaling law for the central electron temperature T_{eo}, where r_1 is the sawtooth inversion radius [i.e., $q(r_1) = 1$] and $\langle T_e \rangle$ is the volume average T_e. Since for a given $T_e(r)$, the ohmic current $j(r)$ can be deduced from Ohm's law, given the function F_1, the function F_2 is uniquely fixed and vice versa. Also given $F_1(1/q_a)$, the central current density $j_o = (V_L/2\pi bRZ_{eff})\ T_{eo}^{3/2} = (I_p/\pi a^2)\ F_3(q_a)$, where the function $F_3 = (q_a/q_o)$ is uniquely fixed by F_1. Here $b \approx 6.53 \times 10^3\ \ell n\Lambda$, and I_p, V_L, Z_{eff}, R, a, and q_o are the plasma current, loop voltage, effective ion charge, major and minor radius, and the central safety factor, respectively. Thus for a fixed $j(r)$ or $T_e(r)$, the set of functions F_1, F_2, and F_3 is uniquely fixed. Further, the principle of profile consistency [i.e., the existence of unique natural equilibrium profile shapes for $j(r)$ and $T_e(r)$ for a fixed q_a] dictates that this set of functions F_1, F_2, and F_3 remain the same for <u>all</u> sawtoothing discharges in <u>any</u> tokamak regardless of its size [i.e., a and R], I_p, V_L, B_T, etc. Here, we present a rather complete and detailed theoretical examination of this self-consistency of the measured values of $T_e(r)$, F_1, F_2, and F_3 for sawtoothing TFTR discharges.

In particular, the theoretical predictions of Coppi's Gaussian, exponential, modified exponential, trapezoidal, Kadomtsev, and Campbell <u>et al.</u> model profiles are compared with TFTR and TFR data. The principal results are: (1) The empirical profile consistency relation $(r_1/a) = (1/q_a)$ is an acceptable solution of $q\ (r_1) = 1$ for all q_a - dependent profiles. (2) A comparison between experiment and theory yields $[\langle T_e\rangle/T_{eo}]_{EXP} \simeq [\langle T_e\rangle/T_{eo}]_{TH} + 0.05$ for Coppi's Gaussian, Kadomtsev, and Campbell <u>et al.</u> model profiles. (3) For all q_a - independent profiles $F_3(q_a) = (q_a/q_o)$ = constant and, consequently $T_{eo}^{3/2} \propto (I_p R\ Z_{eff}/a^2 V_L)$; while for all q_a - dependent profiles $F_3\ (q_a) = (q_a/q_o) \propto q_a$ when $(r_1/a) = (1/q_a)$, and consequently $T_{eo}^{3/2} \propto (B_T\ Z_{eff}/V_L)$, where B_T is the confining toroidal magnetic field. The former T_{eo} scaling is profile consistency independent, and the latter one is profile consistency dependent via the empirical relation $r_1/a = 1/q_a$. (4) Coppi's and Ohkawa's forms of $\chi_e(r)$ yield $T_{eo} \propto B_T^{0.7}$ while the INTOR $\chi_e(r)$ yields $T_{eo} \propto B_T^{0.4}$, where $\chi_e(r)$ is the electron thermal diffusivity. Experimentally, however, the TFTR data yield $T_{eo} \propto B_T^{0.67}$, and the TFR data yield $T_{eo} \propto B_T^{0.86}$. (5) For $(r_1/a) \simeq (1/q_a)$, Coppi's Gaussian, Kadomtsev, and Campbell <u>et al.</u> model profiles all predict that $(\Delta T_e/T_e) \propto (1/q_a)$ in agreement with the experimental observations. Here $(\Delta T_e/T_e)$ is the normalized sawtooth amplitude. (6) The experimental $(\Delta T_e/T_e)$ vs r is consistent with the notion that during a sawtooth crash the profiles get flattened over the range $0 \le r \le \sqrt{2}\ r_1 \simeq \sqrt{2}\ a/q_a$, keeping the total plasma current constant. (7) For q_a - dependent models there exist universality of profiles in suitable reduced coordinates when $(r_1/a) = (1/q_a)$.

CONTENTS

I. PRELIMINARIES

A. Introduction

In 1975 the TFR group [1] reported some of the general features of their measured radial profiles of the electron temperature $T_e(r)$ for sawtoothing ohmic tokamak discharges. These features are: (1) the $T_e(r)$ profiles become more and more peaked as the limiter safety factor q_a increases, and, consequently, the full width at half-maximum of the $T_e(r)$ profiles increases linearly with q_a^{-1}, (2) the normalized radius of the $q = 1$ surface (r_1/a) determined from the position of sawtooth inversion also increases linearly with q_a^{-1}, (3) the central electron temperature T_{eo} increases "almost linearly" with increasing B_T [i.e., $T_{eo} \propto B_T^{0.86}$] or q_a, and (4) the normalized sawtooth amplitude $(\Delta T_e/T_e)$ decreases with increasing B_T or q_a. These measurements were done by changing B_T keeping I_p and $\bar{n}_e$ approximately constant. Subsequently, Manheimer et al. [2] have given a somewhat satisfactory theoretical explanation of some of the observed general features of the tokamak profiles. They used a marginal stability approach for the dissipative trapped-electron instability for $r > r_1$ assuming that the inner core region for $r < r_1$ is marginally stable to the internal kink and tearing modes (with $m = n = 1$ structure observed as sawtooth oscillations in the soft x-ray and electron cyclotron emission signals). These two earlier works are the experimental and theoretical genesis of what is now popularly known as the "profile consistency" in tokamak discharges.

In the literature many authors [2-13] have proposed various different profile shapes to explain (either directly or indirectly) some or all of the observed general features of profile consistency. The primary objective of some of these models was to understand the nature of the energy and particle transport processes in tokamak plasmas, while others concentrated on understanding the macroscopic stability of the plasma column for magnetohydrodynamic (MHD) modes (via, for example, minimum energy principle, principle of minimum entropy production, etc.) with profile consistency as a by-product. But none of these authors have examined the intrinsic self-consistency of their models. It is our aim in this paper to approach the problem from an altogether different point of view and examine the theoretical and experimental self-consistency of these various models [see Fig. 1 and Sec. IB]. After all, what good is any model if it is not physically self-consistent?

In general, the tokamak discharges may be broadly classified into two groups. Type 1 discharges are those which have profile shapes for the current density $j(r)$, the electron temperature $T_e(r)$, and the electron density $n_e(r)$ that are single valued and a monotonically decreasing function of r. For these discharges the safety factor $q(r)$ is single valued and a monotonically increasing function of r. Type 2 discharges are those which have hollow profile shapes for one or all of the three plasma parameters $j(r)$, $T_e(r)$, and $n_e(r)$. If, for example, $T_e(r)$ is hollow, then by Ohm's law $j(r)$ is hollow. Consequently $q(r)$ is multivalued. In this paper we will consider only type 1 discharges. Here again we distinguish two types. Type 1A discharges are those which have $q(o) \leq 1$ such that there exists a core region $[q(r) \leq 1]$ where internal disruptions (MHD activity) maintain a high thermal conduction. These are the sawtoothing discharges. Type 1B discharges are those which have $q(0) > 1$ and $q(r) > 1$ everywhere. Here the core region of internal disruption is absent. These are the non-sawtoothing discharges. Here we will only consider type 1A discharges.

It is believed that during a sawtooth oscillation magnetic reconnection occurs across the $q = 1$ surface [5,6,9,14-25]. During the rising portion of the sawtooth, the $T_e(r)$ profiles keep on peaking up and at the end of the sawtooth crash these profiles get flattened over the entire core region [i.e., up to the sawtooth inversion radius where $q = 1$]. In a sawtooth period a certain fraction of the central core [i.e., inside the $q = 1$ surface] energy is transferred into the region of pressure gradient. Thus, the energy transport for sawtoothing tokamak discharges can be described by a three-region model [26]: (1) a core region [$q \leq 1$], where internal disruptions maintain a high thermal conduction, (2) a confinement region of large pressure gradient, and (3) an edge region dominated by a combination of atomic processes [i.e., radiation, charge exchange, ionization, etc.] and recycling. *Hence the sawtooth period* τ_{ST} *is a measure of the time scale in* which the energy is sloshed back and forth across the $q = 1$ surface. Thus, a core "confinement time" associated with the sawtooth oscillations can be defined as $\tau_{core} = (T_e/\Delta T_e)\tau_{ST}$, where ΔT_e is the sawtooth amplitude. Typically [14,20,21,25] $\tau_{ST} \approx (\tau_E/5)$, where τ_E is the global energy confinement time and $(\Delta T_e/T_e) < (1/5)$ [see also Sec. IX]. That is, $\tau_{core} > \tau_E$. Hence for sawtoothing discharges the core confinement is usually better than the over-all confinement.

What is the "principle of profile consistency?" In the literature there does not seem to exist a fully satisfactory mathematically quantitative and rigorous definition of this principle. It is physically instructive to examine how other authors have attempted to define this principle. Coppi [3] states: "We present a set of criteria that appear to lead to a consistent description of both the electron thermal energy transport and the particle transport. We label this set of criteria as the principle of profile consistency. In fact, this is based on assuming that the observed flows of thermal energy and particles are those needed to reach a consistent set of radial profiles for the current density, the particle temperatures and the plasma density, while satisfying the equilibrium conditions for the considered plasma column." Tang [5] states: "The principle of profile consistency basically involves the empirical observation that dynamical processes in well-behaved tokamak discharges tend to maintain the same relative electron temperature profiles, $T_e(r)/T_{eo}$, and associated current profiles. $T_e(r)/T_{eo}$ is indeed found to be sensitive mainly to q_a irrespective of changes in density, plasma size, central temperature, and heating method. Although no specific mechanisms have as yet been identified to enforce the observed global profiles, the allowed shapes are at least consistent with macroscopic stability requirements (i.e., long wavelength MHD instabilities)." Kadomtsev [9] states: "An unusual phenomenon of sustaining certain optimal profiles with a tendency to retain them even at considerable change in the deposited profile in a plasma arises. It is more natural to assume the existence of tearing modes at low pressures, as it has been emphasized by Furth [6], who has paid attention to the fact that the experimental profiles are close to the stability boundary for tearing modes."

If tearing mode stability is what determines the profiles in tokamaks, then it follows that the fundamental profile is the current density profile $j(r)$ [6,9,10,16,19,26]. The temperature profile $T_e(r)$ must then conform to $j(r)$ so as to satisfy the Ohm's law [27]:

$$j(r) = \sigma[T_e(r)]E = (1/\eta[T_e(r)])(V_L/2\pi R) \ , \qquad (1.1)$$

where $\sigma[T_e(r)]$ and $\eta[T_e(r)]$ are the temperature-dependent plasma conductivity and resistivity, respectively, and E is the electric field in the plasma [28]. Then, as pointed out by Furth [27], the density profile $n_e(r)$ and the thermal transport coefficient $\chi_e(r)$ must conform to the electron thermal energy-balance equation:

$$Q(r) = \frac{-1}{r}\frac{d}{dr}\left[r\chi_e(r)\, n_e(r)\, \frac{dT_e(r)}{dr}\right] + Q_{ei}, \qquad (1.2)$$

where

$$Q_{ei} = (3m_e/m_i)\ \nu_{ei}\ n_e\ T_e(1 - T_i/T_e) \tag{1.3}$$

is the rate of energy transfer from the electrons to the ions and m_e, m_i, ν_{ei} are the electron mass, ion mass, and electron-ion collision frequency, respectively. In Eq. (1.2) Q(r) denotes the sum of all heat sources and sinks in the plasma. For example, $Q = Q_{ohm} + Q_{aux} - Q_{rad}$ in which $Q_{ohm} = E \cdot j(r)$ is the Ohmic power input, Q_{aux} is the auxiliary heating power input, and Q_{rad} is the radiative power loss, all per unit volume. For Ohmic impurity-free plasmas $Q_{aux} = 0$, $Q_{ohm} >> Q_{rad}$ and hence $Q \approx Q_{ohm} = E \cdot j(r)$. In the literature [2-5,29-34] several authors have used widely different forms for the electron heat diffusion coefficient $\chi_e(r)$. For example, Callen et al. [29] have pointed out that either a constant χ_e independent of r or a non-linear χ_e model which takes $\chi_e \propto n_e \nabla T_e$ can explain the JET electron heat flux data [35]. The INTOR studies have proposed [32] a "standard" electron thermal diffusivity for use in computer modeling studies, $\chi_e(r) \propto [n_e(r)]^{-1}$. That is, the heat conduction coefficient $\kappa_e = n_e(r)\ \chi_e(r) \approx$ constant [$\approx 5 \times 10^{17}$ cm^{-1} sec^{-1}] independent of r. This form of $\chi_e(r)$ which was based on informal studies of data from Alcator A seems to be the most popular one [30-34,36]. Ohkawa [33,34] has also proposed a constant κ_e model for $\chi_e(r)$. In Sec. IID we will compare the T_{eo}-scaling predictions of the Coppi's form of $\chi_e(r)$ with those of INTOR and the Ohkawa's forms of $\chi_e(r)$.

Hence, we will take as an operational working definition of the principle of profile consistency for sawtoothing tokamak discharges as stating that for a fixed limiter q_a, there exists unique natural equilibrium profile shapes for j(r) [and consequently q(r)], and $T_e(r)$ independent of the shapes of the heating power deposition profiles as a consequence of the stability requirements for long-wavelength tearing modes. These profiles are such that the three basic consequences of this principle for sawtoothing discharges are: (1) $(r_1/a) = F_1(1/q_a)[\approx 1/q_a$, empirically], (2) $\langle T_e\rangle/T_{eo} = F_2(1/q_a)$, and (3) $T_{eo}^{3/2} \propto (I_p R Z_{eff}/a^2 V_L)F_3(q_a)$. Since for a given $T_e(r)$, the Ohmic current $j(r)$ can be deduced from Ohm's law, it follows that the set of functions F_1, F_2, and F_3 is uniquely fixed. Further, this set of functions remains the same for <u>all</u> sawtoothing discharges in <u>any</u> tokamak regardless of its size [i.e., a and R], I_p, V_L, B_T, etc. Also, by definition the set of relations (1), (2), and (3) necessarily implies that j, q, and T_e are not only functions of r but also are functions of q_a [i.e., $j = j(r, q_a)$, $q = q(r, q_a)$, and $T_e = T_e(r, q_a)$].

We pointed out earlier in Eq. (1.1) that Ohm's law relates $j(r)$ to $T_e(r)$ via the temperature-dependent resistivity $\eta[T_e(r)]$. This η may be written

$$(1/\eta) = (1/\eta_s)\ f_\sigma(r), \tag{1.4}$$

where $f_\sigma(r)$ is the neoclassical conductivity form factor [37], and

$$\eta_s = (b\ Z_{eff}/T_e^{3/2})\ \text{Ohms-cm} \tag{1.5}$$

is the Spitzer resistivity [38] and $b \approx 6.53 \times 10^3\ \ell n\Lambda$. Then

$$j(r) = \beta(r)\{T_e(r)\}^{3/2}, \tag{1.6}$$

where

$$\beta(r) = (V_L/2\pi bR)[f_\sigma(r)/Z_{eff}(r)]. \tag{1.7}$$

It may be noted that for a given j(r)-profile, Ohm's law specifies the steady-state $T_e(r)$-profile and vice versa [27,38] only for ohmically heated plasmas with no appreciable amount of runaway and/or slideaway populations of electrons [38,39]. For auxiliary heated plasmas [such as neutral beam heating, electron-cyclotron resonance heating (ECRH), ion cyclotron resonance heating (ICRH), lower-hybrid resonance heating, etc.] in general the current density $j(r) = j_{ohm}(r) + j_{aux}(r)$, where j_{ohm} is the Ohmic heating current and j_{aux} is the induced current due to auxiliary heating. Hence for "mildly" auxiliary heated plasmas with $j_{ohm} >> j_{aux}$, one can use the Ohmic relations of Eqs. (1.1), (1.6), and (1.7) and make no appreciable error in the final results. However, when $j_{ohm} >> j_{aux}$, Q_{ohm} can either be greater or less than Q_{aux} depending on the Ohkawa steady-state current drive efficiency criterion for that auxiliary heating method [40]. If $Q_{aux} >> Q_{ohm}$, then in Eq. (1.2) $Q(r) \approx Q_{aux}(r)$, regardless of whether j_{aux} is greater than or less than j_{ohm}. That is, what is mild auxiliary heating for Ohm's law Eqs. (1.1), (1.6), and (1.7) is not necessarily mild for the electron thermal energy-balance Eq. (1.2). In this paper we consider only cases where $j_{ohm} >> j_{aux}$ and for all but the T_{eo}-scaling law $Q_{ohm} \gtrless Q_{aux}$. In deriving the T_{eo}-scaling law we further restrict ourselves to cases where $Q_{ohm} >> Q_{aux}$ in Eq. (1.2) [see also Eqs. (1.15), (2.47), and (2.52) for example].

By the self-consistency of the principle of profile consistency results for sawtoothing tokamak discharges we mean that having obtained the analytic functions that reasonably fit the experimentally measured $T_e(r)$ and/or $j(r)$, can one analytically derive the unique set of functions F_1, F_2, and F_3 that will reasonably fit the experimentally measured plots of (r_1/a) vs $(1/q_a)$, $(\langle T_e\rangle/T_{eo})$ vs $(1/q_a)$, and the T_{eo} scaling law simultaneously, and are these analytic functions for $T_e(r)$ and/or $j(r)$ unique for all sawtoothing discharges in any tokamak [see also Fig. 1]? In this paper we will examine in sufficient detail and rigor this theoretical and experimental self-consistency of the various model profiles that are found in the literature. We will find that some of these profiles are naturally inconsistent with the basic notion of profile consistency for sawtoothing discharges. Indeed, all the q_a-independent profiles are at variance with the notion that $(r_1/a) = F_1(1/q_a)$, $\langle T_e\rangle/T_{eo} = F_2(1/q_a)$, $j_o = (I_p/\pi a^2)\ F_3(q_a)$, and $(\Delta T_e/T_e)$ decreases with increasing q_a [see also Table 1]. That is, for these profiles F_1, F_2, F_3 and $(\Delta T_e/T_e)$ are some fixed numbers regardless of the value of q_a. All the q_a-dependent profiles do show that F_1, F_2, and $(\Delta T_e/T_e)$ decrease with increasing q_a while F_3 increases with increasing q_a, in qualitative agreement with experimental observations. But none of these models are in exact quantitative agreement with the experimental measurements. Nevertheless, the Coppi-Tang diffusive model, Kadomtsev optimal profile model, and the Campbell et al. model do come fairly close to being in quantitative agreement with the experimental measurements for the full range of q_a values studied here. Also we will find that the Coppi's and Ohkawa's forms of $\chi_e(r)$ yield the profile-consistency dependent T_{eo}-scaling laws which are closer to physical reality than that given by the INTOR form of $\chi_e(r)$. Finally, it will be seen that precise measurements of the radial dependence of the normalized sawtooth amplitude $\Delta T_e/T_e$ can, in principle, yield not only the temperature and current profiles but also shed light on the "heat pulse" propagation $\chi_e(r)$[35].

B. Outline of the Theoretical Procedure

We will now outline the general theoretical procedure that we will use to examine the self-consistency of the principle of profile consistency results for sawtoothing tokamak discharges. As we stated earlier, if tearing mode stability is what determines the profiles in tokamaks, then the fundamental profile is the current density profile $j(r)$. This $j(r)$ profile is very hard to measure experimentally. Measurements of $j(r)$ have been attempted with some success by (1) far-infrared Faraday rotation [41], (2) Zeeman splitting of excited levels of Li using Li^{O} beams excited by tunable dye lasers [42], (3) Thomson laser scattering in a direction perpendicular to both the toroidal and poloidal magnetic fields [43] (i.e., a manifestation of the familiar Mössbauer effect [44]), (4) the magnetic field pitch angle-dependent widths of He^{+} ion lines from injected He^{O} beams [45], and (5) the displacement of D^{+} and/or H^{+} ion orbits from flux surfaces from injected D° or H° diagnostic beams due to the conservation of total angular momentum [46]. At the present time methods (1) and (2) have yielded $j(r)$ profile measurements to about 15% accuracy at the plasma center. But the accuracy is rather poor near the edge. However, fairly precise measurements of $T_e(r)$ profiles are available via (1) laser Thomson scattering [47], (2) black-body electron cyclotron emission [48,49,50], and (3) soft X-ray energy spectrum measurements along radial chords and subsequent Abel inversion [51]. Hence, in this paper we will take the $T_e(r)$ profile and not the $j(r)$ profile as the only reasonably precisely measurable profile at the present time. With this in mind the self-consistency examination procedure we will use is as follows:

Step 1: Since we know the total plasma current I_p and hence the limiter q_a, we will first fit a reasonable analytic function $T_e[r, \alpha_T(q_a)]$ for the measured $T_e(r)$ profile, where the function $\alpha_T(q_a)$ is a measure of the q_a-dependent width of the measured temperature profile.

Step 2: Now we deduce $j[r, \alpha_j(q_a)] = \beta(r) \{T_e[r, \alpha_T(q_a)]\}^{3/2}$ from Ohm's law [see Eq. (1.6)]. Here the measure of the current profile width $\alpha_j(q_a)$ is determined by the corresponding measure of the temperature profile width $\alpha_T(q_a)$. In almost all cases $\alpha_j = (3\alpha_T/2)$. First, as is usually done by theoreticians, we will assume for simplicity a Spitzer form of resistivity and Z_{eff} independent of r. This implies that β is a constant independent of r. Later we will try some reasonable neoclassical form factors. The procedure from step 1 to step 2 is illustrated by the reversible lines [with arrows pointing in both directions] connecting the box $T_e(r, \alpha_T)$ with the box $j(r, \alpha_j)$ in the flow chart diagram of Fig. 1. Ideally, a pure theorist will follow the reversed direction. If $j(r)$ is more precisely measurable than $T_e(r)$, then we would have first fitted a reasonable analytic function $j[r, \alpha_j(q_a)]$ and then deduced $T_e[r, \alpha_T(q_a)]$ from Ohm's law in agreement with the procedure used by the theorist.

Step 3: We now calculate the poloidal magnetic field from Biöt and Savart (and/or Ampere's law) [52]:

$$B_\theta[r, \alpha_j(q_a)] = \frac{\mu_o}{r} \int_0^r dr\, r\, j[r, \alpha_j(q_a)], \qquad (1.8)$$

where μ_o is the free-space permeability.

Step 4: Thus, we calculate

$$q[r,\ \alpha_j(q_a)] = \{rB_T/RB_\theta[r,\ \alpha_j(q_a)]\}.$$

Hence

$$q[r,\ \alpha_j(q_a)] = q_a\{rB_\theta[a,\ \alpha_j(q_a)]/aB_\theta[r,\ \alpha_j(q_a)]\}. \qquad (1.9)$$

Step 5: Now we solve for the normalized sawtooth inversion radius (r_1/a) as a function of $\alpha_j(q_a)$ from the equation

$$q[r_1,\ \alpha_j(q_a)] = q_a\{r_1B_\theta[a,\ \alpha_j(q_a)]/aB_\theta[r_1,\ \alpha_j(q_a)]\} = 1. \qquad (1.10)$$

Since it is found experimentally that $(r_1/a) = F_1(1/q_a) \approx (1/q_a)$, we demand that this experimentally measured function is a solution of Eq. (1.10). This, in turn, yields the explicit functional dependence of α_j on q_a such that $(r_1/a) \approx (1/q_a)$ is a solution of Eq. (1.10). It is interesting to note from Eqs. (1.8) and (1.10) that $[I_p(o\ \text{to}\ r_1)/I_p(o\ \text{to}\ a)] = (q_a r_1^2/a^2)$, where $I_p(o\ \text{to}\ r)$ is the plasma current inside the minor radius r. That is, the empirical profile-consistency relation $(r_1/a) \approx (1/q_a)$ implies that $[I_p(o\ \text{to}\ r_1)/I_p(o\ \text{to}\ a)] \approx (1/q_a)$.

Step 6: We then calculate the volume-averaged electron temperature

$$\frac{\langle T_e \rangle}{T_{eo}} = \frac{1}{T_{eo}} \frac{\int_o^a dr\ r\ \{T_e[r,\ \alpha_T(q_a)]\}}{\int_o^a dr\ r\ dr} . \qquad (1.11)$$

Since we know $\alpha_T(q_a)$ in terms of $\alpha_j(q_a)$, we now express $[\langle T_e \rangle / T_{eo}]$ of Eq. (1.11) as a function of $(1/q_a)$ and obtain the theoretically predicted function $F_2(1/q_a)$ which is consistent with the function $F_1(1/q_a) = (1/q_a)$. If this theoretically predicted function $F_2(1/q_a)$ describes well the experimentally measured plot of $[\langle T_e \rangle / T_{eo}]$ vs $(1/q_a)$, then there is self-consistency in the predictions of the principle of profile consistency.

Step 7: From step 5 we know α_j as an explicit function of q_a. Then from Eq. (1.9) one can easily show that the central peak current density j_o may be written

$$j_o = (I_p/\pi a^2)\ F_3(q_a) = \langle j \rangle\ (q_a/q_o) \qquad (1.12)$$

[see Sec. IID], where $F_3(q_a) = (q_a/q_o)$, $\langle j \rangle = (I_p/\pi a^2)$, $q_o = (2B_T/\mu_o R j_o)$, and $q_a = (2\pi a^2 B_T/\mu_o R I_p)$. Also from the Ohm's law [i.e., Eqs. (1.6) and (1.7)]

$$j_o = (V_L/2\pi b R Z_{eff})\ T_{eo}^{3/2}, \qquad (1.13)$$

since by definition $f_\sigma(r=o) = 1$.

Thus, from Eqs. (1.12) and (1.13) we get

$$T_{eo}^{3/2} = (2bI_pRZ_{eff}/a^2V_L)\ F_3(q_a). \tag{1.14}$$

It may be noted from Eqs. (1.12) and (1.14) that $T_{eo}^{3/2} \propto (I_p\ R\ Z_{eff}/a^2V_L)$ if $F_3(q_a) = (q_a/q_o) \approx$ constant, a result that is true for all q_a-independent profiles; and $T_{eo}^{3/2} \propto (B_TZ_{eff}/V_L)$ if $F_3(q_a) = (q_a/q_o) \propto q_a$, a result that is true for all q_a-dependent profiles when $(r_1/a) \approx (1/q_a)$. That is, the former T_{eo} scaling is profile consistency independent, and the latter one is profile consistency dependent via the empirical relation $r_1/a \approx 1/q_a$. For low-density regimes, for example, associating $\chi_e(r)$ of the electron thermal energy-balance Eq. (1.2) with the presence of resistive reconnecting modes [see also Eqs. (2.54) and (2.55) for the INTOR and Ohkawa models of $\chi_e(r)$] that allow for a stable j(r) profile, following Coppi's [3] simple dimensional arguments one can easily show that

$$V_L \propto F_4(R,\ a,\ B_T,\ I_p,\ Z_{eff},\ n_e,\ m_i,\ \text{etc.}) \tag{1.15}$$

[see Sec. IID]. Thus from Eqs. (1.14) and (1.15) we get the scaling law for the central electron temperature T_{eo}.

This entire sequence of steps 1 to 7 is shown in the analytic self-consistency loop [or flow chart] diagram of Fig. 1. The reversible lines (with arrows pointing in both directions in this figure) imply that there should exist an intrinsic self-consistency among the forms of j(r), $f_\sigma(r)$, $T_e(r)$, and $\chi_e(r)$ so as to satisfy the Ohm's law and the electron thermal energy balance equation simultaneously as pointed out by Furth [27]. In this figure the two large bold type connecting flow lines emanating from the box labelled "solution $\alpha_j(q_a)$" [one leading to the box labelled "$\langle T_e\rangle/T_{eo} = F_2(q_a)$. Experimental check 4", and the other leading to the box labelled "T_{eo}-scaling law $S_1(V_L)$, Experimental check 5"] are uniquely due to the principle of profile consistency. That is to say that if the tokamak discharges do not satisfy the requirements of the principle of profile consistency these two large bold type connecting flow lines will be absent in the flow chart diagram. In this figure we have also indicated seven distinct boxes where one can experimentally check the corresponding theoretical predictions. For example, first one can check whether the experimentally measured current profile is consistent with the theoretical predictions for macroscopic stability requirements for long-wavelength tearing modes. Second, are the experimentally measured $T_e(r)$ and $j(r)$ profiles consistent with Ohm's law? Finally, are the experimentally measured functions F_1, F_2, $T_{eo}(V_L)$, expression for V_L, and the final form of T_{eo} scaling consistent with the corresponding theoretical predictions based on the principle of profile consistency?

II. *COPPI-TANG MODEL*

A. Coppi-Tang diffusive model for $T_e(r,\ q_a)$ with Spitzer type resistivity.

It is found experimentally in Alcator A and Frascati (FT) tokamaks [3] that the electron temperature takes on a diffusion-like profile in impurity-free plasmas. Also Taroni and Tibone [4] have shown that for regions outside the q = 1 surface [i.e., for $r > r_1$], a Gaussian profile shape provides an excellent fit to the large majority of JET steady-state T_e-profiles. Later, Pfirsch and Pohl [11] have shown theoretically that these Gaussian T_e-profiles lead in many cases to very good agreement with those predicted by their "entropy principle." Then, to the extent that the longitudinal resistivity is proportional to the classical value [i.e., to the extent β of Eq. (1.6) is independent of r], the current density profile j(r) is also Gaussian. Hence, the profile shapes in this model are:

$$T_e(r) = T_{eo} \exp(-\alpha_T r^2/a^2), \tag{2.1}$$

and

$$j(r) = j_o \exp(-\alpha_j r^2/a^2), \tag{2.2}$$

where by Ohm's law $\alpha_j = (3\alpha_T/2)$. Here, α_j and α_T are functions of q_a [i.e., $\alpha_j = \alpha_j(q_a)$ and $\alpha_T = \alpha_T(q_a)$]. From Eq. (2.2) we get the poloidal magnetic field

$$B_\theta(r) = \frac{\mu_o j_o}{r} \int_o^r dr\ r \exp(-\alpha_j r^2/a^2)$$

$$= (\mu_o j_o a^2/2r\alpha_j)\ [1 - \exp(-\alpha_j r^2/a^2)]. \tag{2.3}$$

Then

$$q(r) = [rB_T/RB_\theta(r)] = \frac{(2B_T\alpha_j/R\mu_o j_o)(r^2/a^2)}{1 - \exp(-\alpha_j r^2/a^2)}, \tag{2.4}$$

and

$$q_a = q(a) = (2B_T\alpha_j/R\mu_o j_o)/[1 - \exp(-\alpha_j)]. \tag{2.5}$$

Hence

$$q(r) = \frac{q_a(r^2/a^2)[1 - \exp(-\alpha_j)]}{1 - \exp(-\alpha_j r^2/a^2)} \tag{2.6}$$

and

$$q(o) = (q_a/\alpha_j)[1 - \exp(-\alpha_j)]. \tag{2.7}$$

For sawtoothing discharges $q(o) \le 1$, then from Eq. (2.7) it follows that $\alpha_j > q_a$. The sawtooth inversion radius r_1, is then given by

$$q(r_1) = \frac{q_a(r_1^2/a^2)[1 - \exp(-\alpha_j)]}{1 - \exp(-\alpha_j r_1^2/a^2)} = 1. \tag{2.8}$$

If we demand that $(r_1/a) = (1/q_a)$ is the solution of Eq. (2.8), then

$$\alpha_j = -q_a^2 \log[1 - 1/q_a] + q_a^2 \log[1 - (1/q_a)\exp\{-\alpha_j(1 - 1/q_a^2)\}]. \tag{2.9}$$

The iterative solution of the transcendental Eq. (2.9) may be written

$$\alpha_j \approx \alpha_j^{(o)} + q_a^2 \log[1 - (1/q_a)\exp\{-\alpha_j^{(o)} (1 - 1/q_a^2)\}], \tag{2.10}$$

where the zero-order solution

$$\alpha_j^{(0)} = -q_a^2 \log[1 - 1/q_a]. \tag{2.11}$$

For our cases of interest $q_a > 2$ and hence

$$\alpha_j^{(0)} \approx q_a + 0.5 + (1/3q_a) + \ldots \tag{2.12}$$

This is the solution given by Tang [5]. From Eqs. (1.11) and (2.1) we get

$$\langle T_e \rangle / T_{eo} = (1/\alpha_T)[1 - \exp(-\alpha_T)]$$

$$= (3/2\alpha_j)[1 - \exp(-2\alpha_j/3)]. \tag{2.13}$$

Figure 2 shows clearly that the soft X-ray measurements of the sawtooth inversion radii in TFTR satisfy the relation $(r_1/a) \approx (1/q_a)$. In Fig. 3a we show a comparison between experiment and theory of $[\langle T_e \rangle / T_{eo}]$. The data of this figure include all the discharges used in Fig. 2. It appears that the relationship between the experimental measurements and the theoretical predictions of Coppi-Tang model is $[\langle T_e \rangle / T_{eo}]_{EXP} \approx [\langle T_e \rangle / T_{eo}]_{TH} + 0.05$. At the peak of the sawtooth rise the $T_e(r)$ profile is peaked, while at the bottom of the sawtooth crash the $T_e(r)$ profile is fairly flat up to r_1. Thus, $T_{e1} = T_e(r_1) = T_{eo} \exp(-\alpha_T/q_a^2) = T_{eo} \exp(-2\alpha_j/3q_a^2)$. Hence $[\langle T_e \rangle / T_{e1}]_{TH} = \{[\langle T_e \rangle / T_{eo}]_{TH} \exp(2\alpha_j/3q_a^2)\}$. In Fig. 3b we show a comparison between $[\langle T_e \rangle / T_{eo}]_{EXP}$ and the corresponding $[\langle T_e \rangle / T_{e1}]_{TH}$ for the same set of data as in Fig. 3a. The agreement between the theory using the peak $T_{e1} = T_e(r_1)$ at the bottom of the sawtooth instead of the peak T_{eo} at the top of the sawtooth and experiment is rather poor. In Figs. 4a and 4b we show a comparison between the experimentally measured $T_e(r)$ profiles and the corresponding theoretically predicted ones from Eqs. (2.1) and (2.10) for (low) $q_a \approx 2.9$ and (high) q_a = 6.2 discharges, respectively. These measurements are the second harmonic electron cyclotron black-body emission as measured by a Michelson interferometer, and are averaged over a couple of sawtooth periods. In the Appendix we show that the fraction of the total plasma current that is flowing outside the limiter for this model is

$$[I_p(a \text{ to } \infty)/I_p(o \text{ to } \infty)] = \exp(-\alpha_j). \qquad (2.14)$$

Since $\alpha_j \approx \alpha_j^{(o)} \approx q_a + 0.5$, it appears that from an experimental standpoint this is not an unreasonable fraction for values of $q_a > 2$.

Thus far we have taken the view that the best fit for the experimental plot of Fig. 2 is $(r_1/a) = (1/q_a)$. However, in Fig. 2 one could possibly also fit an equation of the form

$$(r_1/a) = (m/q_a) + b. \qquad (2.15)$$

Then the approximate solution of Eq. (2.8) is

$$\alpha_j(m;b) \approx \alpha_j(1;o)[1 + \{(m^2 - 1) + 2bmq_a + b^2\}/2\alpha_j(1;o)] \qquad (2.16)$$

where $\alpha_j(1;0)$ is the same α_j of Eq. (2.10). Since by definition when $(r_1/a) \to 1$, q_a must also tend to unity, it follows that $b = (1 - m)$ in Eq. (2.15). It is found that it is impossible to find a pair of values of m and b even with $b \neq (1 - m)$ that will yield good fits to both the plots of (r_1/a) vs $(1/q_a)$ and $[\langle T_e\rangle/T_{eo}]_{EXP}$ vs $[\langle T_e\rangle/T_{eo}]_{TH}$ simultaneously. That is, the pair that gives a good fit for one plot yields a very poor fit for the other plot and vice versa.

B. Chopped Coppi-Tang model for $T_e(r, q_a)$ with Spitzer-type resistivity.

This model assumes that the profiles are flat inside some radius $r_f \le r_1$ and is a Gaussian for $r \ge r_f$. That is,

$$T_e(r) = \begin{cases} T_{eo} & \text{for } r \le r_f \\ T_{eo} \exp[-\alpha_T (r^2 - r_f^2)/a^2] & \text{for } r \ge r_f \end{cases}, \tag{2.17}$$

and

$$j(r) = \begin{cases} j_o & \text{for } r \le r_f \\ j_o \exp[-\alpha_j (r^2 - r_f^2)/a^2] & \text{for } r \ge r_f \end{cases}, \tag{2.18}$$

where $\alpha_j = (3\alpha_T/2)$ by Ohm's law. Then one can show that

$$q(r) = \frac{q_a(r^2/a^2)[(r_f^2/a^2) + (1/\alpha_j)(1 - \exp\{-\alpha_j(1 - r_f^2/a^2)\})]}{[(r_f^2/a^2) + (1/\alpha_j)(1 - \exp\{-\alpha_j(r^2 - r_f^2)/a^2\})]} . \tag{2.19}$$

We now write $(r_f/a) = c(r_1/a)$ where $c \le 1$. If we demand that $(r_1/a) = (1/q_a)$ is the solution of $q(r_1) = 1$, then α_j of Eq. (2.19) is given by

$$\alpha_j(c) = \alpha_j(c = o) - q_a^2 [\log (1 + \alpha_j c^2/q_a^2) - (\alpha_j c^2/q_a^2)] \tag{2.20}$$

for c near zero, and

$$\frac{1}{\alpha_j(c)} = \frac{(c^2/q_a)(1 - 1/q_a)}{[(1 - \exp\{-\alpha_j(1 - c^2/q_a^2)\}) - q_a (1 - \exp\{(-\alpha_j/q_a^2)(1 - c^2)\})]} \tag{2.21}$$

for c near unity, where $\alpha_j(c = o)$ is given by Eq. (2.10). It may be noted that the zero-order solutions to the lowest order are

$$\alpha_j^{(o)}(c = o) \approx - q_a^2 \log(1 - 1/q_a) \approx q_a + 0.5 \text{ for } c \approx o, \qquad (2.22)$$

and

$$\alpha_j^{(o)} (c = 1) \approx q_a/(1 - 1/q_a) \approx q_a + 1 \text{ for } c = 1 \text{ and } q_a \geq 2. \qquad (2.23)$$

From Eq. (2.17), we get

$$[\langle T_e\rangle/T_{eo}] = (3/2\alpha_j)[1 - \exp\{- (2\alpha_j/3)(1 - r_f^2/a^2)\}] + (r_f^2/a^2). \qquad (2.24)$$

In Fig. 5 we have shown a comparison of $[\langle T_e\rangle/T_{eo}]_{EXP}$ vs $[\langle T_e\rangle/T_{eo}]_{TH}$ for $c = 1$ and the same set of data as in Fig. 3. Here the agreement between theory and experiment is better than that of Fig. 3a. In Figs. (6a) and (6b) we show a comparison between the experimental and theoretical $T_e(r)$ profiles for discharges with (low) $q_a \approx 2.9$ and (high) $q_a \approx 6.2$, respectively. The overall agreement between the experimental measurements and the theoretical predictions of this chopped Coppi-Tang model with $c = 1$ seems fairly reasonable.

C. Coppi-Tang Model With Some Neoclassical Form Factors.

We now wish to examine the effects of the neoclassical corrections (to the Spitzer resistivity η_s) on the profile consistency set of functions, $F_1(1/q_a) = (r_1/a)$, $F_2(1/q_a) = [\langle T_e\rangle/T_{eo}]$, and $F_3(q_a) = (q_a/q_o)$. An approximate analytic formula for the neoclassical conductivity form factor $f_{NC}(r) = \sigma_{NC}/\sigma_s = \eta_s/\eta_{NC}$ may be written $f_{NC}(r) \approx [1 - f_T/(1 + \xi\, \nu_*)]\ [1 + Cf_T/(1 + \xi\, \nu_*)]$, where f_T is the fraction of trapped particles (with banana orbits), ν_* is the electron collisionality parameter, C is the conductivity reduction coefficient due to electron-electron collisions, and ξ is an effective ion charge-dependent numerical factor. Detailed formulae for these coefficients f_T, ν_*, C and ξ are given by Hirshman and Sigmar [37]. Generally, $0.4 \lesssim f_{NC}(r) \leq 1$, and $f_{NC}(r)$ has a minimum at some value of $r > a/2$. The flatter the temperature profile, the larger is the value of r_{min}. At the plasma center $f_T = 0$ and hence $f_{NC}(r = 0) = 1$. Since $j = \sigma E = \sigma (V_L/2\pi R)$, the neoclassical corrections to η_s tend to narrow the current profile $j(r)$. That is, for a given $T_e(r)$, the neoclassical $j_{NC}(r)$ is narrower than the Spitzer $j_s(r)$. Hence, for a given q_a and $F_1(1/q_a) = (r_1/a) = (1/q_a)$, the value of the current profile width parameter $\alpha_j(q_a)$ for $j_{NC}(r)$ must be less than the corresponding value given by Eq. (2.12) for $j_s(r)$ [i.e., $\alpha_j < q_a + 0.5$]. Thus, for a given q_a and $T_e(r)$, the neoclassical corrections tend to increase the value of $F_2(1/q_a) = [\langle T_e\rangle/T_{eo}] \propto [1/\alpha_j(q_a)]$ since we demand that $F_1(1/q_a) = (1/q_a)$. That is, one would expect the neoclassical corrections to improve the fit between theory and experiment in Fig. 3a since these corrections tend to increase the values of $[\langle T_e\rangle/T_{eo}]_{TH}$.

However, it is extremely difficult if not impossible to derive explicit closed form analytic expressions for this set of functions F_1, F_2, and F_3 even with this approximate $f_{NC}(r)$. Thus, it is natural to assume that a point by point computer numerical solution for each q_a is the most effective one. But, this way does not help very much in comprehension of the physics of the phenomena. Hence, we will now try to mock up this $f_{NC}(r)$ via conductivity form factors $f_\sigma(r)$ that are some simple but physically reasonable functions of (r/a). We find that $f_\sigma(r) = (1 - d\ r^2/a^2)$ and $f_\sigma(r) = \exp(- r^2/a^2)$ fit reasonably well with the JET group resistivity measurements of Campbell et al., [Figs. 3 and 13 of Ref 13] and Bartlett et al., [Fig. 9 of Ref. 31]. Further, since these functions F_1, F_2, and F_3 depend only on the moments of

$j(r)$ and $T_e(r)$ and not on their local derivatives and since these functions are sensitive primarily to the behavior of $f_\sigma(r)$ in the main body of the plasma and are fairly insensitive to the nature of $f_\sigma(r)$ near the plasma edge, we feel that these $f_\sigma(r)$ are reasonably adequate approximations to $f_{NC}(r)$ for the problem under study.

Case 1: First we will try

$$f_\sigma(r) = (1 - dr^2/a^2) \tag{2.25}$$

where $d < 1$. Hence, the profiles are

$$T_e(r) = T_{eo}\ \exp(-\alpha_T r^2/a^2), \tag{2.26}$$

and

$$j(r) = j_o\ (1 - d\ r^2/a^2)\exp(-\alpha_j r^2/a^2), \tag{2.27}$$

where $\alpha_T = (2\alpha_j/3)$. Then

$$q(r) = \frac{q_a\ (r^2/a^2)[(1 - d/\alpha_j) - (1 - d/\alpha_j - d)\exp(-\alpha_j)]}{[(1 - d/\alpha_j) - (1 - d/\alpha_j - dr^2/a^2)\exp(-\alpha_j r^2/a^2)]}\ . \tag{2.28}$$

If we demand that $(r_1/a) = (1/q_a)$ is the solution of the transcendental equation $q(r_1) = 1$, then we get for α_j of Eq. (2.28)

$$\alpha_j = \alpha_j^{(0)} + \delta\ , \tag{2.29}$$

where

$$\alpha_j^{(0)} = - q_a^2 \log(1 - 1/q_a), \tag{2.30}$$

and

$$\delta = - q_a^2[\log(1 - d/\alpha_j) - \log(1 - d/\alpha_j - d/q_a^2)]$$
$$+ q_a^2 \log[1 - \frac{(1 - d/\alpha_j - d)}{q_a(1 - d/\alpha_j - d/q_a^2)} \exp\{-\alpha_j(1 - 1/q_a^2)\}]. \tag{2.31}$$

For our cases of interest $q_a > 2$. Then the zero-order solution of Eq. (2.29) to the lowest order is

$$\alpha_j \approx \alpha_j^{(0)} - q_a^2 [\log(1 - d/\alpha_j) - \log(1 - d/\alpha_j - d/q_a^2)]$$
$$\approx q_a + 0.5 - d + (1/3q_a)\ldots. \tag{2.32}$$

From Eq. (2.26) we get

$$[\langle T_e\rangle/T_{eo}] = (3/2\alpha_j)[1 - \exp(-2\alpha_j/3)]. \tag{2.33}$$

In Fig. 7 we show a comparison between the $[\langle T_e\rangle/T_{eo}]_{EXP}$ and the corresponding $[\langle T_e\rangle/T_{eo}]_{TH}$ for $d = 0.5$ and the same set of data as in Fig. 3. Here the agreement between theory and experiment is better than that of Fig. 3a and is somewhat similar to that of Fig. 5

Case 2: Second we will try

$$f_\sigma(r) = \exp(-r^2/a^2). \tag{2.34}$$

For this conductivity form factor, it is relatively easy to show from Eq. (2.9) that if $(r_1/a) = (1/q_a)$ is the solution of $q(r_1) = 1$, then the corresponding α_j is given by

$$\alpha_j = -1 - q_a^2 \log[1 - 1/q_a] + q_a^2 \log[1 - (1/q_a) \exp\{-(\alpha_j + 1)(1 - 1/q_a^2)\}]. \tag{2.35}$$

For our cases of interest $q_a > 2$, then the lowest order form of Eq. (2.35) may be written

$$\alpha_j \approx -1 - q_a^2 \log[1 - 1/q_a] \approx q_a - 0.5 + (1/3\ q_a)\ldots. \tag{2.36}$$

Comparing Eq. (2.36) with Eq. (2.32), it is apparent that this case 2 is more or less the same as the previous case 1 with $d \approx 1$ in Eq. (2.32). This is a reflection of the fact that the functions, F_1, F_2, and F_3 are sensitive primarily to the behavior of $f_\sigma(r)$ in the main body of the plasma and are fairly insensitive to its behavior near the plasma edge since $f_\sigma(r) = \exp(-r^2/a^2) \approx (1 - r^2/a^2)$ for $r^2 < a^2$. Also it is now apparent why both the conductivity form factors $f_\sigma(r)$ of case 1 [see Eq. (2.25)] and case 2 [see Eq. (2.34)] fit reasonably well with the JET group measurements of Campbell et al. [13] and Bartlett et al. [31] for the main body of the plasma. They do however differ near the plasma edge.

Case 3: Third we will try the theoretically expected conductivity form factor $f_\sigma(r)$ when $\chi_e(r)\, n_e(r) \approx$ constant independent of r [i.e., the INTOR and the Ohkawa type $\chi_e(r)$] in the electron thermal energy-balance Eq. (1.2). Then from the low-density regime [i.e., neglecting the Q_{ei} term] of Eq. (1.2), we get for Ohmic impurity-free plasmas

$$f_\sigma(r) \propto [\frac{1}{r}\ \frac{d}{dr}\ (r\ \frac{dT_e}{dr})]/T_e^{3/2}$$

$$\simeq [1 - (\alpha_T r^2/a^2)]\exp(\alpha_T r^2/2a^2) \qquad (2.37)$$

for $T_e(r) \simeq T_{eo}\exp(-\alpha_T r^2/a^2)$. Then,

$$j(r) = j_o[1 - (\alpha_T r^2/a^2)]\exp(-\alpha_T r^2/a^2). \qquad (2.38)$$

It should be noted from Eqs. (1.1), (1.2) and (2.37) that for low density Ohmic impurity-free plasmas with a constant $\kappa_e = \chi_e(r)\, n_e(r)$, a given $T_e(r)$ uniquely determines $f_\sigma(r)$ and vice versa. Thus, if $T_e(r)$ is a Gaussian of Eq. (2.1), then $f_\sigma(r) \neq f_{NC}(r)$ [or equivalently, if $f_\sigma(r) = f_{NC}(r)$, then $T_e(r)$ cannot be a Gaussian] for these Ohmic plasmas with a constant κ_e. This is a natural consequence of the fact that there must exist an intrinsic self-consistency among the forms of $j(r)$, $f_\sigma(r)$, $T_e(r)$, $\chi_e(r)$, and $n_e(r)$ so as to satisfy the Ohm's law and the electron thermal energy balance equation simultaneously as pointed out by Furth [27] and illustrated by the reversible lines in Fig. 1.

Comparing Eq. (2.38) with Eq. (2.27) of case 1 [with α_T replacing both d and α_j], it follows from Eq. (2.28) that

$$q(r) = q_a \exp[-\alpha_T(1 - r^2/a^2)]. \tag{2.39}$$

If we now demand that $(r_1/a) = (1/q_a)$ is the solution of the equation $q(r_1) = 1$, then from Eq. (2.39) we get

$$\alpha_T = (\log q_a)/(1 - 1/q_a^2). \tag{2.40}$$

Since $T_e(r) = T_{eo} \exp(-\alpha_T r^2/a^2)$, we get

$$[\langle T_e\rangle/T_{eo}] = (1/\alpha_T)[1 - \exp(-\alpha_T)]. \tag{2.41}$$

It is found that a comparison between the $[\langle T_e\rangle/T_{eo}]_{EXP}$ and the corresponding $[\langle T_e\rangle/T_{eo}]_{TH}$ for the same set of data as in Fig. 3 yields $[\langle T_e\rangle/T_{eo}]_{EXP} \approx [\langle T_e\rangle/T_{eo}]_{TH} - 0.15$. This is a poorer agreement than that of case 1. This may imply that either $\chi_e(r)\, n_e(r) \neq$ constant or the $T_e(r)$ is not really Gaussian for the discharges under study.

D. Principle of profile consistency predictions for central electron temperature T_{eo} scaling from Coppi-Tang model.

By definition

$$q_a = [aB_T/RB_\theta(a)] = [2\pi a^2 B_T/\mu_o R I_p]. \tag{2.42}$$

Also from Eq. (2.5)

$$q_a = (2B_T\alpha_j/\mu_o R j_o)/[1 - \exp(-\alpha_j)]. \tag{2.5}$$

The principle of profile consistency for sawtoothing discharges implies that $(r_1/a) \approx (1/q_a)$ which in turn demands [see Eq. (2.12)] that $\alpha_j \approx \alpha_j^{(o)} \approx q_a + 0.5$. For $q_a > 2$, $[1 - \exp(-\alpha_j)] \approx 1$. Then from Eqs. (2.42) and (2.5) we get

$$j_o \approx (I_p \alpha_j/\pi a^2) \approx (I_p/\pi a^2)(q_a + 0.5). \tag{2.43}$$

From Eqs. (1.12) and (2.43) it is seen that $F_3(q_a) = (q_a/q_o) \approx q_a + 0.5$ for this model. By Ohm's law [see Eqs. (1.6) and (1.7)]

$$j_o = (V_L/2\pi b Z_{eff} R)\, T_{eo}^{3/2}. \tag{2.44}$$

Then from Eqs. (2.42), (2.43), and (2.44) we get

$$T_{eo} \approx (4\pi b/\mu_o)^{2/3}\, (Z_{eff} B_T/V_L)^{2/3}\, [1 + (\mu_o R I_p/4\pi a^2 B_T)]^{2/3}. \tag{2.45}$$

For $q_a > 2$, $(\mu_o R I_p/4\pi a^2 B_T) = (0.5/q_a) \ll 1$. Hence, the profile consistency dependent scaling law for large q_a is

$$T_{eo} \propto (Z_{eff} B_T/V_L)^{2/3} \tag{2.46}$$

and there is no explicit dependence on I_p, R, and a.

We now wish to obtain an expression for the loop voltage V_L. Here we will follow the dimensional analysis arguments of Coppi [3]. First we consider the low-density regime where the Q_{ei} term in the electron thermal energy-balance Eq. (1.2) can be neglected. If we associate $\chi_e(r)$ with the presence of resistive reconnecting modes that allow for stable $j(r)$ profile, following Coppi [3], it is relatively easy to show that

$$V_L = (\pi\epsilon_D/2e)(3\pi^{1/2}bem_e c^2/2)^{2/5}(RZ_{eff}^{3/5}n_e^{1/5}/am_i^{1/5}), \qquad (2.47)$$

where ϵ_D is a numerical coefficient [of order $0.3/8\pi \sim 10^{-2}$] that is evaluated by a fit to the experimental data. One may note from Eqs. (1.15) and (2.47) that the function $F_4 \propto R\ Z_{eff}^{3/5}\ n_e^{1/5}\ a^{-1}\ m_i^{-1/5}$ for this model profile and Coppi's form of $\chi_e(r)$. Hence from Eqs. (2.46) and (2.47), it follows that the scaling law in the low-density regime is

$$T_{eo} \propto B_T^{2/3}\ R^{-2/3}\ a^{2/3}\ Z_{eff}^{4/15}\ m_i^{2/15}\ n_e^{-2/15}. \qquad (2.48)$$

This may be compared with the Taylor et al. [25] regression analysis of the TFTR data which yielded

$$T_{eo} \propto B_T^{0.78}\ R^{-0.31}\ a^{1.1}\ Z_{eff}^{0.45}\ I_p^{-0.24}, \qquad (2.49)$$

and the TFR data [1] which yield $T_{eo} \propto B_T^{0.86}$ for constant I_p, n_e, R, a, and m_i.

We now consider the high-density regimes where $T_i(r)$ is strongly coupled to $T_e(r)$. That is, when the electron-ion equilibration time is much shorter than the energy replacement time the approximate form of Eq. (1.2) and (1.3) become

$$E \cdot j(r) \approx Q_{ei} \propto \nu_{ei}(r)\, n_e(r)\, T_e(r)[1 - T_i(r)/T_e(r)]/m_i. \tag{2.50}$$

That is,

$$(E^2/\eta) = (V_L/2\pi R)^2\,(1/\eta) \propto \nu_{ei}\, n_e\, T_e\,[1 - T_i/T_e]/m_i. \tag{2.51}$$

Since $\eta = (m_e c^2\, \nu_{ei}/n_e\, e^2)$, Eq. (2.5') yields

$$V_L \propto (RT_e^{1/2}\,[1 - T_i/T_e]^{1/2}\,\nu_{ei}/m_i^{1/2})$$

$$\propto (Rn_e Z_{eff}[1 - T_i/T_e]^{1/2}/T_e\, m_i^{1/2}), \tag{2.52}$$

where we have used the fact that $\nu_{ei} \propto (n_e Z_{eff}/T_e^{3/2})$. Thus, from Eqs. (2.46) and (2.52), the high-density regime scaling law may be written

$$(T_{eo} - T_{io}) \propto B_T^2\; R^{-2}\, m_i\, n_e^{-2}\,. \tag{2.53}$$

In deriving Eq. (2.53) we have used the values of Eqs. (2.50), (2.51) and (2.52) at $r = o$. However, a better form of the scaling law can be obtained by using the volume-averaged forms of Eqs. (2.50), (2.51), and (2.52).

Equation (2.48) gives the T_{eo} scaling if we associate $\chi_e(r)$ with the presence of resistive reconnecting modes that allow for stable $j(r)$ profiles [3]. In the literature several authors [2-5,29-34] have used various different models for the electron thermal diffusivity $\chi_e(r)$. The INTOR studies [32] have used a constant electron heat conduction coefficient $\kappa_e = n_e(r)\,\chi_e(r) = 5 \times 10^{17}$ cm^{-1} sec^{-1}. Ohkawa [33] has proposed a $\chi_e(r)$ model based on magnetic reconnection due to the small-scale current filamentation around the singular points $\mu = 1/q = n/m$. He argues that the mixing length or the "random walk" step length is the collisionless skin depth c/ω_{pe} and the characteristic time is the transit time of the electrons around the closed field lines (qR/v_e) where the electron thermal speed $v_e = (2\kappa T_e/m_e)^{1/2}$. That is, $\chi_e \approx (c^2/\omega_{pe}^2)(v_e/\pi Rq_a)$. Hence for the Ohkawa model

$$\kappa_e = \chi_e(r)\, n_e(r) \propto (T_{eo}^{1/2}/Rq_a). \tag{2.54}$$

Subsequently, Kadomtsev and Pogutse [34] have shown that this Ohkawa result also follows from considerations of the magnetic reconnection [around flux surfaces where q takes on rational values] as a result of microturbulence in the drift frequency range. It is physically instructive to examine the T_{eo} scaling for the INTOR and the Ohkawa χ_e's using the Coppi-Tang diffusive profiles of Eqs. (2.1) and (2.2).

On making use of Eqs. (1.7), (2.1), and (2.2) in Eq. (1.2) one can show that for low-density Ohmic impurity-free plasmas with constant $\kappa_e = \chi_e(r)\, n_e(r)$[i.e., $Q \approx Q_{ohm} = E \cdot j$ and $\kappa_e \neq \kappa_e(r)$]

$$V_L^2 \approx (32\pi^2 b/3)(\kappa_e \alpha_j R^2 Z_{eff}/a^2 T_{eo}^{1/2}). \tag{2.55}$$

When $r_1/a \approx 1/q_a$, $\alpha_j \approx q_a + 0.5 \approx q_a$ for large q_a [see Eq. (2.12)]. Hence, from Eqs. (2.46) and (2.55) we find that the profile consistency-dependent T_{eo} scaling law may be written

$$T_{eo} \propto B_T^{2/5}\, I_p^{2/5}\, Z_{eff}^{2/5}\, R^{-2/5} \tag{2.56}$$

for the INTOR form of $\chi_e(r)$, and

$$T_{eo} \propto B_T^{2/3}\, a^{2/3}\, Z_{eff}^{1/3}\, R^{-1/3} \tag{2.57}$$

for the Ohkawa form of $\chi_e(r)$. Comparing Eqs. (2.48), (2.56), and (2.57) with the empirical Eq. (2.49) and with the TFR data [1], which yield $T_{eo} \propto B_T^{0.86}$, one can see that Coppi's and Ohkawa's forms of $\chi_e(r)$ yield T_{eo} scalings that are closer to physical reality than the INTOR form of $\chi_e(r)$.

III. EXPONENTIAL PROFILES

Electron temperature profiles have been measured under a wide range of discharge conditions in TFTR. Boyd and Stauffer [7] have presented these normalized T_e-profiles [i.e., plots of $T_e(r)/T_e(o)$ vs r/a] for a wide range of values of the limiter q. They find that for low q_a the shape is trapezoidal, and at higher q_a the profile is centrally peaked and falls exponentially in the range $0.1 < r/a < 0.6$. However, Fredrickson et al. [8] have taken an altogether different viewpoint in analyzing these $T_e(r)$ profiles in TFTR. In particular, these authors chose to normalize the $T_e(r)$ profiles to the value at the half minor radius point and have presented plots of $T_e(r)/T_e(a/2)$ vs r/a. That is, Boyd and Stauffer have put more emphasis on the data for $(r/a) < 0.6$ and less emphasis on the data for $(r/a) > 0.6$; while Fredrickson et al. have put more emphasis on the data for $(r/a) > 0.4$ and less emphasis on the data for $(r/a) < 0.4$, particularly for high q_a discharges. Taking their empirically fitted profile for high q_a Ohmic discharges (with very small sawteeth) as the "limit" profile, Fredrickson et al. found that the profile shapes outside the core region can be approximately fitted with a modified exponential function [see Sec. IV, Eqs. (4.1), (4.2) and (4.15)]. Inside the core region this limit profile shape is flattened for sawtoothing discharges.

A comparison of the conventional normalizing procedure used by Boyd and Stauffer [i.e., plots of $T_e(r)/T_e(o)$ vs r/a] with those used by Fredrickson et al. [i.e., plots of $T_e(r)/T_e(a/2)$ vs r/a] can be found in the paper by Becker et al. [30]. In this Sec. III and in Secs. IV and V we will examine the predictions of the generalized versions of these profile shapes [i.e., exponential, modified exponential, and trapezoidal profile shapes, respectively].

A. q_a - dependent exponential profile fits for $T_e(r,q_a)$

In this model, the profiles are given by

$$T_e(r) = T_{eo} \exp(-\alpha_T r/a), \tag{3.1}$$

and

$$j(r) = j_o \exp(-\alpha_j r/a), \tag{3.2}$$

where $\alpha_T = (2\alpha_j/3)$. Then,

$$q(r) = \frac{q_a(r^2/a^2)[1 - (\alpha_j + 1)\exp(-\alpha_j)]}{[1 - \{(\alpha_j r/a) + 1\}\exp(-\alpha_j r/a)]}, \tag{3.3}$$

where

$$q_a = (B_T\alpha_j^2/\mu_o R j_o)/[1 - (\alpha_j + 1)\exp(-\alpha_j)] . \tag{3.4}$$

From Eq. (3.3), we get

$$q\ (o) = (2q_a/\alpha_j^2)[1 - (\alpha_j + 1)\exp(-\alpha_j)]. \tag{3.5}$$

For sawtoothing discharges $q(o) \leq 1$ and, therefore, $\alpha_j^2 > 2q_a$. If $(r_1/a) = (1/q_a)$, then from Eq. (3.3) the iterative solution of the transcenaental equation $q(r_1) = 1$ may be written

$$\alpha_j^2 = [\alpha_j^{(o)2} + 2q_a^2 \log(1 - \frac{\alpha_j^{(o)} + 1}{\alpha_j^{(o)} + q_a} \exp\{-\alpha_j^{(o)}\ (1 - 1/q_a)\})]/Y(\alpha_j^{(o)}/q_a) \tag{3.6}$$

where

$$Y\ (\alpha_j^{(o)}/q_a) = - 2\{\log\ (1 + \alpha_j^{(o)}/q_a) - (\alpha_j^{(o)}/q_a)\}/(\alpha_j^{(o)}/q_a)^2 \tag{3.7}$$

and the zero order solution

$$\alpha_j^{(o)^2} = - 2q_a^2 \log(1 - 1/q_a) \approx 2q_a + 1. \tag{3.8}$$

From Eq. (3.1) we get

$$\begin{aligned}\langle T_e\rangle/T_{eo} &= (2/\alpha_T^2)[1 - (\alpha_T + 1)\exp(-\alpha_T)] \\ &= (9/2\alpha_j^2)[1 - (1 + 2\alpha_j/3)\exp(-2\alpha_j/3)].\end{aligned} \tag{3.9}$$

It is found that the $T_e(r)$ profiles of Eq. (3.1) witn α_j of Eq. (3.6) in general gives a very poor fit to the experimentally measured $T_e(r)$, profiles. The agreement between $[\langle T_e\rangle/T_{eo}]_{EXP}$ and the corresponding $[\langle T_e\rangle/T_{eo}]_{TH}$ of Eq. (3.9) is also found to be rather poor. Further, in the Appendix we show that the fraction of the total plasma current flowing outside the limiter for this model is

$$[I_p(a \text{ to } \infty)]/I_p(o \text{ to } \infty)] = (\alpha_j + 1)\exp(-\alpha_j). \tag{3.10}$$

Since $\alpha_j \approx \alpha_j^{(0)} \approx (2c_a+1)^{1/2}$, it appears that from an experimental standpoint this is an unacceptable fraction for values of $q_a > 2$.

B. T_{eo} scaling for q_a - dependent exponential profiles.

From Eqs. (2.42) and (3.4) we get

$$q_a = \frac{2\pi a^2 B_T}{\mu_o R I_p} = \frac{(B_T \alpha_j^2/\mu_o R j_o)}{[1 - (\alpha_j + 1)\exp(-\alpha_j)]} . \tag{3.11}$$

If $(r_1/a) = (1/q_a)$, then from Eq. (3.8) $\alpha_j{}^2 \approx \alpha_j{}^{(0)^2} \approx (2q_a + 1)$. For our cases of interest $q_a > 2$, then $[1 - (\alpha_j + 1)\exp(-\alpha_j)] \approx 1$. Thus from Eq. (3.11) we get

$$j_o \approx (I_p \alpha_j^2/2\pi a^2) \approx (I_p/\pi a^2)(q_a + 0.5). \tag{3.12}$$

Then using Eq. (2.44) we find that for $q_a \gg 1$

$$T_{eo} \propto (Z_{eff} B_T/V_L)^{2/3}. \tag{3.13}$$

Using Eq. (3.1) in the electron thermal energy-balance Eq. (1.2) for low-density regimes [i.e., neglecting the Q_{ei} term in Eq. (1.2)] and since by definition $\langle j/j_o \rangle = q_a/q(o)$ and $rj = (c/4\pi)\, d\,(rB_\theta)/dr$, one can show that [3]

$$\chi_e = \left(\frac{c^2 q_o \Omega_{\theta e}}{\omega_{pe}^2 q_a}\right)\left[\frac{eV_L}{(8\pi q_o \alpha_T/q_a)T_e}\,\frac{4a}{R}\right], \qquad (3.14)$$

where $\alpha_T = (2\alpha_j/3)$ and for $(r_1/a) = (1/q_a)$, $\alpha_j^2 = \alpha_j^{(0)^2} = (2q_a + 1) = 2q_a$ for $q_a > 2$ and $\Omega_{\theta e} = (eB_\theta(r)/m_e c)$. Since the general properties of resistive reconnecting modes depend on characteristic fractional powers (1/3 to 2/5) of the classical electrical resistivity, following Coppi [3], in Eq. (3.14) one may take

$$\left[\frac{eV_L}{(8\pi q_o \alpha_T/q_a)\; T_e}\;\frac{4a}{R}\right] = \epsilon_D \left(\chi_\eta \frac{\omega_{pi}}{v_{TH}}\right)^{2/5}, \qquad (3.15)$$

where $\chi_\eta = (\eta_\perp c^2/4\pi)$ and $\eta_\perp = (3\pi/32)\,\eta_\parallel = (3\pi/32)(bZ_{eff}/T_e^{3/2})$, ϵ_D is a numerical coefficient that is evaluated by a fit to the experimental data and $\omega_{pi} = (4\pi Z_{eff} n_e e^2/m_i)^{1/2}$. Thus, from Eq. (3.15) we get for the low-density regime

$$V_L \approx (\pi^{1/2}\mu_o^{1/2}\epsilon_D/3e)(3\pi^{1/2} b e m_e c^2/2)^{2/5} \left(\frac{R^{3/2}\; I_p^{1/2}\; Z_{eff}^{3/5}\; n_e^{1/5}}{a^2\; B_T^{1/2}\; m_i^{1/5}}\right), \qquad (3.16)$$

where from Eqs. (3.5) and (3.8) we have used $[q(o)\alpha_T/q_a] \approx (2/\alpha_j^2)\,(2\alpha_j/3) \approx (2/3)\,(2/q_a)^{1/2} = (2/3)\,(\mu_o/\pi)^{1/2}\,(R^{1/2}\, I_p^{1/2}/a\, B_T^{1/2})$. Hence from Eq. (3.13), for the low-density regime we get

$$T_{eo} \propto (Z_{eff} B_T/V_L)^{2/3} \propto B_T\, R^{-1}\, a^{4/3}\, Z_{eff}^{4/15}\, I_p^{-1/3}\, n_e^{-2/15}. \qquad (3.17)$$

It is interesting and physically instructive to note from Eqs. (2.46) and

(3.13) that the profile consistency dependent T_{eo} scaling law for sawtoothing tokamak discharges in terms of the loop voltage $T_{eo} \propto (Z_{eff}B_T/V_L)^{2/3}$ is universal and unique and is independent of the profile shapes. However, the expression for V_L for macroscopic stability requirements for the plasma column under study depends critically on the profile shapes and, in particular, on the $T_e(r)$ profiles. This is due to the fact that the electron thermal energy-balance equation which determines the macroscopic stability of the plasma column is a very sensitive function of the profile shapes for low-density regimes. This is the reason that the Gaussian temperature profile scaling law of Eq. (2.48) is somewhat different from the corresponding exponential $T_e(r)$ profile scaling law of Eq. (3.17). However, in the high-density regime, the dominant term in the electron energy-balance Eq. (1.2) is Q_{ei} and consequently the T_{eo} scaling is still given by Eq. (2.53) and is independent of the $T_e(r)$ profile.

C. q_a-dependent chopped exponential profile fits for $T_e(r,q_a)$.

The profile shapes for this model are

$$T_e(r) = \begin{cases} T_{eo} & \text{for } r \le r_f \\ T_{eo} \exp\{-\alpha_T(r - r_f)/a\} & \text{for } r \ge r_f \ , \end{cases} \tag{3.18}$$

and

$$j(r) = \begin{cases} j_o & \text{for } r \le r_f \\ j_o \exp\{-\alpha_j(r - r_f)/a\} & \text{for } r \ge r_f \ , \end{cases} \tag{3.19}$$

where $\alpha_T = (2\alpha_j/3)$. These profiles are flat up to some radius $r_f \le r_1$ and are exponential for $r \ge r_f$. Then for $r \ge r_f$,

$$q(r) = \frac{q_a(r^2/a^2)[(r_f^2/a^2) + (1/\alpha_j^2)\,((1 + \alpha_j r_f/a) - (1 + \alpha_j)\exp\{-\alpha_j(1-r_f/a)\})]}{(r_f^2/a^2) + (1/\alpha_j^2)[(1 + \alpha_j r_f/a) - (1 + \alpha_j r/a)\exp\{-\alpha_j(r - r_f)/a\}]},$$

(3.20)

where

$$q_a = \frac{(2B_T/\mu_o R j_o)}{(r_f^2/a^2) + (1/\alpha_j^2)[(1 + \alpha_j\, r_f/a) - (1 + \alpha_j)\exp\{-\alpha_j(1 - r_f/a)\}]}\,. \tag{3.21}$$

If $(r_1/a) = (1/q_a)$ and $(r_f/a) = (cr_1/a) = (c/q_a)$ with $c \le 1$, then from Eq. (3.20) the iterative solution of the transcendental equation $q(r_1) = 1$ may be written

$$\alpha_j^2(c) = \alpha_j^2(c{=}o) - 2q_a^2\{\log(1 + c\alpha_j^{(0)}/q_a + c^2\alpha_j^{(0)^2}/q_a^2) - (c\alpha_j^{(0)}/q_a)\}/Y(\alpha_j^{(0)}/q_a) \tag{3.22}$$

for c near zero, and for c near unity

$$\alpha_j^{-2}(c) = (c^2/q_a)(1-1/q_a)[(1+\alpha_j c/q_a)(1-q_a) - (1+\alpha_j)\exp\{-\alpha_j(1+c/q_a)\} + (\alpha_j+q_a)\exp(-(\alpha_j/q_a)(1-c)\}]^{-1}, \tag{3.23}$$

where $\alpha_j(c{=}0)$, $Y(\alpha_j^{(0)}/q_a)$ are given by Eqs. (3.6) and (3.7), and the zero-order solutions to the lowest order are

$$\alpha_j^{(0)}\,(c = 0) = [-2q_a^2\,\log(1 - 1/q_a)]^{1/2} \approx (2q_a + 1)^{1/2}, \tag{3.24}$$

and

$$\alpha_j^{(0)}\ (c = 1) \approx [q_a/(1 - 1/q_a)]^{1/2} \approx (q_a + 1)^{1/2}, \tag{3.25}$$

for c near zero and c near unity, respectively. From Eq. (3.18) we get

$$\langle T_e\rangle/T_{eo} = (9/2\alpha_j^2)[1 + (2c\alpha_j/3q_a) + (2c^2\alpha_j^2/9q_a^2)$$

$$- (1 + 2\alpha_j/3)\exp\{-(2\alpha_j/3)(1 - c/q_a)\}], \tag{3.26}$$

where we have set $\alpha_T = (2\alpha_j/3)$ and $(r_f/a) = (c\ r_1/a) = (c/q_a)$. Here again it is found that the $T_e(r)$ of Eq. (3.18) with α_j of Eq. (3.22) and (3.23) gives a very poor fit to the experimentally measured $T_e(r)$ profiles for any value of c ≤ 1. For $c = 1$, the agreement between $[\langle T_e\rangle/T_{eo}]_{EXP}$ and the corresponding $[\langle T_e\rangle/T_{eo}]_{TH}$ of Eq. (3.26) is found to be extremely poor. However, it is shown in Fig. 8 that the agreement between $[\langle T_e\rangle/T_{eo}]_{EXP}$ and the corresponding $[\langle T_e\rangle/T_{eo}]_{TH}$ of Eq. (3.26) for $c \approx 0.5$ is reasonably good.

D. q_a - independent exponential profile fits for $T_e(r)$.

In this model we assume the following profile shapes

$$T_e(r) = T_{eo}\exp(-4r/3a), \tag{3.27}$$

and

$$j(r) = j_o\exp(-2r/a). \tag{3.28}$$

Then

$$q(r) = \frac{q_a(r^2/a^2)[1 - 3\exp(-2)]}{[1 - (1 + 2r/a)\exp(-2r/a)]}, \tag{3.29}$$

where

$$q_a \approx (4B_T/0.594\mu_o Rj_o) \tag{3.30}$$

since $[1 - 3\ \exp\ (-2)] \approx 0.594$. If $(r_1/a) = (1/q_a)$ is the solution of the equation $q\ (r_1) = 1$, then

$$0.594/q_a = 1 - (1 + 2/q_a)\exp(-2/q_a). \tag{3.31}$$

The solution of Eq. (3.31) is $(1/q_a) = 0.8$ and, therefore, $q_a \approx 1.25$. Also, one can easily show that $(r_1/a) \geq o$ implies that $(1/q_a) \geq 0.297$, i.e., $q_a \leq 3.367$. From Eq. (3.27) we get

$$\langle T_e\rangle/T_{eo} = (9/8)[1 - (7/3)\exp(-4/3)] = 0.433 \tag{3.32}$$

regardless of the value of q_a. It is clear that q_a - independent profiles cannot have $(r_1/a) = (1/q_a)$ as a solution of $q\ (r_1) = 1$ for any continuous range of values of q_a and, consequently, $\langle T_e\rangle/T_{eo} \neq F_2(1/q_a)$ for any finite range of q_a.

E. T_{eo} scaling for q_a - independent exponential profiles, a scaling that does not depend on the principle of profile consistency.

From Eqs. (2.42) and (3.30), we get

$$q_a = (2\pi a^2 B_T/\mu_o RI_p) \approx (6.734B_T/\mu_o Rj_o). \tag{3.33}$$

That is,

$$j_o = (6.734 I_p / 2\pi a^2). \tag{3.34}$$

Then using Eq. (2.44), we get

$$T_{eo} = \left(\frac{6.734 b I_p R Z_{eff}}{V_L a^2} \right)^{2/3} \propto (I_p R Z_{eff} / V_L a^2)^{2/3}. \tag{3.35}$$

By comparing Eqs. (2.46), (3.13), and (3.35), it is apparent that if $j(r)$ and $T_e(r)$ profiles are q_a - dependent, then T_{eo} scales as $T_{eo} \propto (B_T Z_{eff}/V_L)^{2/3}$ for large q_a as a consequence of the principle of profile consistency relation $(r_1/a) \approx (1/q_a)$, while if these profiles are q_a - independent then $T_{eo} \propto (I_p R Z_{eff}/V_L a^2)^{2/3}$, a scaling law that does not depend on the principle of profile consistency. These two types of T_{eo} scaling laws are indeed a consequence of the fact that for q_a-dependent profiles which satisfy the empirical relation $(r_1/a) \approx (1/q_a)$, $F_3(q_a) = (q_a/q_o) \propto q_a$ [i.e., $q_o \approx$ constant] for large q_a; while for q_a-independent profiles $F_3(q_a) = (q_a/q_o) \approx$ constant [i.e., $q_o \propto q_a$] for all q_a and is independent of the condition $(r_1/a) \approx (1/q_a)$. It is our belief that these are the only two fundamental types of T_{eo} scaling laws for all tokamak discharges when $Q \approx Q_{ohm}$ in Eq. (1.2). However, the expression for V_L depends on the type of mode that determines the stable $j(r)$ profile for the plasma column under study. Again in this case following Coppi [3], one can easily show that V_L is roughly given by Eq. (2.47) and (2.52) for the low-density and the high-density regimes, respectively. Hence for the low-density regime

$$T_{eo} \propto I_p^{2/3} \, Z_{eff}^{4/15} \, a^{-2/3} \, m_i^{2/15} \, n_e^{-2/15}, \tag{3.36}$$

and for the high-density regime

$$(T_{eo} - T_{io}) \propto I_p^2 \, m_i \, n_e^{-2} \, a^{-4}. \tag{3.37}$$

It is interesting to note that there is no B_T or R dependence on these T_{eo} scaling laws.

F. q_a- independent chopped exponential fits for T_e (r).

In this model we assume that the profiles are given by

$$T_e(r) = \begin{cases} T_{eo} & \text{for } r \le r_f \\ T_{eo} \exp\{-4(r - r_f)/3a\} & \text{for } r \ge r_f \end{cases}, \tag{3.38}$$

and

$$j(r) = \begin{cases} j_o & \text{for } r \le r_f \\ j_o \exp\{-2(r - r_f)/a\} & \text{for } r \ge r_f \end{cases}. \tag{3.39}$$

Then

$$q(r) = \frac{q_a(r^2/a^2)[(r_f^2/a^2) + (1/4)((1 + 2r_f/a) - 3\exp\{-2(1 - r_f/a)\})]}{[(r_f^2/a^2) + (1/4)((1 + 2r_f/a) - (1 + 2r/a)\exp\{-2(r - r_f)/a\})]}, \tag{3.40}$$

and

$$\langle T_e \rangle / T_{eo} = (9/8)[1 + (4r_f/3a) + (8r_f^2/9a^2) - (7/3)\exp\{-(4/3)(1 - r_f/a)\}]. \tag{3.41}$$

For $r_f = r_1$, $q(r_1) = 1$ yields

$$1/q_a = (r_1^2/a^2) + (1/4)[(1 + 2r_1/a) - 3\exp\{-2(1 - r_1/a)\}] . \qquad (3.42)$$

If $(r_1/a) = (1/q_a)$ is the solution of the Eq. (3.42), then

$$1/q_a = 1/q_a^2 + (1/4)[(1 + 2/q_a) - 3\exp\{-2(1 - 1/q_a)\}] . \qquad (3.43)$$

The graphical solution of Eq. (3.43) is $(1/q_a) \approx 0.32$, i.e., $q_a = 3.125$. Then from Eq. (3.41) we get $\langle T_e\rangle/T_{eo} = 0.647$. However, for $0 \le (r_1/a) = F_1(1/q_a) \neq (1/q_a)$, Eq. (3.42) has solutions for all values of $q_a \le [4/\{1 - 3\exp(-2)\}] \approx 6.7$, and this is shown in curve A of Fig. 9. In this figure the agreement between theory and experiment is good for medium and low values of q_a and is poor for high values of q_a. But the corresponding agreement in curve A of Fig. 10 is terrible. This curve A is obtained from Eq. (3.41) with $r_f = r_1$, where r_1 is given by Eq. (3.42).

IV. MODIFIED EXPONENTIAL PROFILES

In contrast to the exponential profiles of the previous section, the modified exponential profiles to be considered here will have a natural cutoff at a certain value of r/a. Thus, the purpose of this section is primarily to ilustrate the effects of profile truncation on the consistent set of functions F_1, F_2, and F_3.

A. q_a - dependent modified exponential profile fits for $T_e(r,q_a)$.

In this model we will assume the following profile shapes:

$$j(r) = j_o(1 - \alpha_j r/ca)\exp(-\alpha_j r/a), \tag{4.1}$$

and

$$T_e(r) = T_{eo}(1 - \alpha_j r/ca)^{2/3} \exp(-2\alpha_j r/3a). \tag{4.2}$$

Then

$$q(r) = \frac{q_a(r^2/a^2)[\{(\alpha_j^2/c) - (1 + \alpha_j)(1 - 2/c)\}\exp(-\alpha_j) + (1 - 2/c)]}{[\{(\alpha_j^2 r^2/ca^2) - (1 + \alpha_j r/a)(1 - 2/c)\}\exp(-\alpha_j r/a) + (1 - 2/c)]}, \tag{4.3}$$

where

$$q_a = \frac{(B_T\alpha_j^2/\mu_o R j_o)}{\{(\alpha_j^2/c) - (1 + \alpha_j)(1 - 2/c)\}\exp(-\alpha_j) + (1 - 2/c)}, \tag{4.4}$$

and

$$q(o) = (2q_a/\alpha_j^2)[\{(\alpha_j^2/c) - (1 + \alpha_j)(1 - 2/c)\}\exp(-\alpha_j) + (1 - 2/c)]. \tag{4.5}$$

Since it is impossible to obtain a closed analytic form for $\langle T_e \rangle$ of Eq. (4.2), we will approximate this $T_e(r)$ profile as

$$T_e(r) \approx T_{eo}(1 - \alpha_T r/ca)\exp(-\alpha_T r/a), \tag{4.6}$$

where $\alpha_T = (2\alpha_j/3)$. Then

$$\langle T_e \rangle / T_{eo} = (2/\alpha_T^2)[\{(\alpha_T^2/c) - (1 + \alpha_T)(1 - 2/c)\}\exp(-\alpha_T) + (1 - 2/c)]. \tag{4.7}$$

It may be noted that when $c \to \infty$, Eqs. (4.1), (4.2), (4.3), (4.4), (4.5) and (4.7) reduces to the Eqs. (3.2), (3.1), (3.3), (3.4), (3.5) and (3.9), respectively, as they should. It is clear from Eqs. (4.3), (4.4), (4.5), and (4.7) that the simplest case occurs for $c = 2$. For this simplest case

$$j(r) = j_o(1 - \alpha_j r/2a)\exp(-\alpha_j r/a). \tag{4.8}$$

From Eq. (4.5) for $c = 2$ we get

$$q(0) = q_a \exp(-\alpha_j). \tag{4.9}$$

For sawtoothing discharges $q(0) \leq 1$, and hence $\alpha_j > \log q_a$. From Eq. (4.3)

$$q(r) = q_a \exp\{-\alpha_j(1 - r/a)\}. \tag{4.10}$$

If $(r_1/a) = (1/q_a)$ is the solution of $q(r) = 1$, then

$$\alpha_j = \log q_a/(1 - 1/q_a). \tag{4.11}$$

Then from Eq. (4.7)

$$\langle T_e\rangle/T_{eo} = \exp(-\alpha_T) = \exp(-2\alpha_j/3). \tag{4.12}$$

Here again it is found that the agreement between $[\langle T_e\rangle/T_{eo}]_{EXP}$ and $[\langle T_e\rangle/T_{eo}]_{TH}$ is very poor.

B. q_a - independent modified exponential profile fits for $T_e(r)$.

In this model we will examine the following two cases: case 1, $c = 2$ and $\alpha_j \neq \alpha_j(q_a) = 2$, and case 2, $(\alpha_j/c) = 0.95$ and $\alpha_j \neq \alpha_j(q_a) = 2$ in Eq. (4.1). In the literature, the second case with a flattened core has been considered by Fredrickson et al. [8].

Case 1: $c = \alpha_j = 2$ in Eq. (4.1).

That is

$$j(r) = j_o(1 - r/a)\exp(-2r/a). \tag{4.13}$$

If $(r_1/a) = (1/q_a)$ is the solution of $q\ (r_1) = 1$, then from Eq. (4.11) we get

$$\log q_a = 2(1 - 1/q_a). \tag{4.14}$$

The graphical solution of Eq. (4.14) is $(1/q_a) = 0.203$, i.e., $q_a \approx 4.92$ and from Eq. (4.7), $\langle T_e\rangle/T_{eo} \approx e^{-2} \approx 0.135$. These results are, of course, in complete disagreement with the existing experimental measurements [1,25,53]. In particular, for example, the temperature profile peakedness $T_{eo}/\langle T_e \rangle$ is not a function of q_a.

Case 2: $\alpha_j = 2$ and $(\alpha_j/c) = 0.95$ in Eq. (4.1).

That is

$$j(r) = j_o(1 - 0.95r/a)\exp(-2r/a). \tag{4.15}$$

Then from Eq. (4.3) we get

$$q(r) \approx \frac{5.736q_a(r^2/a^2)}{[1 + \{38\ (r^2/a^2) - 2(r/a) - 1\}\exp(-2r/a)]}, \tag{4.16}$$

and from Eq. (4.5) we get

$$q(0) \approx 0.1434q_a = q_a/6.973. \tag{4.17}$$

For sawtoothing discharges $q(o) \le 1$ and hence $q_a \le 6.973$. Now $q(r_1) = 1$ implies that

$$[1 - 5.736q_a\ (r_1^2/a^2)] = [1 + 2\ (r_1/a)$$

$$- 38(r_1^2/a^2)]\exp(-2r_1/a). \tag{4.18}$$

If $(r_1/a) = (1/q_a)$ is the solution of the Eq. (4.18), then

$$1/q_a = (1/2)\ \log[(1 + 2/q_a - 38/q_a^2)/(1 - 5.736/q_a)]. \tag{4.19}$$

The graphical solution of Eq. (4.19) yields $(1/q_a) = 0$, or $(1/q_a) \approx 0.222$, i.e., $q_a = \infty$ or $q_a \approx 4.505$. Since for sawtoothing discharges $q_a \lesssim 6.973$, the only physically meaningful solution of Eq. (4.19) is $q_a \approx 4.505$. Setting $\alpha_j = 2$ in Eq. (4.12), we find that $\langle T_e \rangle / T_{eo} = \exp(-4/3) \approx 0.264$. Again these results are in complete disagreement with the existing experimental measurements [1,25,53]. In particular, neither the sawtooth inversion radius nor the temperature profile peakedness is a function of the limiter safety factor [i.e., $F_1 \neq F_1(1/q_a)$ and $F_2 \neq F_2(1/q_a)$ for any finite range of values of q_a]. It may be noted that in general F_1, F_2, and F_3 cannot be functions of q_a for any q_a-independent profile.

C. T_{eo} scaling from q_a-dependent modified exponential profile.

Here we will only consider the simplest case of $c = 2$ in Eqs. (4.1) and (4.2). For $(r_1/a) \approx 1/q_a$, one can show from Eqs. (1.12), (4.5), and (4.11) that

$$F_3(q_a) = (q_a/q_o) = \exp[\log q_a/(1 - 1/q_a)] = q_a^{1/(1 - 1/q_a)}$$

$$\approx q_a \text{ for } q_a \gg 1. \tag{4.20}$$

Using Eq. (4.2) [with $c = 2$] in Eq. (1.2) we get for the low-density regime

$$\chi_e(r) \approx \left(\frac{3c^2 q_o \Omega_{\theta e}}{4\pi \omega_{pe}^2 q_a}\right) \left[\frac{eV_L (1 - \alpha_j r/2a)}{(\alpha_j q_o/q_a)\, T_e(r)} \quad \frac{a}{R}\right] , \tag{4.21}$$

where

$$(\alpha_j\, q_o/q_a) = \alpha_j \exp(-\alpha_j) = [\log q_a/(1 - 1/q_a)]\, q_a^{-1/(1 - 1/q_a)}$$

$$\approx q_a^{-1} \log q_a \text{ for } q_a \gg 1. \qquad (4.22)$$

Following Coppi [3] and associating $\chi_e(r)$ with the presence of resistive reconnecting modes that allow for stable $j(r)$ profile, one can show from dimensional analysis arguments that

$$V_L \propto (\alpha_j q_o/q_a)(RZ_{eff}^{3/5} \dot{n}_e^{1/5}/am_i^{1/5}). \qquad (4.23)$$

Hence from Eqs. (1.14), (4.20), (4.22), and (4.23), it follows that the scaling law in the low-density regime is

$$T_{eo} \propto \alpha_j^{-1} \exp(2\alpha_j)\;\; I_p\, m_i^{1/5}\, Z_{eff}^{2/5}\, a^{-1}\, n_e^{-1/5}$$

$$\approx (B_T^{4/3}\, a^2\, Z_{eff}^{4/15}\, m_i^{2/15}\, n_e^{-2/15}\, R^{-4/3}\, I_p^{-2/3})$$

$$[\log(2\pi a^2 B_T/\mu_o R I_p)]^{-2/3} \qquad (4.24)$$

for $q_a \gg 1$.

In the high-density regime V_L is again given by Eq. (2.52). From Eqs. (4.20) and (2.52) one can easily show that the high-density regime scaling law for large q_a is again given by Eq. (2.53).

D. T_{eo} scaling from q_a-independent modified exponential profiles.

Here again we will examine the following two cases: Case 1, $\alpha_j = c = 2$, and Case 2, $\alpha = 2$ and $(\alpha_j/c) = 0.95$ in Eqs. (4.1) and (4.2). From Eqs.

(1.12), (4.9), and (4.17) we get

$$F_3(q_a) = (q_a/q_o) = \text{constant} \approx \begin{cases} 7.389 \text{ for Case 1} \\ 6.973 \text{ for Case 2} \end{cases} \qquad (4.25)$$

and is independent of the condition $(r_1/a) \approx (1/q_a)$. That is, for q_a-independent profiles $q_o \propto q_a$ for all values of q_a; while for q_a-dependent profiles $q_o \approx$ constant for large q_a when $(r_1/a) \approx 1/q_a$ [see Figs. 15a and 15b]. Again in these cases following Coppi [3] one can easily show that V_L is roughly given by Eqs. (2.47) and (2.52) for the low-density and the high-density regimes, respectively. Hence for the low and high density regimes the T_{eo} scaling law is given by Eqs. (3.32) and (3.33), respectively.

E. Fredrickson <u>et al.</u> model.

In this model the profile shapes are:

$$j(r) = \begin{cases} j_o & \text{for } r \le r_f \\ j_o[(1 - 0.95\, r/a)/(1 - 0.95\, r_f/a)]\exp\{-2(r - r_f)/a\} & \text{for } r \ge r_f \end{cases} \qquad (4.26)$$

and

$$T_e(r) = \begin{cases} T_{eo} & \text{for } r \le r_f \\ T_{eo}[(1 - 0.95\, r/a)/(1 - 0.95\, r_f/a)]^{2/3} \exp\{-4(r - r_f)/3a\} & \text{for } r \ge r_f \end{cases} \qquad (4.27)$$

where we have assumed Spitzer resistivity and thus $j \propto T_e^{3/2}$. This model is a special case of the q_a-independent chopped modified exponential profiles. Here we will only consider the case where $r_f = r_1$. That is, we will assume that the profiles are flat up to the sawtooth inversion radius. Then from Eq.(4.26) one can show that $q(r_1) = 1$ yields

$$(1/q_a) = (r_1{}^2/a^2) + (1/40)(1 - 0.95\ r_1/a)^{-1} \quad [35 \exp\{-2(1 - r_1/a)\}$$
$$- \{ 38\ r_1{}^2/a^2 - 2\ r_1/a - 1\}]. \qquad (4.28)$$

If we now demand that $(r_1/a) = F_1(1/q_a) = (1/q_a)$, then Eq. (4.28) has a solution for only one value of q_a, namely for $q_a = 1$. However, for $0 \le (r_1/a) = F_1(1/q_a) \ne (1/q_a)$, Eq. (4.28) has solutions for all values of $q_a \le [40/\{35 \exp(-2) + 1\}] \approx 7$ and this is shown in curve B of Fig. 9. In this figure the agreement between theory and experiment is good for medium and low values of q_a and is poor for high values of q_a. Indeed for $q_a > 7$, $(r_1/a) < 0$. Hence, tokamak discharges with this model profile cannot be sawtoothing for values of $q_a > 7$. It should be noted that the critical value of $q_a \approx 7$ below which the discharges are sawtoothing and above which the discharges are nonsawtoothing in this model is only true for $r_f = r_1$. If r_f is different from r_1, then this critical value of q_a will also be different from 7.

Since Eq. (4.27) contains powers of r that are nonintegers, it is impossible to obtain a closed analytic form for $\langle T_e \rangle$ of Eq. (4.27). For $r \ll a$, $(1 - 0.95\ r/a)^{2/3} \approx (1 - 0.63\ r/a)$. Thus for the sake of analytical simplicity we will approximate $[(1 - 0.95\ r/a)/(1 - 0.95\ r_f/a)]^{2/3}$ in Eq. (4.27) by $[(1 - cr/a)/(1 - cr_f/a)]$, where $0.63 < c \approx (0.63 + 0.95)/2 \approx 0.8 < 0.95$. As we will see later, choosing this mean value of $c \approx 0.8$ is not a bad approximation for the range of q_a values studied in Figs. 9 and 10. With this approximation, one can show from Eqs. (4.27) and (1.11) that

$$\langle T_e\rangle/T_{eo} = (r_f^2/a^2) + (9/8)(1 - cr_f/a)^{-1} [(4.833c - 2.333)$$
$$\exp\{-(4/3)(1 - r_f/a)\} - c\{(4/3)(r_f/a)^2 + 2(r_f/a) + 1.5\} + (4/3)(r_f/a) + 1], \tag{4.29}$$

where for our purposes $r_f = r_1$ and (r_1/a) is given by Eq. (4.28). This self-consistent theoretical prediction of Eqs. (4.29) and (4.28) is shown in curve B of Fig. 10 for $c = 0.8$. In this figure the agreement between the theory and experiment is indeed remarkable. For a given q_a, the higher (or lower) values of c in Eq. (4.29) tend to lower (or raise) the predicted values of $\langle T_e\rangle/T_{eo}$ (by approximately equal amounts). For example, for $c = 0.95$ (or $c = 0.63$) one gets a parallel curve displaced downwards (or upwards) from that for $c = 0.8$ by approximately 0.05 along the $\langle T_e\rangle/T_{eo}$ axis. Thus, from Figs. 9 and 10 in conjunction with the earlier $T_e(r)$ profile - fit studies of Fredrickson et al. [8], it is apparent that these chopped modified exponential profiles are in good overall agreement with the existing TFTR data. It is interesting to note from Eqs. (4.12), (4.28), and (4.29) that by chopping a q_a-independent profile such that $r_f \approx r_1$, one ends up with a q_a-dependent profile. That is, for a q_a-independent profile the inverse of the temperature profile peakedness $\langle T_e\rangle/T_{eo} \neq F_2(1/q_a)$, while the same profile when chopped up to the sawtooth inversion radius yields $\langle T_e\rangle/T_{eo} = F_2(1/q_a)$ via the relation $(r_1/a) = F_1(1/q_a) \neq (1/q_a)$.

V. TRAPEZOIDAL FITS FOR $T_e(r)$.

In this model we take the profiles to be given by

$$T_e(r) = \begin{cases} T_{eo} & \text{for } r \le r_f \\ T_{eo}\,[(1 - r/a)/(1 - r_f/a)] & \text{for } r \ge r_f\,, \end{cases} \tag{5.1}$$

and

$$j(r) = \begin{cases} j_o & \text{for } r \le r_f \\ j_o\,[(1 - r/a)/(1 - r_f/a)]^{3/2} & \text{for } r \ge r_f \,, \end{cases} \qquad (5.2)$$

Then

$$q(r) = q_a(r^2/35a^2)[8 + 12(r_f/a) + 15(r_f/a)^2][(r_f/a)^2 + (4/7)(1 - r_f/a)^{-3/2}$$

$$\{(1 - r/a)^{7/2} - (1 - r_f/a)^{7/2}\} - (4/5)(1 - r_f/a)^{-3/2}\,\{(1 - r/a)^{5/2} - (1 - r_f/a)^{5/2}\}]^{-1}, \qquad (5.3)$$

where

$$q_a = \frac{(2B_T/\mu_o R j_o)}{[(8/35) + (12/35)(r_f/a) + (3/7)(r_f/a)^2]}\,, \qquad (5.4)$$

and

$$q(o) = (2B_T/\mu_o R j_o). \qquad (5.5)$$

If the flat region of the profile $r_f = r_1$, then from Eq. (5.3) $q(r_1) = 1$ yields

$$(1/q_a) = (8/35) + (12/35)(r_1/a) + (3/7)(r_1/a)^2. \qquad (5.6)$$

It may be noted that for $r_f = r_1$, $q(0) = 1$ and hence Eq. (5.6) also follows trivially from Eqs. (5.4) and (5.5). Equation (5.6) can easily be rewritten as

$$[(r_1/a) + (2/5)]^2 = (7/3)[(1/q_a) - (4/25)]. \tag{5.7}$$

This is the equation for a parabola with the vortex $1/q_a = 4/25 = 0.16$ and $r_1/a = -2/5 = -0.4$ and this is shown in curve C of Fig. 9. If we demand that $r_1/a = 1/q_a$ is the solution of Eq. (5.6), then $1/q_a = 1$ or $(16/30) = 0.533$. From Eq. (5.1) we get

$$\langle T_e\rangle/T_{eo} = (1/3)[1 + (r_f/a) + (r_f/a)^2]. \tag{5.8}$$

For $r_f = r_1$

$$\langle T_e\rangle/T_{eo} = (1/3)[1 + (r_1/a) + r_1/a)^2]$$

$$= (1/9) + (35/36)(1/q_a) - (1/12)(r_1/a)^2, \tag{5.9}$$

where we have made use of Eq. (5.6). If we neglect the $(1/12)(r_1/a)^2$ in Eq. (5.9), this is the equation for a straight line with a slope $(35/36) = 0.972$ and intercept on the $[\langle T_e\rangle/T_{eo}]$ axis of $(1/9) = 0.111$. We have illustrated this in curve C of Fig. 10. In this figure the agreement between the theory and experiment is indeed remarkable for medium and low values of q_a. However, the corresponding agreement in Fig. 9 is poor for high and medium values of q_a, and is fair for low values of q_a. The trapezoidal fits to the experimentally measured $T_e(r)$ profiles are very good for low q_a - discharges and are poor for the high q_a - discharges. Indeed it is interesting to note from Figs. 6a, 9, and 10 that the trapezoidal profile is an "ideal limit profile" for very low values of q_a [i.e., for $q_a < 3$] in agreement with the experimental observations of Boyd and Stauffer [7]. It is clear from Eqs. (5.6) or (5.7) that $(r_i/a) \geq 0$ only when $(1/q_a) \geq (8/35)$, i.e., only when $q_a \leq (35/8) \approx 4.4$. Hence, tokamak discharges with trapezoidal profiles cannot be sawtoothing for $q_a > 4.4$. It may be noted that this critical value of $q_a = 4.4$ for the trapezoidal model is much less than the corresponding value of $q_a \approx 7$ for the Fredrickson et al. model of Sec. IVE. Finally, since in this model the current is automatically truncated at $r = a$, no current flows outside the limiter.

VI. KADOMTSEV MODEL

A. Kadomtsev optimal profile fits for $T_e(r, q_a)$.

Kadomtsev [9-11] argues that the optimal profiles with respect to perturbations of the tearing mode type are the ones that satisfy the variational minimum energy principle for the total energy with the current conservation constraint. If we assume that the toroidal coils fix the longitudinal flux and hence the longitudinal magnetic field energy remains unchanged, then the integral

$$F = \int dr\ 2\pi r\ [(B_\theta^2/8\pi) + (p/(\gamma - 1)) + \lambda j] \qquad (6.1)$$

is a minimum for the correct flux function $\Psi(r)$ where $(d\Psi/dr) = B_\theta(r)$, λ is the Lagrange undetermined multiplier, and γ is the adiabatic index. The current conservation constraint is a consequence of the indestructibility of the magnetic configuration far from the islands [i.e., far from the singular points of $\mu = 1/q = n/m$]. Let $\dot{\Psi} = (d\Psi/dr^2) = (1/2r)\ (d\Psi/dr) = (B_\theta/2r) = (B_T/2R)\{1/q(r)\} = (B_T/2R)\mu(r)$; then from Eq. (6.1), the variational minimum energy principle yields that

$$\delta F = \int dr^2\, \delta\Psi\, [\frac{\partial f}{\partial\Psi} - \frac{d}{dr^2}\, \frac{\partial f}{\partial\dot{\Psi}}] = 0\ , \tag{6.2}$$

where

$$f[r^2,\ \Psi(r^2),\ \dot{\Psi}] = [(1/2)\ r^2\ \dot{\Psi}^2 + \{\pi p/(\gamma - 1)\} + \pi\lambda j]. \tag{6.3}$$

Hence, the optimal profiles must satisfy

$$\frac{\partial f}{\partial\Psi} - \frac{d}{dr^2}\, \frac{\partial f}{\partial\dot{\Psi}} = 0. \tag{6.4}$$

If we now assume that p and j are not explicit functions of Ψ [i.e., $(\partial f/\partial\Psi) = 0$] and since $\dot{\Psi} = (B_T/2R)\mu$, Eq. (6.4) yields that the optimal profiles must then satisfy

$$[r^2\mu + (4R^2/B_T)\{(\pi/\gamma - 1)(\partial p/\partial\mu) + \pi\lambda\ (\partial j/\partial\mu)\}] = \text{constant}. \tag{6.5}$$

The simplest choice that will satisfy Eq. (6.5) is $(\partial p/\partial\mu) \propto \mu$ and $(\partial j/\partial\mu) \propto \mu$. That is, $p = p_o'\mu^2$ and $j = j_o'\mu^2$. Then from Eq. (6.5) we get

$$\mu(r) = \frac{(\text{constant}/a_*^2)}{[1 + r^2/a_*^2]} = \frac{1}{q(r)}\ , \tag{6.6}$$

where

$$a_*^2 = (8\pi R^2/B_T^2)[(p_o'/\gamma - 1) + \lambda\ j_o']. \tag{6.7}$$

From Eq. (6.6) we get

$$(1/q_a) = (\text{constant}/a_*^2)/[1 + a^2/a_*^2],$$

and

$$\mu(r) = [1/q(r)] = [(1 + a^2/a_*^2)/(1 + r^2/a_*^2)](1/q_a). \qquad (6.8)$$

From Eq. (6.8)

$$q(o) = q_a/(1 + a^2/a_*^2). \qquad (6.9)$$

Hence, Kadomtsev optimal profiles are:

$$j(r) = j_o/(1 + r^2/a_*^2)^2 , \qquad (6.10)$$

and

$$p(r) \propto n_e(r)\ T_e(r) = p_o/(1 + r^2/a_*^2)^2. \qquad (6.11)$$

It may be noted from Eqs. (6.10) and (6.11) that if $j \propto T_e^{3/2}$, then $n_e \propto T_e^{1/2}$ [11].

Now from Eq. (6.10) and Biöt and Savart's law, it is relatively easy to show that

$$q(r) = q_a(1 + r^2/a_*^2)/(1 + a^2/a_*^2), \qquad (6.12)$$

where

$$q_a = (2B_T/\mu_o R j_o)(1 + a^2/a_*^2). \qquad (6.13)$$

If we now demand that $(r_1/a) = (1/q_a)$ is the solution of the equation $q(r_1) = 1$, then from Eq. (6.12) we get

$$(a_*^2/a^2) = (1/q_a) \text{ for } q_a \neq 1. \tag{6.14}$$

Hence, the Kadomtsev optimal profiles that satisfy the principle of profile consistency relation $(r_1/a) = (1/q_a)$ are [9,10]

$$j(r) = [j_o/(1 + r^2/a_*^2)^2] = [j_o/(1 + q_a r^2/a^2)^2], \tag{6.15}$$

and

$$T_e(r) = [T_{eo}/(1 + r^2/a_*^2)^{4/3}] = [T_{eo}/(1 + q_a r^2/a^2)^{4/3}], \tag{6.16}$$

where we have assumed that $j \propto T_e^{3/2}$. Then,

$$\langle T_e\rangle/T_{eo} = (3/q_a)[1 - 1/(q_a + 1)^{1/3}]. \tag{6.17}$$

These are also the same profiles given by Biskamp [10]. This $T_e(r)$ profile of Eq. (6.16) gives a fairly reasonable fit for high q_a - discharges, but yields a very poor fit to the low q_a - discharges, particularly for larger values of (r/a). This is tied to the fact that this Kadomtsev model allows an appreciable fraction of the total plasma current to flow outside the limiter for low q_a - discharges. Indeed, we show in the Appendix that this fraction is given by

$$[I_p(a \text{ to } \infty)/I_p(o \text{ to } \infty)] = [1 + a^2/a_*^2]^{-1} = (1 + q_a)^{-1} \tag{6.18}$$

for $(r_1/a) = (1/q_a)$. In Fig. 11a we show a comparison between $[\langle T_e\rangle/T_{eo}]_{EXP}$ and the corresponding $[\langle T_e\rangle/T_{eo}]_{TH}$. It appears that the relationship between the experimental measurements and the theoretical predictions of the Kadomtsev model is $[\langle T_e\rangle/T_{eo}]_{EXP} = [\langle T_e\rangle/T_{eo}]_{TH} + 0.05$. This result is exactly the same as that of the Coppi-Tang model of Fig. 3a.

B. Chopped Kadomtsev Model.

In this model we take

$$j(r) = \begin{cases} j_o & \text{for } r \le r_f \\ j_o[(1 + r_f^2/a_*^2)/(1 + r^2/a_*^2)]^2 & \text{for } r \ge r_f \ , \end{cases} \tag{6.19}$$

and

$$T_e(r) = \begin{matrix} T_{eo} & \text{for } r \le r_f \\ T_{eo}[(1 + r_f^2/a_*^2)/(1 + r^2/a_*^2)]^{4/3} & \text{for } r \ge r_f \ . \end{matrix} \tag{6.20}$$

Here, the profiles are flat up to some radius $r_f \le r_1$, and is of the Kadomtsev type for $r \ge r_f$. Then

$$q(r) = \frac{q_a(r^2/a^2)[\ (r_f^2/a_*^2) + \{(1 + r_f^2/a_*^2)(a^2 - r_f^2)/(a^2 + a_*^2)\}]}{[(r_f^2/a_*^2) + \{(1 + r_f^2/a_*^2)(r^2 - r_f^2)/(r^2 + a_*^2)\}]} \ , \tag{6.21}$$

where

$$q_a = \frac{(2B_T/\mu_o R j_o)(a^2/a_*^2)}{[(r_f^2/a_*^2) + \{(1 + r_f^2/a_*^2)(a^2 - r_f^2)/(a^2 + a_*^2)\}]} \ . \tag{6.22}$$

If $r_f = r_1$ and $(r_1/a) = (1/q_a)$ is the solution of the equation $q(r_1) = 1$, then

$$(a_*^2/a^2) = (1/q_a)[\{1 - (2/q_a) + (1/q_a^3)\}/(1 - 1/q_a)]. \tag{6.23}$$

From Eq. (6.20) we get

$$\langle T_e\rangle/T_{eo} = (r_f^2/a^2) + (3a_*^2/a^2)[(1 + r_f^2/a_*^2)$$

$$- \{(1 + r_f^2/a_*^2)^{4/3}/(1 + a^2/a_*^2)^{1/3}\}]. \qquad (6.24)$$

For $(r_f/a) = (r_1/a) = (1/q_a)$, Eq. (6.24) becomes

$$\langle T_e\rangle/T_{eo} = (1/q_a^2) + (3a_*^2/a^2)[1 + (1/q_a^2)(a^2/a_*^2),$$

$$- \frac{\{1 + (1/q_a^2)(a^2/a_*^2)\}^{4/3}}{(1 + a^2/a_*^2)^{1/3}}], \qquad (6.25)$$

where (a_*^2/a^2) is given by Eq. (6.23). In Fig. 11b we have shown a comparison of $[\langle T_e\rangle/T_{eo}]_{EXP}$ vs $[\langle T_e\rangle/T_{eo}]_{TH}$ of Eqs. (6.25) and (6.23) for the same set of data as in Fig. 3. Here, the agreement between theory and experiment is better than that of Fig. 11a.

C. T_{eo} scaling from Kadomtsev optimal profiles.

For $(r_1/a) \approx 1/q_a$, it can be shown from Eqs. (1.12), (6.9), and (6.14) that the function $F_3(q_a)$ is

$$F_3(q_a) = (q_a/q_o) = q_a + 1. \qquad (6.26)$$

Using Eq. (6.26) in Eq. (1.14) we get

$$T_{eo} = (4\pi b/\mu_o)^{2/3}(B_T Z_{eff}/V_L)^{2/3}[1 + (\mu_o R I_p/2\pi a^2 B_T)]^{2/3}. \qquad (6.27)$$

For $q_a = (2\pi a^2 B_T/\mu_o R I_p) \gg 1$, Eq. (6.27) yields the approximate form of the scaling law as $T_{eo} \propto (B_T Z_{eff}/V_L)^{2/3}$. Then for the low-density regime neglecting the Q_{ei} term in the electron thermal energy balance Eq. (1.2) and making use of Eq. (6.16) we get

$$\chi_e(r) \approx \left(\frac{3c^2 a q_o \Omega_{\theta e}}{16\pi\omega_{pe}^2 r q_a}\right) \left[\frac{eV_L(1 + q_a r^2/a^2)}{q_o T_e(r)} \frac{a}{R}\right] . \tag{6.28}$$

Since $q_o = [q_a/(q_a + 1)] \approx 1$ for $q_a \gg 1$, following Coppi [3] one can show from Eq. (6.28) that the T_{eo} scaling law in the low-density regime for large values of q_a is again given by Eq. (2.48). Also, for large values of q_a it can easily be seen from Eq. (6.27) and (2.52) that the T_{eo} scaling law in the high-density regime is again given by Eq. (2.53). That is, the Kadomtsev model yields the same T_{eo} scaling law as that of the Coppi-Tang model for both the low-and high-density regimes.

VII. CAMPBELL et al. MODEL

A. Fits for $T_e(r,q_a)$ used by Campbell et al. of the JET group.

Campbell et al. of the JET group [13] have claimed that the theoretical predictions of the behavior of tokamak discharges based on a simplified current profile of the form $j(r) = j_o\,[1 - r^2/a^2]^\nu$, where $\nu = [(q_a/q(0)) - 1]$ is in remarkable agreement with their experimental observations in JET. This model was used earlier by Wesson [12] to examine the various MHD instability regimes in tokamaks. Here, we will generalize this model and take the profiles as given by

$$T_e(r) = T_{eo}[1 - r^2/a^2]^{\nu_T}, \tag{7.1}$$

and

$$j(r) = j_o[1 - r^2/a^2]^{\nu_j}, \tag{7.2}$$

where by Ohm's law $\nu_T = (2\nu_j/3)$. Then

$$q(r) = q_a(r^2/a^2)/[1 - (1 - r^2/a^2)^{\nu_j+1}], \tag{7.3}$$

where

$$q_a = (2B_T/\mu_o R j_o)(\nu_j + 1). \tag{7.4}$$

From Eq. (7.3)

$$q(0) = q_a/(\nu_j + 1), \tag{7.5}$$

i.e., $[\nu_j = (q_a/q(0)) - 1]$ in complete agreement with Campbell et al. If we demand that $(r_1/a) = (1/q_a)$ is the solution of $q(r_1) = 1$, then

$$(\nu_j + 1) = \log(1 - 1/q_a)/\log(1 - 1/q_a^2). \tag{7.6}$$

It may be noted from Eq. (7.6) that for $q_a >> 1$, $\nu_j = (q_a - 0.5)$.
From Eq. (7.1) we get

$$\langle T_e\rangle/T_{eo} = (\nu_T + 1)^{-1} = [(2/3)(\nu_j + 1) + (1/3)]^{-1}, \tag{7.7}$$

where $(\nu_j + 1)$ is given by Eq. (7.6).

In Figs. (12a) and (12b) we show a comparison between the experimentally measured $T_e(r)$ profiles and the corresponding theoretically predicted ones from Eqs. (7.1) and (7.6) for low q_a ($\approx$2.9), and high q_a (= 6.2) discharges, respectively. Here, the agreement between theory and experiment for $T_e(r)$ profiles is better than that of the Kadomtsev model and is somewhat similar to that of the Coppi-Tang model for both the low and high q_a - discharges. This is tied to the fact that these profiles have an automatic cut-off at r = a, and thus no current flows outside the limiter. In Fig. 13a we show a comparison between $[\langle T_e\rangle/T_{eo}]_{EXP}$ and the corresponding $[\langle T_e\rangle/T_{eo}]_{TH}$ for the same set of data as in Fig. 3. It appears that the relationship between the experimental measurements and the theoretical predictions of the Campbell et al. model is $[\langle T_e\rangle/T_{eo}]_{EXP} = [\langle T_e\rangle/T_{eo}]_{TH} + 0.05$. It is indeed remarkable that this result is identical to that of both the Coppi-Tang model of Fig. 3a and the Kadomtsev model of Fig. 11a. It is not very clear to us what intrinsic connection exists among these three models [i.e., the Coppi-Tang, Kadomtsev, and Campbell et al. models] that leads to the same relationship of $[\langle T_e\rangle/T_{eo}]_{EXP} = [\langle T_e\rangle/T_{eo}]_{TH} + 0.05$ for all these three models.

B. Chopped Campbell et al. Model.

In this model we will take the profiles as flat up to some radius $r_f \le r_1$, and is of the Campbell et al. type for $r \ge r_f$.
That is, the profiles are:

$$T_e(r) = \begin{cases} T_{eo} & \text{for } r \le r_f \\ T_{eo}\,[(1 - r^2/a^2)/(1 - r_f^2/a^2)]^{\nu_T} & \text{for } r \ge r_f\,, \end{cases} \tag{7.8}$$

and

$$j(r) = \begin{cases} j_o & \text{for } r \le r_f \\ j_o\,[(1 - r^2/a^2)/(1 - r_f^2/a^2)]^{\nu_J} & \text{for } r \ge r_f\,, \end{cases} \tag{7.9}$$

where $\nu_T = (2\,\nu_J/3)$ by Ohm's law. Then

$$q(r) = \frac{q_a(r^2/a^2)[(r_f^2/a^2) + (1-r_f^2/a^2)/(\nu_j+1)]}{[(r_f^2/a^2) + (1-r_f^2/a^2)/(\nu_j+1) - \{(1-r^2/a^2)^{\nu_j+1}/(1-r_f^2/a^2)^{\nu_j}(\nu_j+1)\}]} \tag{7.10}$$

where

$$q_a = (2B_T/\mu_o R j_o)/[(r_f^2/a^2) + (1 - r_f^2/a^2)/(\nu_j + 1)] \tag{7.11}$$

For $r_f = r_1$ and if $(r_1/a) = (1/q_a)$ is the solution of the equation $q(r_1) = 1$, then we get

$$\nu_j = q_a \text{ for } q_a \neq 1. \tag{7.12}$$

From Eq. (7.8) we get

$$\langle T_e \rangle / T_{eo} = [(r_f^2/a^2) + (1 - r_f^2/a^2)/(\nu_T + 1)]. \tag{7.13}$$

Then for $(r_f/a) = (r_1/a) = (1/q_a)$, Eq. (7.13) becomes

$$\langle T_e \rangle / T_{eo} = [(1/q_a^2) + \{1 - 1/q_a^2\}/\{1 + (2q_a/3)\}]. \tag{7.14}$$

Here the agreement between theory and experiment for $T_e(r)$ profiles is somewhat better for low q_a - discharges than those for the high q_a - discharges and is fair for all discharges. In Fig. 13b we show a comparison of $[\langle T_e \rangle / T_{eo}]_{EXP}$ vs $[\langle T_e \rangle / T_{eo}]_{TH}$ of Eq. (7.14) for the same set of data as in Fig. 3. The agreement between theory and experiment is rather poor for $q_a > 4$ and is somewhat reasonable for $q_a < 4$.

C. T_{eo} scaling from Campbell et al. Model

For $(r_1/a) \approx 1/q_a$ one can show from Eqs. (1.12), (7.5), and (7.6) that

$$F_3(q_a) = (q_a/q_o) = [\log(1 - 1/q_a)/\log(1 - 1/q_a^2)]$$

$$\approx (q_a + 0.5) \text{ for } q_a \gg 1. \tag{7.15}$$

From Eqs. (1.14) and (7.15) one finds that T_{eo} is given by Eq. (2.45) which for large q_a reduces to Eq. (2.46). Using Eq. (7.1) in Eq. (1.2) we get for the low-density regime

$$\chi_e(r) \approx \left(\frac{3c^2 a q_o \Omega_{\theta e}}{8\pi\omega_{pe}^2 r q_a}\right) \left[\frac{eV_L(\nu_j + 1)(1 - r^2/a^2)}{\nu_j T_e(r)} \frac{a}{R}\right]. \tag{7.16}$$

Since from Eq. (7.6), $[(\nu_j + 1)/\nu_j] \approx [(q_a + 0.5)/(q_a - 0.5)] \approx (1 + 1/q_a) \approx 1$ for $q_a \gg 1$, we find that V_L is given by Eq. (2.47). Thus, here again we find that the Campbell et al. model yields the same T_{eo} scaling law as that of the Coppi-Tang model for both the low [Eq. (2.48)] and the high [Eq. (2.53)] density regimes.

VIII. PROFILE CONSISTENCY AND THE UNIVERSALITY OF PROFILES IN THE REDUCED COORDINATES

Recently, Soltwisch et al. [41] have measured the current density j(r) and, hence, the safety factor q(r) profiles by the Faraday rotation method in the Textor tokamak (to about 15% accuracy at the center). Also West et al. [42] have measured the axial safety factor q_o in the Texas Experimental Tokamak by the use of laser-induced fluorescence of an injected Li° beam. Their experimental results show that for sawtoothing discharges $q_o < 1$, and when the sawtooth phenomenon is not observed, q_o is measured to be above one and when q_a is raised, q_o also increases. We have also shown their measurements of q_o vs q_a in Fig. 15a.

Further, Soltwisch et al. have observed that in stationary conditions in sawtoothing discharges, current density and q-profiles assume a unique shape. They find that this can be expressed in reduced coordinates (depending only on the "external" tokamak parameters R, B_T, and I_p) as a result of the critical effect of the m = 1 tearing mode on transport: $[j/(B_T/\mu_o R)]$, $[r/(\mu_o R I_p/B_T)^{1/2}]$. It is physically instructive to note that $(B_T/\mu_o R) = (I_p/\pi a^2)q_a = q_o j_o$ [see Eq. (1.12)] and $(\mu_o R I_p/B_T) = (2\pi a^2/q_a)$. Hence the reduced coordinates of Soltwisch et al. are $[j/q_o j_o]$ and $[r/a_{eff}]$ where $a_{eff}^2 = (2\pi a^2/q_a)$. That is, their empirical observation of the universality of the current profiles imply that the normalized current profiles are functions of $r/a_{eff} = (r\, q_a^{1/2}/a)$ [11,41].

One can show that all the q_a-dependent profiles considered in this paper except the ones used by Campbell et al. [see Eq. (7.2)] will lead to the universality of profiles in some reduced coordinates (j/j_o) and (r/a_{eff}) where (a_{eff}/a) is some function of $q_a^{-1/2}$. For example, it is apparent from Eq. (2.2) that if we plot $[j(r)/j_o]$ vs (r/a_{eff}) where $a_{eff}^2 = (a^2/\alpha_j)$ we will obtain a universal Coppi-Tang diffusive profile. Here it follows from Eqs. (2.5) and (2.7) that the reduced coordinates j_o and a_{eff} are given by

$$j_o = (2B_T/\mu_o R q_o), \tag{8.1}$$

and

$$a_{eff}^2 = (a^2/\alpha_j) = a^2(q_o/q_a)[1 - \exp(-\alpha_j] \approx a^2(q_o/q_a)$$

$$= (q_o \mu_o R I_p / 2\pi B_T), \tag{8.2}$$

respectively, since for sawtoothing discharges $q_o < 1$ implies that $\alpha_j > q_a$ which in turn yields that $[1 - \exp(-\alpha_j)] \approx 1$ for large q_a. Now if the sawtooth inversion radius r_1 satisfies the empirical principle of profile consistency relation $(r_1/a) \approx 1/q_a$, then $\alpha_j \approx \alpha_j^{(0)} \approx q_a + 0.5$ [see Eq. (2.12)]. Hence $q_o \approx (q_a/\alpha_j) \approx [q_a/(q_a + 0.5)] \approx [1 - 0.5/q_a] \approx 1$ for $q_a \gg 1$. Since $q_a = (2\pi a^2 B_T/\mu_o R I_p)$, if $(r_1/a) = 1/q_a$, then the reduced coordinates j_o and a_{eff} of Eqs. (8.1) and (8.2) depend only on the "external" tokamak parameters B_T, I_p, R, and a. The weak dependence on the limiter radius a comes from the weak dependence of q_o on q_a when $(r_1/a) \approx 1/q_a$. Hence, for large q_a and when $(r_1/a) \approx 1/q_a$, our reduced coordinates of Eqs. (8.1) and (8.2) become equal to those of Soltwisch <u>et al.</u> It is interesting to note that if Soltwisch <u>et al.</u> would have used the reduced coordinate of Eq. (8.1) in their Fig. 6, then the central current density (for r = 0) would have taken the values 0.67 × 2.95 ≈ 1.98, 0.74 × 2.64 ≈ 1.95, 0.72 × 2.75 ≈ 1.98, 0.78 × 2.55 ≈ 1.99, 0.80 × 2.50 = 2.00, and 0.88 × 2.30 ≈ 2.02 for the curves 1, 2, 3, 4, 5, and 6, respectively, thus yielding a reduced spread from 1.9 to 2.02 instead of the spread from 2.30 to 2.95. Also, if one used the a_{eff} of Eq. (8.2), then the values of r have to be divided by the corresponding $q_o^{1/2}$. Hence, it appears that the use of the reduced coordinates of Eqs. (8.1) and (8.2) would improve the universality of Soltwisch <u>et al.'s</u> profile plots of Fig. 6.

Similarly, one can show from Eqs. (3.2), (3.4), (3.5), and (3.8) that the proper reduced coordinates for the q_a-dependent exponential profiles to yield the universality of the profiles are (j/j_o) and r/a_{eff}, where $j_o = (2B_T/\mu_o R q_o)$ and $a_{eff}^2 = a^2/\alpha_j^2 \approx (q_o/2q_a)a^2 = (q_o \mu_o R I_p/4\pi B_T)$ for large q_a. From Eqs. (4.1), (4.4), (4.5), (4.8), (4.9), and (4.11), the reduced coordinates for the q_a-dependent modified exponential profiles for the simplest case of $c = 2$ may be written (j/j_o) and r/a_{eff}, where $j_o = (2B_T/\mu_o R q_o)$ and $a_{eff} = (a/\alpha_j) = [a/\log(q_a/q_o)] = [a/(1 - 1/q_a)\log q_a] \approx (a/\log q_a)$ for large q_a. Also, from Eqs. (6.9), (6.10), (6.13), and (6.14) it follows that the proper reduced coordinates for the Kadomtsev optimal profiles are (j/j_o) and r/a_{eff}, where $j_o = (2B_T/\mu_o R q_o)$ and $a_{eff}^2 = (a^2/q_a) = (\mu_o R I_p/2\pi B_T)$.

It is, of course, apparent that for q_a-independent profiles (such as the q_a-independent exponential and modified exponential, and trapezoidal profiles) and for the profile used by Campbell et al. of the JET group, it is not possible to find any suitable reduced coordinates that will lead to a universality of profiles as observed by Soltwisch et al.

IX. RADIAL AND q_a DEPENDENCE OF THE NORMALIZED SAWTOOTH AMPLITUDE

We now wish to examine the dependence of the normalized sawtooth amplitude on the limiter safety factor q_a for those models which satisfy the empirical profile consistency relation $(r_1/a) \approx (1/q_a)$. During the rising portion of the sawtooth, which occurs on a slow resistive Joule heating time scale [14-23], the $T_e(r)$ profile, and presumably the $j(r)$ profile, keeps on peaking up and the central q_o keeps on decreasing steadily from unity. At the end of the sawtooth crash, which occurs on a fast time scale associated with either the resistive internal kink mode [15-20], the pressure-driven ideal kink mode [19,22,23], or with enhanced transport due to micro-turbulence and/or global stochastization of the magnetic field lines by the overlap of secondary islands [23,26,55], these profiles get flattened over the entire core region of the plasma [15,16,17,24,25]. Kadomtsev [15,16,17] has shown that this flat core region extends up to a minor radius $r_o = c_o r_1 = \sqrt{2}\, r_1$ and in this region q = 1. This is shown schematically by the dashed lines in the inserts of Figs. 14a and b. Here the volume integrals of the two shaded regions are equal to each other, implying the conservation of total plasma thermal energy and total plasma current for the $T_e(r)$ profile [of Fig. 14a] and j(r) profile [of Fig. 14b], respectively. Hence, the radial dependence of the normalized sawtooth amplitude is given by

$$(\Delta T_e/T_e) = 2[T_e^{(B)}(r) - T_e^{(T)}(r)]/[T_e^{(B)}(r) + T_e^{(T)}(r)], \qquad (9.1)$$

where $T_e^{(B)}(r)$ and $T_e^{(T)}(r)$ are the temperature profiles at the bottom of the sawtooth [i.e., the dashed lines in the inserts of Figs. 14a and b] and at the top of the sawtooth [i.e., the solid lines in these inserts of Figs. 14a and b], respectively. Thus, the normalized sawtooth amplitude at the plasma center [i.e., at r = 0].

$$(\Delta T_e/T_e)_o = 2[T_e(a/q_a) - T_{eo}]/[T_e(a/q_a) + T_{eo}], \qquad (9.2)$$

where we have set $T_e(r) = T_e^{(T)}(r)$ and $T_{eo} = T_e(o)$ and we have used the empirical profile consistency relation $(r_1/a) \approx (1/q_a)$.

From Eqs. (2.1), (2.9), (2.12), and (9.2) we get for the Coppi-Tang model

$$(\Delta T_e/T_e)_o \approx -2[1 - \exp(-2\alpha_j/3q_a^2)]/[1 + \exp(-2\alpha_j/3q_a^2)]$$

$$\approx -(2/3q_a) \text{ for } q_a \gg 1, \qquad (9.3)$$

since when $(r_1/a) \approx (1/q_a)$, $\alpha_j \approx -q_a^2 \log(1 - 1/q_a) \approx q_a + 0.5$. That is, the normalized sawtooth amplitude increases linearly with increasing limiter rotational transform q_a^{-1} for large q_a. From Eq. (9.3) we get $(\Delta T_e/T_e)_o \approx 0.28$ and 0.12 for $q_a = 2.9$ and 6.2, respectively, while experimentally $(\Delta T_e/T_e)_o \approx$

0.18 and 0.10 for $q_a \approx 2.9$ and 6.2, respectively. Similarly, from Eqs. (3.1), (3.6), (3.8), and (9.2) we get for the q_a-dependent exponential profiles

$$(\Delta T_e/T_e)_o \approx -2[1 - \exp(-2\alpha_j/3q_a)]/[1 + \exp(-2\alpha_j/3q_a)]$$

$$\approx -(8/9q_a)^{1/2} \text{ for } q_a \gg 1, \qquad (9.4)$$

since when $(r_1/a) \approx (1/q_a)$, $\alpha_j^2 \approx -2q_a^2 \log(1 - 1/q_a) \approx (2q_a + 1)$. Equation (9.4) yields $(\Delta T_e/T_e)_o \approx 0.58$ and 0.39 for $q_a \approx 2.9$ and 6.2, respectively. From an experimentalist point of view these are very unreasonable numbers. Also for the q_a-dependent modified exponential of Eq. (4.8), we find that

$$(\Delta T_e/T_e)_o \approx -[1 - (1 - \alpha_j/3q_a)\exp(-2\alpha_j/3q_a)]/[1 + (1 - \alpha_j/3q_a)\exp(-2\alpha_j/3q_a)]$$

$$\approx (\log q_a)/(q_a - 1) \text{ for } q_a \gg 1, \qquad (9.5)$$

where α_j is given by Eq. (4.11). This gives $(\Delta T_e/T_e)_o \approx 0.56$ and 0.35 for $q_a \approx 2.9$ and 6.2, respectively. For the Kadomtsev model, we get from Eqs. (6.16) and (9.2)

$$(\Delta T_e/T_e)_o \approx -2[1 - (1 + 1/q_a)^{-4/3}]/[1 + (1 + 1/q_a)^{-4/3}] \approx -(4/3q_a) \qquad (9.6)$$

for $q_a \gg 1$. This yields $(\Delta T_e/T_e)_o \approx 0.39$ and 0.20 for $q_a \approx 2.9$ and 6.2, respectively. For the Campbell <u>et al.</u> model we find from Eqs. (7.1), (7.6), and (9.2) that

$$(\Delta T_e/T_e)_o \approx -2[1 - (1 - 1/q_a^2)^{2\nu_j/3}]/[1 + (1 - 1/q_a^2)^{2\nu_j/3}]$$

$$\approx - (2/3q_a) \text{ for } q_a >> 1. \tag{9.7}$$

This yields $(\Delta T_e/T_e)_o \approx 0.20$ and 0.11 for $q_a \approx 2.9$ and 6.2, respectively, while the corresponding experimental values are $(\Delta T_e/T_e)_o \approx 0.18$ and 0.10. It is interesting to note that all the q_a-dependent profiles considered here predict that $(\Delta T_e/T_e)_o$ decreases with increasing q_a when $(r_1/a) \approx (1/q_a)$, and at the end of the sawtooth crash these profiles get flattened over the entire core region such that in this flat region $q \approx 1$. This qualitative behavior is in good agreement with the experimental observations of the TFR group [1]. It appears, however, that quantitatively speaking only the Campbell et al. and the Coppi-Tang models are reasonably close to the experimental observations in TFTR and TFR.

Let us now examine the radial dependence of the sawtooth amplitude $(\Delta T_e/T_e)$ of Eq. (9.1) for the two simple cases illustrated by the inserts in Figs. 14a and 14b. According to Kadomtsev [15,16,17] the transfer of heat from the shaded region of $r \le r_1$ to the shaded region in the range $r_1 \le r \le r_o$ is by convection induced by the tearing-mode perturbations to the magnetic field. Thus, the evolution of the excess heat or "heat pulse" in the region $r \ge r_o = \sqrt{2}\, r_1$ should be determined only by the transport properties of the stable plasma since the tearing-mode perturbations do not exist in this region. In the light of such a transport study by Jahns et al. [see Fig. 2 of Ref. 17], it is apparent that a straight line approximation for $T_e^{(B)}(r)$ and $j^{(B)}(r)$ [at the bottom of the sawtooth crash] in the region $r_o \le r \le c_T\, r_1$ and $c_j\, r_1$ for these inserts in Figs. 14a and 14b, respectively, is a very reasonable one. For the Coppi-Tang diffusive profiles of Eqs. (2.1) and (2.2), it is relatively easy to show that the equation of this straight line is

$$y(c;\ c_o) = (c - c_o)^{-1}[(c - r/r_1)\exp(-\alpha\ r_1^2/a^2)$$

$$- (c_o - r/r_1)\exp(-c^2\alpha\ r_1^2/a^2)], \qquad (9.8)$$

where $y(c;\ c_o) = (T_e(r)/T_{eo})$, $c = c_T$, and $\alpha = \alpha_T$ for the flattened $T_e^{(B)}(r)$ profile of Fig. 14a; and $y(c;\ c_o) = (j(r)/j_o) = (T_e(r)/T_{eo})^{3/2}$, $c = c_j$, and $\alpha = \alpha_j$ for the flattened $j^{(B)}(r)$ profile of Fig. 14b. By equating the volume integrals of the two shaded regions [i.e., by the conservation of total plasma thermal energy and/or total plasma current], one can show after a certain amount of lengthy algebra that c of Eq. (9.8) is given by

$$(c + c_o/2)^2 = \{[(3a^2/\alpha r_1^2)\exp(\alpha r_1^2/a^2) - (3c_o^2/4)] - [(3a^2/\alpha r_1^2) + (2c^2 - c\ c_o - c_o^3)]\exp[(1 - c^2)\ \alpha r_1^2/a^2)]\}. \qquad (9.9)$$

Here $\alpha_j = (3\alpha_T/2)$ is given by Eqs. (2.10) and (2.11) for $(r_1/a) = (1/q_a)$. For iterative purposes the lowest order solution c_L of Eq. (9.9) may be written

$$(c_L + c_o/2)^2 = [(3a^2/\alpha\ r_1^2)\exp(\alpha r_1^2/a^2) - (3c_o^2/4)], \qquad (9.10)$$

since $c > c_o \geq 1$ and $(\alpha\ r_1^2/a^2) \sim q_a^{-1} \ll 1$ for large q_a. By using this value of c_L for c on the right side of Eq. (9.9), one obtains the more accurate first order iterative solution for c. Thus, from Eqs. (2.1), (2.2), (2.10), (2.11), (9.1), (9.8), (9.9), and (9.10) one can obtain the radial dependence of the normalized sawtooth amplitude, i.e., $(\Delta T_e/T_e)$ vs r. For the flattened $T_e^{(B)}$ profile of Fig. 14a with conservation of total plasma thermal energy we get

$$(\Delta T_e/T_e) = \begin{cases} \dfrac{-2(1 - \exp[-\alpha_T(r_1^2 - r^2)/a^2])}{(1 + \exp[-\alpha_T(r_1^2 - r^2)/a^2])} & \text{for } r \le c_o\, r_1 \\ \\ \dfrac{2(y(c_T;c_o) - \exp(-\alpha_T r^2/a^2))}{(y(c_T;c_o) + \exp(-\alpha_T r^2/a^2))} & \text{for } c_o\, r_1 \le r \le c_T\, r_1 \end{cases} \tag{9.11}$$

and is zero for $r \geq c_T r_1$. Similarly, for the flattened $j(r)$ profile of Fig. 14b with conservation of total plasma current we get

$$(\Delta T_e/T_e) = \frac{2([y(c_j;c_o)]^{2/3} - \exp(-\alpha_T r^2/a^2))}{([y(c_j;c_o)]^{2/3} + \exp(-\alpha_T r^2/a^2))} \tag{9.12}$$

for $c_o\, r_1 \leq r \leq c_j r_1$, is given by Eq. (9.11) for $r \leq c_o\, r_1$, and is zero for $r \geq c_j\, r_1$. These radial dependences of $(\Delta T_e/T_e)$ for $q_a = 4$ are shown in Figs. 14a and 14b. In both these figures the solid line corresponds to the Kadomtsev case of $c_o = \sqrt{2}$, and the dashed line is for $c_o = 1$. The somewhat symmetric solid line curve of Fig. 14b for the Kadomtsev case of $c_o = \sqrt{2}$ with the current conservation constraint seems to have the same shape as the experimental results of Fig. 3 of Ref. 21 and Fig. 5 of Yamada et al. [20]. However, the experimental curve of Fig. 2C of Ref. 14 has a rather assymmetric shape for $r > r_1$. Finally, it is interesting to note from our simple physical picture that one can, in principle, unfold the $T_e^{(T)}(r)$ [and presumably $j^{(T)}(r)$ via Ohm's law] profiles from precise measurements of $(\Delta T_e/T_e)$ vs r for $r \leq c_o\, r_1 = \sqrt{2}\, a/q_a$. Then the precise measurement of $(\Delta T_e/T_e)$ vs r for $r \geq c_o\, r_1$ will yield $T_e^{(B)}(r)$ in this range, which in turn will shed light on the heat pulse propagation diffusion coefficient $\chi_e(r)$.

X. CONCLUSIONS

In this paper we have presented a rather complete and detailed theoretical examination of the self-consistency of the principle of profile consistency results for sawtoothing tokamak discharges. In Sec. I we have outlined very clearly the theoretical procedure that we used to examine this self-consistency. It should be apparent from our procedural outline that the method used here is for the most part a pedestrian approach. Table 1 summarizes our principal results and conclusions. Most of these models in this table have been proposed earlier in the literature and used with computer simulation techniques. Here, we have tried to present a rather rigorous theoretical analysis of these models and compare them with some of the existing TFTR data for sawtoothing Ohmic and low-power neutral beam injection discharges. We have not included any high-power neutral beam injection results from TFTR, since: (1) for the sawtoothing high-power neutral beam injection TFTR discharges the beam-induced plasma current is an appreciable fraction of the total plasma current and it is not clear what type of Ohm's law relates this part of $j(r)$ to $T_e(r)$ [while for the Ohmic part of the current $j(r) \propto f_\sigma(r)\ T_e^{3/2}(r)$], and (2) most of the high-power neutral beam injection TFTR discharges are high-T_i discharges with no sawtooth behavior [54], and in this case there exists no function F_1. Now we will present a section by section summary and conclusions.

In Sec. I we have presented an operational working definition of the principle of profile consistency for sawtoothing tokamak discharges. The three basic mathematical statements of this principle for sawtoothing discharges [i.e., discharges with $q(0) < 1$] are: (1) $(r_1/a) = F_1(1/q_a)$ [$\approx (1/q_a)$ empirically], (2) $[\langle T_e\rangle/T_{eo}] = F_2(1/q_a)$, and (3) the scaling law for the central electron temperature $T_{eo}^{3/2} \propto (I_p R Z_{eff}/a^2 V_L)\ F_3(q_a)$. In the rest of the sections we have examined the self-consistency of the measured $T_e(r)$

profiles, the functions F_1, F_2, and F_3 for sawtoothing TFTR discharges with the corresponding ones predicted by the various theoretical models proposed earlier in the literature by several authors.

In general, as seen from Fig. 2, $(r_1/a) = F_1(1/q_a) \approx (1/q_a)$ gives a very good fit to the experimental data. Because of the limited range of q_a - measurements, one can also get a reasonable fit to the experimental data of Fig. 2 with an equation of the form $(r_1/a) = (m/q_a) + b$. For example, the pair of values $m \approx 1.23$ and $b \approx 0.076$ and the pair $m \approx 1.6$ and $b \approx -0.2$ both yield a reasonably good fit to the experimental data of Fig. 2. However, from a theoretical standpoint the relation $(r_1/a) = (1/q_a)$ seems much more fundamental and physically appealing than the relation $(r_1/a) = (m/q_a) + b$. This observed functional relationship $(r_1/a) \approx (1/q_a)$ for the range of q_a - values necessarily implies that for these TFTR discharges $j(r)$ and, hence, by Ohm's law $T_e(r)$ are both not only functions of r but also functions of q_a, i.e., $j = j(r, q_a)$ [and consequently $q = q\ (r, q_a)$] and $T_e = T_e(r, q_a)$.

In Sec. II, we find that $(r_1/a) = (1/q_a)$ is an admissible solution to the transcendental equation $q(r_1) = 1$ for the Coppi-Tang model. Considering the fact that at the top of the sawtooth the measured $T_e(r)$ profile is peaked with a peak value of T_{eo} and at the bottom of the sawtooth crash $T_e(r)$ is flat within the $q = 1$ surface such that $T_{e1} = T_e(r = r_1) = T_{eo}\ \exp(-2\alpha_j/3q_a^2) = T_{eo}\ \exp[-2(q_a + 0.5)/3q_a^2]$, one can see that the Coppi-Tang model with Spitzer-type resistivity is in reasonable agreement with the measured $T_e(r)$ profiles. The best fitting relationship between the experimental measurements and the theoretical predictions of the Coppi-Tang model appears to be $[\langle T_e\rangle/T_{eo}]_{EXP} = [\langle T_e\rangle/T_{eo}]_{TH} + 0.05$. However, the agreement between $[\langle T_e\rangle/T_{eo}]_{EXP}$ and $[\langle T_e\rangle/T_{e1}]_{TH}$ is rather poor. The trial function $(r_1/a) = (m/q_a) + b$ with $b = (1 - m)$ yields a better fit for the plot of $[\langle T_e\rangle/T_{eo}]_{EXP}$ vs $[\langle T_e\rangle/T_{eo}]_{TH}$ but worsens the fit for the plot of (r_1/a) vs $(1/q_a)$ and vice versa. However, unusual and theoretically unrealistic pairs of values of m and $b \neq (1 - m)$, for example $m = 1.6$ and $b = -0.2$, will to some extent yield reasonably good fits to both the plots of (r_1/a) vs $(1/q_a)$ and $[\langle T_e\rangle/T_{eo}]_{EXP}$ vs $[\langle T_e\rangle/T_{eo}]_{TH}$ simultaneously. [These plots are not shown in this paper.]

The Coppi-Tang model with some reasonable neoclassical conductivity form factors yields a better fit than factors with simple Spitzer-type resistivity. However, the theoretically deduced neoclassical correction by assuming that $\chi_e(r)\, n_e(r)$ = constant in the electron thermal energy balance equation yields the best fitting relationship as $[\langle T_e\rangle/T_{eo}]_{EXP} = [\langle T_e\rangle/T_{eo}]_{TH} - 0.15$. This may imply that either $\chi_e(r)\, n_e(r)$ is not really constant but has some weak functional dependence on r or the $T_e(r)$ is not really Gaussian for these TFTR discharges under study.

On the whole, the chopped Coppi-Tang model yields reasonably good fits to all three experimental plots of $T_e(r)$ vs. r, (r_1/a) vs. $(1/q_a)$, and $[\langle T_e\rangle/T_{eo}]_{EXP}$ vs $[\langle T_e\rangle/T_{eo}]_{TH}$ simultaneously.

The principle of profile consistency predictions for the scaling law for the central electron temperature T_{eo} from the Coppi-Tang model is found to be in fairly reasonable agreement with the Taylor et al.'s. regression analysis of the corresponding TFTR data, and the TFR data. The Ohkawa's form of $\chi_e(r)$ yields a T_{eo} scaling law that is rather similar to that yielded by the Coppi's form of $\chi_e(r)$. However, the INTOR form of $\chi_e(r)$ predicts a somewhat different T_{eo} scaling law, in particular, a weaker dependence on B_T and no dependence on the minor radius a.

In Sec. III we have shown that, in general, the q_a - dependent exponential profiles give a poor fit to the experimental data. The fits for $T_e(r)$ vs. r plots are worse for low q_a - data and are somewhat better for the high q_a - data. But the ratio of T_{eo} at the top of the sawtooth to T_{e1} at the bottom of the sawtooth crash, i.e., $T_{eo}/[T_{e1} = T_e(r_1) = T_{eo}\exp(-\alpha_T r_1/a)]$

seems unrealistically large compared to the TFTR data of Taylor et al. The profile consistency predictions of the T_{eo} scaling law for this model are somewhat different from that of the diffusive profiles of the Coppi-Tang model of Sec. II.

The chopped q_a - dependent exponential profiles with $(r_f/a) = (r_1/a) = (1/q_a)$ yield a poor fit for $[\langle T_e\rangle/T_{eo}]_{EXP}$ vs $[\langle T_e\rangle/T_{eo}]_{TH}$ plots. However, when chopped up to $0.5r_1$ [i.e., $(r_f/a) = (0.5r_1/a) = (0.5/q_a)$], they yield reasonably good fits on this plot of $[\langle T_e\rangle/T_{eo}]_{EXP}$ vs $[\langle T_e\rangle/T_{eo}]_{TH}$.

The q_a - independent exponential profiles, in general, give very poor fits all around. Further, the q_a - independent profiles can have $(r_1/a) = (1/q_a)$ as a solution of the equation $q(r_1) = 1$ for only one value of q_a, and they yield a single value for $[\langle T_e\rangle/T_{eo}]_{TH}$ regardless of the value of q_a. These same remarks also apply to the chopped q_a - independent exponential profiles. However, the chopped q_a-independent exponential profiles have $0 \leq (r_1/a) = F_1(1/q_a) \neq (1/q_a)$ as solutions of the equation $q(r_1) = 1$ for all values of $q_a \leq [4/\{1 - 3\exp(-2)\}] \approx 6.7$. That is, when chopped up to the sawtooth inversion radius (or when $r_f \approx r_1$), all q_a-independent profiles [with $\langle T_e\rangle/T_{eo} \neq F_2(1/q_a)$] in general become q_a-dependent [with $\langle T_e\rangle/T_{eo} = F_2(1/q_a)$]. In deriving the T_{eo} scaling law from any q_a - independent profiles one does not make use of the principle of profile consistency in sharp contrast to those of the q_a - dependent profiles. The q_a - independent profiles always seem to yield a scaling law of the form $T_{eo} \propto (I_p R Z_{eff}/V_L a^2)^{2/3}$, while the q_a - dependent profiles always yield $T_{eo} \propto (B_T Z_{eff}/V_L)^{2/3}$ as a direct consequence of the profile consistency relation $(r_1/a) = (1/q_a)$. Further, for q_a - independent profiles T_{eo} is independent of B_T, while for q_a - dependent profiles T_{eo} is a strong function of B_T.

The modified exponential profiles of Sec. IV also seem to give very poor fits to the experimental plots of $[\langle T_e\rangle/T_{eo}]_{EXP}$ vs $[\langle T_e\rangle/T_{eo}]_{TH}$. In a broad sense the same conclusions of the exponential profiles of Sec. III apply equally well here. However, the chopped modified exponential profiles of Fredrickson et al. [8] yield good overall agreement with the existing TFTR data.

As seen from the results in Sec. V, the trapezoidal fits to the experimentally measured $T_e(r)$ profiles are very good for low q_a - discharges and are poor for high q_a - discharges. For these profiles the equation for (r_1/a) as a function of $(1/q_a)$ is a parabola, and is in very poor agreement with the experimental measurements which yield the straight line $(r_1/a) \simeq (1/q_a)$ as the best fit. However, amusingly enough, the trapezoidal model yields $[\langle T_e\rangle/T_{eo}]$ values that are in remarkable agreement with the TFTR experimental measurements.

In general, the behavior of the Kadomtsev model of Sec. VI and the Campbell et al. model of Sec. VII are very similar to those of the Coppi-Tang model of Sec. II. However, from an experimental standpoint the Kadomtsev model yields unrealistically large values for the fractional current flowing outside the limiter, while the other two models yield practically realistic values for this fractional current. It is indeed remarkable and is somewhat amusing to find that all these three models yield $[\langle T_e\rangle/T_{eo}]_{EXP} \simeq [\langle T_e\rangle/T_{eo}]_{TH} + 0.05$ as the best fit to the TFTR data. The exact reason and the intrinsic connection that may exist among these three models [i.e., the Coppi-Tang, Kadomtsev, and the Campbell et al. models] that leads to the same relationship of $[\langle T_e\rangle/T_{eo}]_{EXP} \simeq [\langle T_e\rangle/T_{eo}]_{TH} + 0.05$ for all these three models is not very clear to us.

In Sec. VIII we have shown that all the q_a-dependent profiles considered in this paper, except the ones used by Campbell et al., lead to the universality of profiles in some reduced coordinates which depend mainly on the external tokamak parameters in agreement with the observations of

Soltwisch <u>et al.</u> [41] and also with the predictions of Pfirsch and Pohl [11]. It is, of course, impossible to find any suitable reduced coordinates that will lead to a universality of profiles for all q_a-independent profiles and for the profile used by Campbell <u>et al.</u>

In Sec. IX we have examined the radial and q_a dependence of the normalized sawtooth amplitude $(\Delta T_e/T_e)$. We find that for large q_a, the Coppi-Tang, Kadomtsev, and Campbell <u>et. al</u> models all predict that $(\Delta T_e/T_e) \propto (1/q_a)$ in agreement with the experimental observations. The assumption of the flattening of the current profile for $0 \le r \le c_o r_1 = \sqrt{2}\, a/q_a$ at the end of the sawtooth crash subject to the current conservation constraint, yields a radial dependence of $(\Delta T_e/T_e)$ that is in reasonable semi-quantitative agreement with the existing experimental measurements.

Finally, in the Appendix we have examined the fractional amount of current flowing outside the limiter, and the dependence of the central q(o) on the limiter safety factor q_a. It is interesting to note from Figs. 15a and 15b that the recent measurements of q(o) as a function of q_a by Soltwisch <u>et al.</u> [41] and by West <u>et al.</u> [42] seem to favor the predictions of the Coppi-Tang, Kadomtsev, and Campbell <u>et al.</u> models.

ACKNOWLEDGMENTS

This work was supported by the U.S. Department of Energy Contract No. DE-AC02-76-CHO-3073. We thank the members of both the experimental and the theoretical division of our physics group for useful comments.

APPENDIX

For the sake of completeness in this appendix we will examine the fractional amount of current flowing outside the limiter, and the dependence of the central q(o) on the limiter q_a for these models. From an experimentalist point of view, it is of course physically instructive to know offhand whether the selected profiles predict reasonable values for the fractions $F_p = [I_p(a \text{ to } \infty)/I_p(o \text{ to } \infty)]$, and $[q(o)/q_a]$.

Case A: Coppi-Tang model.

For this model from Eq. (2.2) we get

$$I_p(o \text{ to } r) = \int_o^r dr\ 2\pi r\ j_o\ \exp(-\alpha_j r^2/a^2)$$

$$= (\pi a^2 j_o/\alpha_j)[1 - \exp(-\alpha_j r^2/a^2)]. \qquad (A.1)$$

Hence,

$$I_p(o \text{ to } a) = (\pi a^2 j_o/\alpha_j)\ [1 - \exp(-\alpha_j)], \qquad (A.2)$$

and

$$I_p(o \text{ to } \infty) = (\pi a^2 j_o/\alpha_j). \qquad (A.3)$$

Thus,

$$F_p = [I_p(a \text{ to } \infty)/I_p(o \text{ to } \infty)] = \exp(-\alpha_j). \qquad (A.4)$$

If $(r_1/a) = (1/q_a)$, then from Eq. (2.12) to the lowest order

$$\alpha_j^{(o)} \approx -q_a^2 \log[1 - 1/q_a] \approx q_a + 0.5. \qquad (A.5)$$

Thus, for low $q_a \approx 3$, the fractional current flowing outside the limiter is about 3%; and for high $q_a \approx 8$, this fraction is about 0.02%. From an experimentalist point of view these are very reasonable numbers.

Case B: Exponential profiles.

For this model from Eq. (3.1) we get

$$I_p(o \text{ to } r) = \int_o^r dr 2\pi r j_o \exp(-\alpha_j r/a)$$

$$= (2\pi j_o a^2/\alpha_j^2)[1 - (1 + \alpha_j r/a)\exp[-\alpha_j r/a)]. \qquad (A.6)$$

Hence,

$$F_p = [I_p(a \text{ to } \infty)/I_p(o \text{ to } \infty)] = (1 + \alpha_j)\exp(-\alpha_j). \qquad (A.7)$$

If $(r_1/a) = (1/q_a)$, then from Eq. (3.8) to the lowest order

$$\alpha_j^{(o)} \approx [-2q_a^2 \log(1 - 1/q_a)]^{1/2} \approx (2q_a + 1)^{1/2}. \qquad (A.8)$$

Thus, for low $q_a \approx 3$, this fraction of Eq. (A.7) is about 26% and for high $q_a \approx 8$, this fraction is about 8.3%. From an experimentalist point of view these are very unreasonable numbers.

Case C: Modified exponential profiles.

For this model from Eq (4.1) we get

$$I_p(o \text{ to } r) = \int_o^r dr\, 2\pi r j_o(1 - \alpha_j r/ca)\exp(-\alpha_j r/a) = (2\pi a^2 j_o/\alpha_j^2)$$

$$[\{(\alpha_j^2 r^2/ca^2) - (1 + \alpha_j r/a)(1 - 2/c)\}\exp(-\alpha_j r/a) + (1 - 2/c)]. \tag{A.9}$$

Here again we will only consider the simplest case of $c = 2$. Then, from Eq. (A.9) we get

$$I_p(o \text{ to } r) = (\pi j_o r^2)\exp(-\alpha_j r/a). \tag{A.10}$$

It is clear from Eq. (4.8) that the current profile must truncate when $(1 - \alpha_j r/2a) = o$, i.e., when $r = (2a/\alpha_j)$.

Hence,

$$I_p[o \text{ to } r = (2a/\alpha_j)] = (4\pi j_o a^2/\alpha_j^2)\exp(-2), \tag{A.11}$$

and

$$I_p[o \text{ to } a] = (\pi j_o a^2)\exp(-\alpha_j). \tag{A.12}$$

Thus the fractional current flowing outside the limiter is

$$F_p = [I_p(a \text{ to } r = 2a/\alpha_j)]/[I_p(o \text{ to } r = 2a/\alpha_j)]$$

$$= [1 - (\alpha_j^2/4)\exp(2 - \alpha_j)]. \tag{A.13}$$

For q_a - dependent modified exponential profiles which satisfy the principle of profile consistency relation $(r_1/a) = (1/q_a)$,

$$\alpha_j = \log q_a/(1 - 1/q_a). \tag{A.14}$$

Then, for example, for $q_a = 3$ the fractional current of Eq. (A.13) is about 3.5%; while for $q_a = 8$ this fraction is about 3.1%. From an experimentalist point of view these are very reasonable ·umbers. Finally, it is interesting and physically instructive to note from Eq. (A.13) that for a q_a - independent modified exponential profile with $\alpha_j = 2$, the fractional current flowing outside the limiter is exactly zero.

Case D: Trapezoidal profiles.

These profiles by definition are automatically truncated at $r = a$. Hence, no current flows outside the limiter for these profiles of Eq. (5.2).

Case E: Kadomtsev optimal profiles.

For this model from Eq. (6.10) we get

$$I_p(o \text{ to } r) = \int_o^r dr \frac{2\pi r j_o}{(1 + r^2/a_*^2)^2} = (\pi a_*^2 j_o) \frac{(r^2/a_*^2)}{[1 + (r^2/a_*^2)]} . \tag{A.15}$$

Hence,

$$I_p \text{ (o to a)} = (\pi a_*^2 j_o) \frac{(a^2/a_*^2)}{[1 + (a^2/a_*^2)]} , \tag{A.16}$$

and

$$I_p(o \text{ to } \infty) = (\pi a_*^2 J_o). \tag{A.17}$$

Thus,

$$F_p = [I_p(a \text{ to } \infty)/I_p(o \text{ to } \infty)] = [1/(1 + a^2/a_*^2)]. \tag{A.18}$$

If $(r_1/a) = (1/q_a)$, then from Eq. (6.14)

$$(a^2/a_*^2) = q_a. \qquad (A.19)$$

Thus from Eqs. (A.18) and (A.19) we find for low $q_a \approx 3$ this fraction is about 25%; while for high $q_a \approx 8$ this fraction is 11%. From an experimentalist point of view these are very unreasonable numbers.

Case F: Campbell et al. model.

These profiles of Eq. (7.2) are automatically truncated at $r = a$. Hence, for these profiles no current flows outside the limiter.

In a similar way one can show that the fractional amount of current flowing outside the limiter F_p for the chopped Coppi-Tang, Coppi-Tang with neoclassical $f_\sigma(r) = (1 - d\ r^2/a^2)$, q_a-dependent chopped exponential, q_a-independent exponential, q_a-independent chopped exponential, q_a-independent modified exponential of Eq. (4.13), chopped Kadomtsev, and chopped Campbell et al. models are given by

$$F_p = \frac{I_p(a \text{ to } \infty)}{I_p(o \text{ to } \infty)} = \frac{\exp[-\alpha_J(1 - r_f^2/a^2)]}{1 - \alpha_J r_f^2/a^2}, \tag{A.20}$$

$$F_p = \frac{I_p(a \text{ to } d^{-1/2})}{I_p(o \text{ to } d^{-1/2})} = \frac{(1 - d - d/\alpha_j)\exp(-\alpha_j) + (d/\alpha_j)\exp(-\alpha_j/d)}{1 - d/\alpha_j + (d/\alpha_j)\exp(-\alpha_j/d)} , \quad \text{(A.21)}$$

$$F_p = \frac{I_p(a \text{ to } \infty)}{I_p(o \text{ to } \infty)} = \frac{(1 + \alpha_j)\exp[-\alpha_j(1 - r_f/a)]}{1 + \alpha_j r_f/a + \alpha_j^2 r_f^2/a^2} , \quad \text{(A.22)}$$

$$F_p = \frac{I_p(a \text{ to } \infty)}{I_p(o \text{ to } \infty)} = 3\exp(-2) \approx 0.406 , \quad \text{(A.23)}$$

$$F_p = \frac{I_p(a \text{ to } \infty)}{I_p(o \text{ to } \infty)} = \frac{3\exp[-2(1 - r_f/a)]}{1 + 2r_f/a + 4r_f^2/a^2} , \quad \text{(A.24)}$$

$F_p = 0$ [since these profiles are naturally truncated at $r = a$], (A.25)

$$F_p = \frac{I_p(a \text{ to } \infty)}{I_p(o \text{ to } \infty)} = \frac{(1 + r_f^2/a_*^2)^2}{(1 + a^2/a_*^2)(1 + 2r_f^2/a_*^2)} , \quad \text{(A.26)}$$

and

$F_p = 0$ [since these profiles are automatically truncated at $r = a$] , (A.27)

respectively. For most of the chopped models considered here we have set $(r_f/a) = (r_1/a) \approx (1/q_a)$.

In Figs. 15a and b we show the behavior of the central safety factor q(o) as a function of the limiter q_a for the models considered in this paper. It may again be noted from these two figures that the Coppi-Tang and Campbell *et al.* models are very similar both in magnitude and shape for medium and high q_a discharges; and further the Kadomtsev model is very similar [although slightly low in values of q(o)] to that of Coppi-Tang model. Also, it is interesting to note from these figures that the recent measurements of q(o) as a function of q_a by Soltwisch <u>et al.</u> and by West <u>et al.</u> seem to favor the predictions of the Coppi-Tang, Kadomtsev, and Campbell <u>et al.</u> models. As we pointed out earlier, we see here that for q_a-independent profiles q(o) is proportional to q_a [i.e., $F_3 = (q_a/q_o)$ = constant $\neq F_3\ (q_a)$], while for q_a-dependent profiles q(o) tends to constant values for large q_a [i.e., $F_3 = F_3(q_a) \propto q_a$ for $q_a \gg 1$]. This difference naturally leads to two distinct types of T_{eo} scaling laws for Ohmic plasmas. For q_a-independent profiles one gets the profile consistency independent scaling law $T_{eo} \propto (I_p R Z_{eff}/a^2 V_L)^{2/3}$, and for q_a-dependent profiles one gets the profile consistency dependent scaling law $T_{eo} \propto (B_T Z_{eff}/V_L)^{2/3}$ for large q_a. Here we have used the fact that for q_a-dependent profiles $F_3(q_a) \propto q_a$ for large q_a if and only if $(r_1/a) = F_1(1/q_a) \approx (1/q_a)$.

REFERENCES

1. The TFR Group (presented by P. Platz), in Seventh European Conference on Controlled Fusion and Plasma Physics (Centre de Recherches en Physique des Plasmas, Lausanne, 1975), Vol. 1, p.1.
2. W. M. Manheimer and T. M. Antonson, Jr., Phys. Fluids, 25 (1979) 957; W. M. Manheimer, K. R. Chu, E. Ott, and J. P. Boris, Phys. Rev. Lett. 37 (1976) 286.
3. B. Coppi, Comments Plasma Phys. Cont. Fusion, 5 (1980) 261; B. Coppi, and E. Mazzucato, Phys. Lett. 71A (1979) 337.
4. A. Taroni, and F. Tibone, JET Report JET-IR(87) 02 (1987); A. Taroni, and F. Tibone, in Thirteenth European Conference On Controlled Fusion and Plasma Heating, Schliersee (1986), Vol. 10C, p.160.
5. W. M. Tang, Nucl. Fusion 26 (1986) 1605; W. M. Tang, Comments Plasma Phys. Controlled Fusion 10 (1986) 57.
6. H. P. Furth, P. H. Rutherford, and H. Selberg, Phys. Fluids 16 (1973) 1054; A. H. Glasser, H. P. Furth, and P. H. Rutherford, Phys. Rev. Lett., 38 (1977) 234; A. H. Glasser, W. Park, P. Rutherford, H. Selberg, and R. B. White, in Twelfth European Conference on Controlled Fusion and Plasma Physics, Budapest (1985), Vol. 9F, part II, p.358.
7. D. A. Boyd, and F. J. Stauffer, Comments Plasma Phys. Cont. Fusion 11 (1987) 63.
8. E. D. Fredrickson, K. M. McGuire, R. J. Goldston, M. G. Bell, et al., Nucl. Fusion 27 (1987) 1897.
9. B. B. Kadomtsev, Radio Physics And Quantum Electronics 26 (1987) 781; B. B. Kadomtsev, Comments Plasma Phys. Cont. Fusion 11 (1987) 153.
10. D. Biskamp, Comments Plasma Phys. Cont. Fusion 10 (1986) 165.

11. D. Pfirsch, and F. Pohl, Plasma Physics and Controlled Fusion 29 (1987) 697. These authors use an "entropy principle" and argue that tokamak plasmas should relax towards states described by relations $T_e(r) = T_e[n_e(r)]$ in which the total entropy of the plasma does not change when the plasma performs arbitrary internal motions slow enough not to alter the relation between T_e and n_e. The notion of profile consistency and the universality of profiles in some reduced coordinates appear to be a natural consequence of their entropy principle. They show that the Kadomtsev optimal profile result of $T_e(r) \propto [n_e(r)]^2$ is a special case of their general theory. See also E. Minardi, Plasma Phys. Contr. Fusion 30 (1988) 1701; E. Minardi, Milano IFP Report FP88/18, Oct. 1988.

12. J. A. Wesson, Nucl. Fusion 18 (1978) 87.

13. D. J. Campbell, J. P. Christiansen, J. G. Cordey, E. Lazzaro, M.F.F. Nave, F.C. Schueller, and P.R. Thomas, JET Report JET-P (86) 46 (1986).

14. S. von Goeler, W. Stodiek, and N. Sauthoff, Phys. Rev. Lett. 33 (1974) 1201.

15. B. B. Kadomtsev. Sov. J. Plasma Phys. 1 (1975) 389.

16. B. V. Waddel, M. N. Rosenbluth, D. A. Monticello, and R. B. White, Nucl. Fusion 16 (1976) 528.

17. G. L. Jahns, M. Soler, B. Waddel, J. D. Callen, and H. R. Hicks, Nucl. Fusion 18 (1978) 609.

18. A. Sykes, and J. A. Wesson, Phys. Rev. Lett. 37 (1976) 140.

19. J. A. Wesson, Plasma Physics and Controlled Fusion 28 (1986) 243.

20. K. McGuire and D. C. Robinson, Nucl. Fusion 19 (1979) 505; H. Yamada, K. McGuire, D. Colchin, P. C. Efthimion, *et al.*, Princeton University Plasma Physics Laboratory Report PPPL-2213 (1985).

21. K. McGuire, V. Arunasalam, M. G. Bell, M. Bitter, et al., in Eleventh International Conference On Plasma Physics and Controlled Neulear Fusion Research, Kyoto, 1986 (International Atomic Energy Agency, Vienna, 1987) Vol. 1. p.421.

22. A. W. Edwards, D. J. Campbell, W. W. Engelhart H. U. Fahrbach, et al., Phys. Rev. Lett. 57 (1986) ?10; D. J. Campbell, R. D. Gill, C. W. Gowers, J. A. Wesson, et al., Nucl. Fusion 26 (1986) 1085; D. J. Campbell, P. A. Duperrex, A. W. Edwards, R. D. Gill, et al., in Eleventh International Conference on Plasma Physics and Controlled Nuclear Fusion Research, Kyoto, 1986 (International Atomic Energy Agency, Vienna, 1987) Vol. 1, p.433.

23. A. Y. Aydemir, Phys. Rev. Lett. 59 (1987) 649; E. Westerhof, Comments Plasma Phys. Cont. Fusion, 11 (1987) 79.

24. R. E. Waltz, K. K. Wong, J. M. Greene, and R. R. Dominquez, Nucl. Fusion 26 (1986) 1729. These authors raise the interesting point that the profile consistency applies only to sawtoothing tokamak discharges. See also Ref. 5 and F. W. Perkins, and Y. C. Sun, Princeton University Plasma Physics Laboratory Report PPPL-2261 (1985).

25. G. Taylor, P. C. Efthimion, V. Arunasalam, R. J. Goldston, et al., Nucl. Fusion 26 (1986) 339.

26 P. H. Rebut, and M. Brusati, Plasma Physics and Controlled Fusion 28 (1986) 113.

27. H. P. Furth, Plasma Physics and Controlled Fusion 28 (1986) 1305.

28. In this paper we will assume resistive equilibrium and consequently E is a constant independent of r [i.e., $E \approx (V_L/2\pi R)$]. For transient situations such as the fast current ramp experiments in Ref. 8, E is a function of both the minor radius r and time t and the consistency conditions for the plasma column equilibrium and stability of Refs. 3 and 6 do not apply.

29. J. D. Callen, J. P. Christiansen, J. G. Cordey, P. R. Thomas, and K. Thomsen, Nucl. Fusion 27 (1987) 1857.

30. G. Becker, ASDEX TEAM, and NEUTRAL INJECTION TEAM, Nucl. Fusion 28 (1988) 139.

31. D. V. Bartlett, R. J. Bickerton, M. Brusati, D. J. Campbell et al., Nucl. Fusion 28 (1988) 73.

32. R. J. Goldston, Plasma Physics and Controlled Fusion 26 (1984) 87.

33. T. Ohkawa, Phys. Lett., 67A (1978) 35.

34. B. B. Kadomtsev, and O. P. Pogutse, in Tenth International Conference on Plasma Physics and Controlled Nuclear Fusion Research, London, 1984 (International Atomic Energy Agency, Vienna, 1985) Vol. 2, p.69.

35. B. J. D. Tubbing, N. J. Lopes Cardozo, M. J. Van Der Wiel, Nucl. Fusion 27 (1987) 1843; N.J. Lopes Cardozo, B.J.D. Tubbing, F. Tibone, and A. Taroni, Nucl. Fusion, 28 (1988) 1173; M. Soler and J.D. Callen, Nucl. Fusion 19 (1979) 703; E.D. Fredrickson, J.D. Callen, K. McGuire, T.D. Bell, et.al., Nucl. Fusion 26 (1986) 849. These papers also examine the relationship between the global power balance diffusivity χ_e^{GLO}, the heat pulse propagation diffusivity χ_e^{HP}, and the incremental heat diffusivity χ_e^{INC}.

36. K. Itoh, S. I. Itoh, and F. W. Perkins, Comments Plasma Phys. Cont. Fusion 10 (1986) 103.

37. F. L. Hinton, and R. D. Hazeltine, Rev. Mod. Phys. 48 (1976) 239; S.P. Hirshman and D.J. Sigmar, Nucl. Fusion 21 (1981) 1079; S.P Hirshman, R.J. Hawryluk, and B. Birge, Nucl. Fusion 17 (1977) 611.

38. L. Spitzer, Jr., Physics Of Fully Ionized Gases, 2nd Revised Edition, Interscience, New York (1962).

39. H. Dreicer, Phys. Rev., 115 (1959) 238; B. Coppi, F. Pegoraro, R. Pozzoli, and G. Rewoldt, Nucl. Fusion 16 (1976) 309; B. H. Hui, N. K. Windsor, and B. Coppi, Phys. Fluids 20 (1977) 1275.

40. T. Ohkawa, Nucl. Fusion 10 (1970) 185; N. J. Fisch, Rev. Mod. Phys., 59 (1987) 175; V. Arunasalam, P. C. Efthimion, J. C. Hosea, H. Hsuan, and G. Taylor, Phys. Rev. A 37, (1988) 2063.

41. H. Soltwisch, W. Stodiek, J. Manickam, and J. Schlüter, in Eleventh International Conference on Plasma Physics and Controlled Nuclear Fusion Research, Kyoto, 1986 (International Atomic Energy Agency, Vienna, 1987) Vol. 1, p.263; J. O'Rourke, J. Blum, J. G. Cordey, et al. in Fifteenth European Conference on Controlled Fusion and Plasma Heating, Dubrovnik, 1988, Vol. 12B, part 1, p.155; H. K. Park, D. K. Mansfield, L. C. Johnson, and C. H. Ma, Proceedings of STIE, 787 (1987) 110; H. K. Park, D. K. Mansfield, and L. C. Johnson, Proceedings of the Third International Symposium on Laser Aided Plasma Diagnostics, Los Angeles, CA (1987) p.96.

42. W. P. West. D. H. Thomas, J. S. de Grassie, and S. B. Zheng, Phys. Rev. Lett., 58 (1987) 2758; K. McCormick, A. Eberhagen, H. Murmann, and the ASDEX TEAM, in Fifteenth European Conference on Controlled Fusion and Plasma Heating, Dubrovnik, 1988, Vol. 12B, part 1, p.35; E. Marmer, Bull. Am. Phys. Soc. 32 (1987) 1847.

43. M. J. Forrest, P. G. Carolan, and N. J. Peacock, Nature (London), 271 (1978) 718; ibid, Culham Laboratory Report CLM-P499 (1977); F. W.

Perkins, Princeton Plasma Physics Laboratory Report MATT-818 (1970).

44. Hans Frauenfelder, The Mössbauer Effect, (Frontiers in Physics, W. A. Benjamin, Inc., 1962).

45. F. Jobes, Bull. Am. Phys. Soc. 32 (1987) 1928.

46. R. J. Goldston, Phys. Fluids 21 (1978) 2346; D. D. Meyerhofer, R. J. Goldston, R. Kaita, et al., Nucl. Fusion 25 (1985) 321.

47. D. J. Johnson, B. Grek, D. Dimock, et al., Rev. Sci. Instrum., 56 (1985) 1015.

48. G. Taylor, P. C. Efthimion, M. McCarthy, V. Arunasalam, et al., Rev. Sci. Instrum. 55 (1984) 1739; P. C. Efthimion, V. Arunasalam, R. Bitzer, and J. C. Hosea, Temperature, Vol. 5., (Reinhold, New York, 1982); P. C. Efthimion, V. Arunasalam, and J. C. Hosea, Phys. Rev. Lett. 44 (1980) 396.

49. F. J. Stauffer, D. Boyd, R. Cutler, and M. McCarthy, Rev. Sci. Instrum. 56 (1985) 925.

50. A. Cavalo and R. Cutler, Rev. Sci. Instrum. 56 (1985) 931.

51. E. H. Silver, M. Bitter, et al., Rev. Sci. Instrum. 53 (1982) 1198; K. W. Hill, M. Bitter, et al., Rev. Sci. Instrum. 56 (1985) 840; J. Kiraly, M. Bitter, et al., Nucl. Fusion 27 (1987) 397.

52. J. D. Jackson, Classical Electrodynamics, (John Wiley & Son, Inc., New York, 1967); W. K. H. Panofsky, and M. Phillips, Classical Electricity and Magnetism, (Addison-Wesley Publishing Company, Inc., Reading, Massachusetts, 1955).

53. S. M. Kaye, R. J. Goldston, M. Bell, K. Bol, et al., Nucl. Fusion 24 (1984) 1303; M. Murakami, V. Arunasalam, J. D. Bell, M. G. Bell, et al., Plasma Physics and Controlled Fusion 28 (1986) 17.

54. R. J. Goldston, V. Arunasalam, M. G. Bell, M. Bitter, et al., in Eleventh International Conference on Plasma Physics and Controlled Fusion Research, Kyoto, 1986 (International Atomic Energy Agency, 1987) p.75; R. J. Hawryluk, V. Arunasalam, M. G. Bell, M. Bitter, et al., ibid, p.51.

55. T. H. Stix, Phys. Rev. Lett. 30 (1973) 833; A. B. Rechester and T. H. Stix, Phys. Rev. Lett. 36 (1976) 587; P. H. Rebut, M. Brusati, M. Hugon, and P. Lallia, in Eleventh International Conference on Plasma Physics and Controlled Fusion Research, Kyoto, 1986 (International Atomic Energy Agency, 1987) p.187

FIGURE CAPTIONS

FIG. 1 Analytic self-consistency loop [or the flow chart] diagram for sawtoothing tokamak discharges. Here, the two large bold type connecting flow lines emanating from either side of the box labelled "Solution $\alpha_j(q_a)$" are uniquely due to the principle of profile consistency. The reversible lines with arrows pointing in both directions imply that an intrinsic self-consistency should exist among the forms of $j(r)$, $f_\sigma(r)$, $T_e(r)$, and $\chi_e(r)$ so as to safisfy the Ohm's law and the electron thermal energy-balance equation simultaneously.

FIG. 2 A plot of the normalized sawtooth inversion radius (r_1/a) vs $(1/q_a)$ for some TFTR discharges. Here, q_a is the limiter safety factor, and the dashed line is $(r_1/a) = (1/q_a)$.

FIG. 3a A comparison of $[\langle T_e\rangle/T_{eo}]_{EXP}$ vs $[\langle T_e\rangle/T_{eo}]_{TH}$ for Coppi-Tang model for some TFTR discharges including all those of Fig. 2. Here, —— is $[\langle T_e\rangle/T_{eo}]_{EXP} = [\langle T_e\rangle/T_{eo}]_{TH}$, and --- is $[\langle T_e\rangle/T_{eo}]_{EXP} = [\langle T_e\rangle/T_{eo}]_{TH} + 0.05$.

FIG. 3b A comparison of $[\langle T_e\rangle/T_{eo}]_{EXP}$ vs $[\langle T_e\rangle/T_{e1}]_{TH}$. for the same TFTR discharges. Here, $[\langle T_e\rangle/T_{e1}]_{TH} = [\langle T_e\rangle/T_{eo}]_{TH} \exp\{2(q_a + 0.5)/3q_a^2\}$. Here, the solid line is $[\langle T_e\rangle/T_{eo}]_{EXP} = [\langle T_e\rangle/T_{e1}]_{TH}$.

FIG. 4a A comparison of the theoretical and the experimental $T_e(r)$ profiles for a low q_a [= 2.9] TFTR discharge from Coppi-Tang model. Here, —— is experimental, and --- is theoretical.

FIG. 4b A comparison of the theoretical and the experimental $T_e(r)$ profiles for a high q_a [= 6.2] TFTR discharge from Coppi-Tang model. Here, —— is experimental, and --- is theoretical.

FIG. 5 A comparison of $[\langle T_e\rangle/T_{eo}]_{EXP}$ vs $[\langle T_e\rangle/T_{eo}]_{TH}$ for the chopped Coppi-Tang model for the same TFTR discharges with c = 1, i.e., $(r_f/a) = (r_1/a) = (1/q_a)$. Here, the solid line is theory.

FIG. 6a A comparison of the theoreticl and experimental $T_e(r)$ profiles for a low q_a [= 2.9] TFTR discharge from the chopped Coppi-Tang model with c = 1. Here, —— is experimental, and --- is theoretical.

FIG. 6b A comparison of the theoretical and experimental $T_e(r)$ profiles for a high q_a [= 6.2] TFTR discharge from the chopped Coppi-Tang model with c = 1. Here, —— is experimental, and --- is theoretical.

FIG. 7 A comparison of $[\langle T_e\rangle/T_{eo}]_{EXP}$ vs $[\langle T_e\rangle/T_{eo}]_{TH}$ for the Coppi-Tang model with a neoclassical conductivity from factor $f_\sigma(r) = (1 - 0.5\, r^2/a^2)$. Here, the solid line is theory.

FIG. 8 A comparison of $[\langle T_e\rangle/T_{eo}]_{EXP}$ vs $[\langle T_e\rangle/T_{eo}]_{TH}$ for q_a-dependent chopped exponential model with $(r_f/a) = (0.5r_1/a) = (0.5/q_a)$. Here, the solid line is theory.

FIG. 9 A plot of (r_1/a) vs $(1/q_a)$ for some TFTR discharges. Here, the curves A, B, and C are the theory for the chopped q_a-independent exponential, Fredrickson <u>et al.</u>, and the trapezoidal models, respectively, and the dashed line is $(r_1/a) = (1/q_a)$.

FIG. 10 A plot of $[\langle T_e\rangle/T_{eo}]$ vs $(1/q_a)$ for some TFTR discharges. Here the curves A, B, and C are the theory for the chopped q_a-independent exponential, Fredrickson et al., and the trapezoidal models, respectively.

FIG. 11a A comparison of $[\langle T_e\rangle/T_{eo}]_{EXP}$ vs $[\langle T_e\rangle/T_{eo}]_{TH}$ for the Kadomtsev optimal profile fits. Here, —— is $[\langle T_e\rangle/T_{eo}]_{EXP} = [\langle T_e\rangle/T_{eo}]_{TH}$, and --- is $[\langle T_e\rangle/T_{eo}]_{EXP} = [\langle T_e\rangle/T_{eo}]_{TH} + 0.05$.

FIG. 11b A comparison of $[\langle T_e\rangle/T_{eo}]_{EXP}$ vs $[\langle T_e\rangle/T_{eo}]_{TH}$ for the chopped Kadomtsev model. Here the solid line is theory.

FIG. 12a A comparison of the theoretical and experimental $T_e(r)$ profiles for a low q_a ($\approx$ 2.9) TFTR discharge from Campbell et al. of JET model. Here, —— is experimental, and --- is theoretical.

FIG. 12b A comparison of the theoretical and experimental $T_e(r)$ profiles for a high q_a ($\approx$ 6.2) TFTR discharge from Campbell et al. model. Here, —— is experimental, and --- is theoretical.

FIG. 13a A comparison of $[\langle T_e\rangle/T_{eo}]_{EXP}$ vs $[\langle T_e\rangle/T_{eo}]_{TH}$ for the Campbell et al. model. Here, —— is $[\langle T_e\rangle/T_{eo}]_{EXP} = [\langle T_e\rangle/T_{eo}]_{TH}$, and --- is $[\langle T_e\rangle/T_{eo}]_{EXP} = [\langle T_e\rangle/T_{eo}]_{TH} + 0.05$.

FIG. 13b A comparison of $[\langle T_e\rangle/T_{eo}]_{EXP}$ vs $[\langle T_e\rangle/T_{eo}]_{TH}$. for the chopped Campbell et al. model. Here, the solid line is theory.

FIG. 14a Radial dependence of the sawtooth amplitude for the flattened $T_e(r)$ profile with conservation of total plasma thermal energy as shown in the insert. The solid line is for the Kadomtsev value of $c_o = \sqrt{2}$ and the dashed line is for $c_o = 1$.

FIG. 14b Radial dependence of the sawtooth amplitude for the flattened $j(r)$ profile with conservation of total plasma current as shown in the insert. The solid line is for the Kadomtsev value of $c_o = \sqrt{2}$ and the dashed line is for $c_o = 1$.

FIG. 15a Plots of the central safety factor q(0) vs the limiter q_a for Coppi-Tang, Kadomtsev, and exponential models. Here, o and • are the measurements of Soltwisch et al. and West et al. respectively.

FIG. 15b. Plots of q(0) vs q_a for the modified exponential, and the Campbell et al. models.

TABLE 1A

SUMMARY TABLE

MODEL PROFILE	If $(r_1/a) = F_1(1/q_a) \approx (1/q_a)$, then	$F_2(1/q_a) = [\langle T_e\rangle/T_{eo}]_{TH}$	$[\langle T_e\rangle/T_{eo}]_{EXP}$ vs $[\langle T_e\rangle/T_{eo}]_{TH}$
1. Coppi-Tang (Spitzer η_s)	$\alpha_j \approx q_a + 0.5$	$F_2 = (3/2\alpha_j)[1-\exp(-2\alpha_j/3)]$	EXP ≈ TH + 0.05
2. Chopped Coppi-Tang (c=1, Spitzer η_s)	$\alpha_j \approx q_a^2(q_a-1)^{-1}$	$F_2 = (3/2\alpha_j)\{1-\exp[-(2\alpha_j/3)(1-q_a^{-2})]\} + q_a^{-2}$	Good fit for $q_a < 5$, poor fit for higher q_a.
3. Coppi-Tang [$\eta_{nc} = \eta_s(1-d\,r^2/a^2)^{-1}$]	$\alpha_j \approx q_a + 0.5 - d$	$F_2 = (3/2\alpha_j)[1-\exp(-2\alpha_j/3)]$	Good fit for $q_a < 6$, poor fit for higher q_a.
4. Exponential (q_a-dependent)	$\alpha_j \approx (2q_a + 1)^{1/2}$	$F_2 = (9/2\alpha_j^2)[1-(1 + 2\alpha_j/3)\exp(-2\alpha_j/3)]$	Bad fit.
5. Chopped Exponential (c=1, q_a-dependent)	$\alpha_j \approx (q_a + 1)^{1/2}$	$F_2 = (9/2\alpha_j^2)\{1 + (2\alpha_j/3q_a) + (2\alpha_j^2/9q_a^2)-(1 + 2\alpha_j/3)\exp[-(2\alpha_j/3)(1-1/q_a)]\}$	Bad fit for c = 1, but fair fit for c ≈ 0.5.
6. Exponential (q_a-independent)	$q_a \approx 1.25$	$F_2 \neq F_2(1/q_a) \approx 0.43$	Meaningless for $(r_1/a) \approx (1/q_a)$ since $F_2 \neq F_2(1/q_a)$.
7. Chopped Exponential (c=1, q_a-independent)	$q_a \approx 3.13$	$F_2 \neq F_2(1/q_a) \approx 0.65$	Meaningless for $(r_1/a) \approx (1/q_a)$ since $F_2 \neq F_2(1/q_a)$.

TABLE 1A (continued)

MODEL PROFILE	If $(r_1/a) = F_1(1/q_a)$ $\approx (1/q_a)$, then	$F_2(1/q_a) = [\langle T_e\rangle/T_{eo}]_{TH}$	$[\langle T_e\rangle/T_{eo}]_{EXP}$ vs $[\langle T_e\rangle/T_{eo}]_{TH}$
8. Modified Exponential [q_a-dependent, Eq. (4.8)]	$\alpha_J = (1-1/q_a)^{-1}\log q_a$	$F_2 = \exp(-2\alpha_J/3)$	Bad fit.
9. Modified Exponential [q_a-independent, Eq. (4.13)]	$q_a \approx 4.92$	$F_2 \neq F_2(1/q_a) \approx 0.14$	Meaningless for $(r_1/a) \approx (1/q_a)$ since $F_2 \neq F_2(1/q_a)$.
10. Trapezoidal	$q_a \approx 1$ or 1.88 [(r_1/a) vs q_a^{-1} is parabola]	$F_2 \neq F_2(1/q_a) = 1$ or 0.61 [$F_2 \approx (1/9) + (35/36)\, q_a^{-1}$]	Meaningless for $(r_1/a) \approx (1/q_a)$ since $F_2 \neq F_2(1/q_a)$. [Excellent fit for $q_a < 4.4$]
11. Kadomtsev	$(a_*/a)^2 = q_a{}^{-1}$	$F_2 = 3q_a^{-1}[1-(q_a + 1)^{-1/3}]$	EXP $\approx$ TH + 0.05
12. Chopped Kadomtsev (c=1)	$(a_*/a)^2=(q_a-1)^{-1}$ $[1-2q_a^{-1}+q_a^{-3}]$	$F_2 = q_a^{-2}+3(a_*/a)^2\{1 + q_a^{-2}$ $(a^2/a_*^2)-(1 + a^2/a_*^2)^{-1/3}$ $[1 + q_a^{-2}(a^2/a_*^2)]\}^{4/3}$	Good fit for $q_a < 6$, poor fit for higher q_a.
13. Campbell et al.	$\nu_J \approx q_a - 0.5$	$F_2 = (1 + 2\nu_J/3)^{-1}$	EXP $\approx$ TH + 0.05.
14. Chopped Campbell et al. (c=1)	$\nu_J = q_a$	$F_2=q_a^{-2}+(1-q_a^{-2})(1+2q_a/3)^{-1}$	Fair fit for $q_a < 4$, poor fit for higher q_a.

TABLE 1B

SUMMARY TABLE

MODEL PROFILE	MEASURED $T_e(r)$ FIT WHEN $(r_1/a) \approx 1/q_a$		REDUCED COORDINATES; (UNIVERSALITY OF PROFILES)	$F_p = [I_p(a \text{ to } \infty)/I_p(0 \text{ to } \infty)]$
	FOR LOW q_a	FOR HIGH q_a		
1.	Good for $r > r_1$	Good	$j_o = (2B_T/\mu_o R q_o)$, $a_{eff}^2 \approx (q_o \mu_o R I_p / 2\pi B_T)$; (Yes)	$F_p = \exp(-\alpha_j)$
2.	Good	Fair for $r > r_1$	$j_o = (2B_T/\mu_o R q_o)$, $a_{eff}^2 \approx (q_o \mu_o R I_p / 2\pi B_T)$; (Yes)	$F_p = (1+\alpha_j^2/q_a^2)^{-1} \exp[-\alpha_j(1-1/q_a^2)]$
3.	Good for $r > r_1$	Fair	Same as 1 for $d \propto \alpha_j$, do not exist for $d \neq d(\alpha_j)$	$F_p = [(d/\alpha_j)\exp(-\alpha_j/d) + (1-d-d/\alpha_j)\exp(-\alpha_j)] [(d/\alpha_j)\exp(-\alpha_j/d)+(1-d/\alpha_j)]^{-1}$
4.	Bad	Fair for $r > r_1$	$j_o = (2B_T/\mu_o R q_o)$, $a_{eff}^2 \approx (q_o \mu_o R I_p / 4\pi B_T)$; (Yes)	$F_p = (1 + \alpha_j)\exp(-\alpha_j)$
5.	Bad	Bad for c=1, but fair for $r > r_1$ and c=0.5	$j_o = (2B_T/\mu_o R q_o)$, $a_{eff}^2 \approx (q_o \mu_o R I_p / 4\pi B_T)$; (Yes)	$F_p = \{(1+\alpha_j)\exp[-\alpha_j(1-1/q_a)]\} \{1+\alpha_j/q_a+\alpha_j^2/q_a^2\}^{-1}$
6.	Meaningless for $r_1/a \approx 1/q_a$	Meaningless for $r_1/a \approx 1/q_a$	Do not exist; (No)	$F_p = 3\exp(-2) \approx 0.406$

TABLE 1B (continued)

MODEL PROFILE	MEASURED $T_e(r)$ FIT WHEN $(r_1/a) \approx 1/q_a$ FOR LOW q_a	FOR HIGH q_a	REDUCED COORDINATES; (UNIVERSALITY OF PROFILES)	$F_p = [I_p(a \text{ to } \infty)/I_p(o \text{ to } \infty)]$
7.	Meaningless for $r_1/a \approx 1/q_a$	Meaningless for $r_1/a \approx 1/q_a$	Do not exist; (No)	$F_p = \{3\exp[-2(1-1/q_a)]\}$ $\{1+2/q_a+4/q_a^2\}^{-1}$
8.	Good for $r > r_1$	Fair for $r > 0.4a$	$j_o = (2B_T/\mu_o R q_o)$, $a_{eff} \approx (a/\log q_a)$; (Yes)	$F_p = [1-(\alpha_J^2/4)\exp(2-\alpha_J)]$
9.	Meaningless for $r_1/a \approx 1/q_a$	Meaningless for $r_1/a \approx 1/q_a$	Do not exist; (No)	$F_p = 0$
10.	Meaningless for $r_1/a \approx 1/q_a$	Meaningless for $r_1/a \approx 1/q_a$	Do not exist; (No)	$F_p = 0$
11.	Bad	Fair	$j_o = (2B_T/\mu_o R q_o)$, $a_{eff}^2 = (\mu_o R I_p/2\pi B_T)$; (Yes)	$F_p = (1+a^2/a_*^2)^{-1}$
12.	Fair for $r < 0.9a$	Fair for $r > r_1$	$j_o = (2B_T/\mu_o R q_o)$, $a_{eff}^2 \approx (\mu_o R I_p/2\pi B_T)$; (Yes)	$F_p = (1+r_f^2/a_*^2)^2\ [(1+2r_f^2/a_*^2)$ $(1+a^2/a_*^2)]^{-1}$
13.	Good for $r > r_1$	Fair	Do not exist; (No)	$F_p = 0$
14.	Good	Fair for $r > r_1$	Do not exist; (No)	$F_p = 0$

TABLE 1C

SUMMARY TABLE

MODEL PROFILE	$F_3(q_a) = (q_a/q_o) = (\pi a^2 j_o/I_p)$ $= (a^2 V_L T_{eo}^{3/2}/2b\ I_p\ R\ Z_{eff})$	T_{eo}-SCALING LAW FOR LOW n_e	FOR HIGH n_e
1	$F_3 = \alpha_j[1 - \exp(-\alpha_j)]^{-1}$	$T_{eo} \propto [B_T^{2/3}\ a^{2/3}\ Z_{eff}^{4/15}\ m_i^{2/15}\ R^{-2/3}\ n_e^{-2/15}]$	$(T_{eo} - T_{io}) \propto B_T^2\ m_i\ R^{-2}\ n_e^{-2}$
2	$F_3 = q_a$		
3	$F_3 = \alpha_j[1 - d/\alpha_j - (1 - d - d/\alpha_j)\ \exp(-\alpha_j)]^{-1}$	$T_{eo} \propto [B_T^{2/3}\ a^{2/3}\ Z_{eff}^{4/15}\ m_i^{2/15}\ R^{-2/3}\ n_e^{-2/15}]$	$(T_{eo} - T_{io}) \propto B_T^2\ m_i\ R^{-2}\ n_e^{-2}$
4	$F_3 = (\alpha_j^2/2)[1 - (\alpha_j + 1)\ \exp(-\alpha_j)]^{-1}$	$T_{eo} \propto [B_T\ a^{4/3}\ Z_{eff}^{4/15}\ R^{-1}\ I_p^{-1/3}\ n_e^{-2/15}]$	$(T_{eo} - T_{io}) \propto B_T^2\ m_i\ R^{-2}\ n_e^{-2}$
5	$F_3 = q_a$		
6	$F_3 \approx 3.367$	$T_{eo} \propto [I_p^{2/3}\ Z_{eff}^{4/15}\ m_i^{2/15}\ a^{-2/3}\ n_e^{-2/15}]$	$(T_{eo} - T_{io}) \propto I_p^2\ m_i\ n_e^{-2}\ a^{-4}$
7	$F_3 = q_a$		

TABLE 1C (continued)

MODEL PROFILE	$F_3(q_a) = (q_a/q_o) = (\pi a^2 j_o/I_p)$ $= (a^2 V_L\, T_{eo}^{3/2}/2b\, I_p\, R\, Z_{eff})$	T_{eo}-SCALING LAW FOR LOW n_e	FOR HIGH n_e
8	$F_3 = \exp \alpha_j$	$T_{eo} \propto [B_T^{4/3}\, a^2\, Z_{eff}^{4/15}\, m_i^{2/15}\, n_e^{-2/15}\, R^{-4/3}\, I_p^{-2/3}]\, [\log(2\pi a^2 B_T/\mu_o R I_p]^{-2/3}$	$(T_{eo} - T_{io}) \propto B_T^2\, m_i\, R^{-2}\, n_e^{-2}$
9	$F_3 = 7.407$	$T_{eo} \propto [I_p^{2/3}\, Z_{eff}^{4/15}\, m_i^{2/15}\, a^{-2/3}\, n_e^{-2/15}]$	$(T_{eo} - T_{io}) \propto I_p^2\, m_i\, n_e^{-2}\, a^{-4}$
10	$F_3 = q_a$		
11	$F_3 = [(a^2/a_*^2) + 1]$	$T_{eo} \propto [B_T^{2/3}\, a^{2/3}\, Z_{eff}^{4/15}\, m_i^{2/15}\, R^{-2/3}\, n_e^{-2/15}]$	$(T_{eo} - T_{io}) \propto B_T^2\, m_i\, R^{-2}\, n_e^{-2}$
12	$F_3 = q_a$		
13	$F_3 = (\nu_j + 1)$	$T_{eo} \propto [B_T^{2/3}\, a^{2/3}\, Z_{eff}^{4/15}\, m_i^{2/15}\, R^{-2/3}\, n_e^{-2/15}]$	$(T_{eo} - T_{io}) \propto B_T^2\, m_i\, R^{-2}\, n_e^{-2}$
14	$F_3 = \nu_j$		

#88X0717

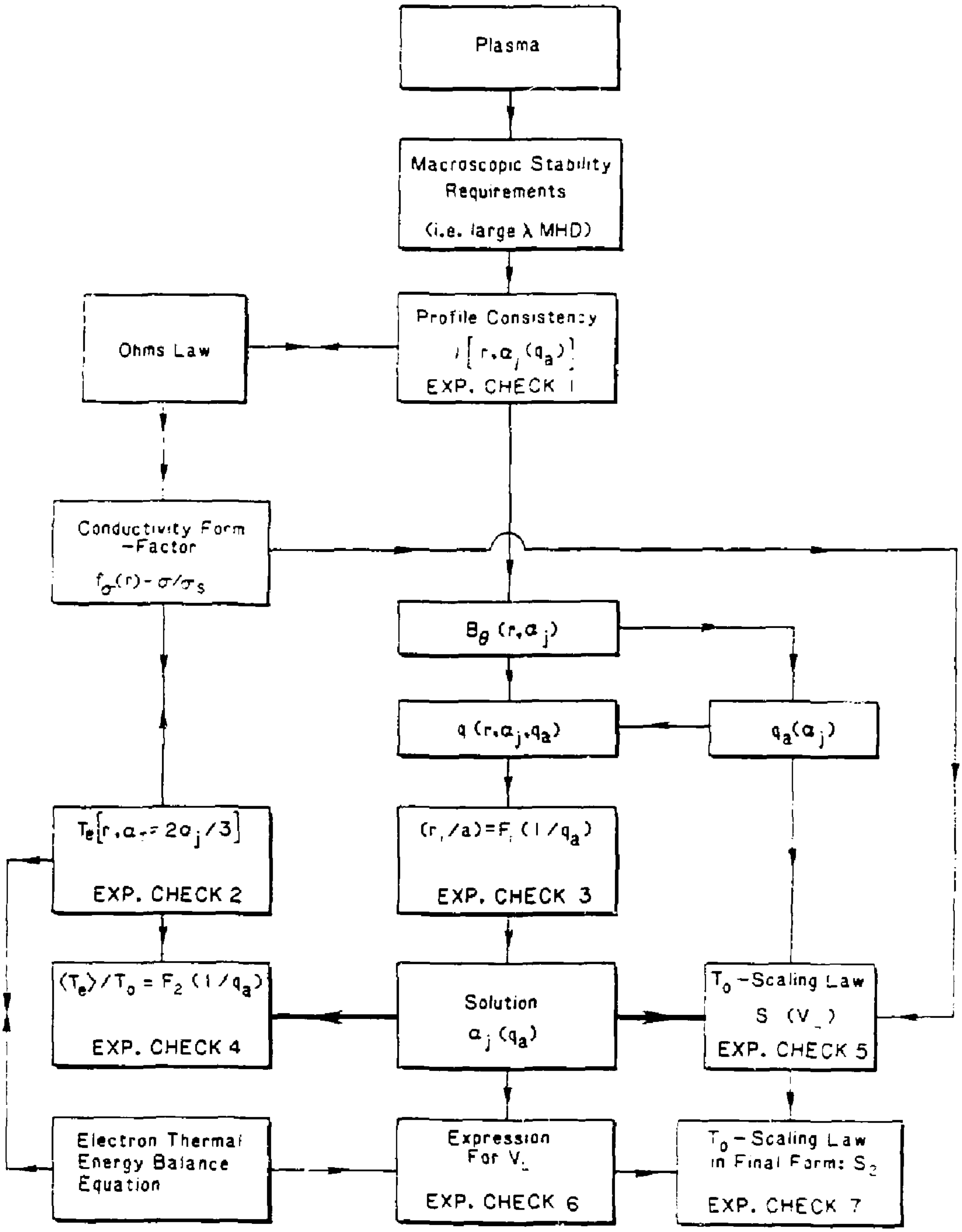

Fig. 1

#88X0041

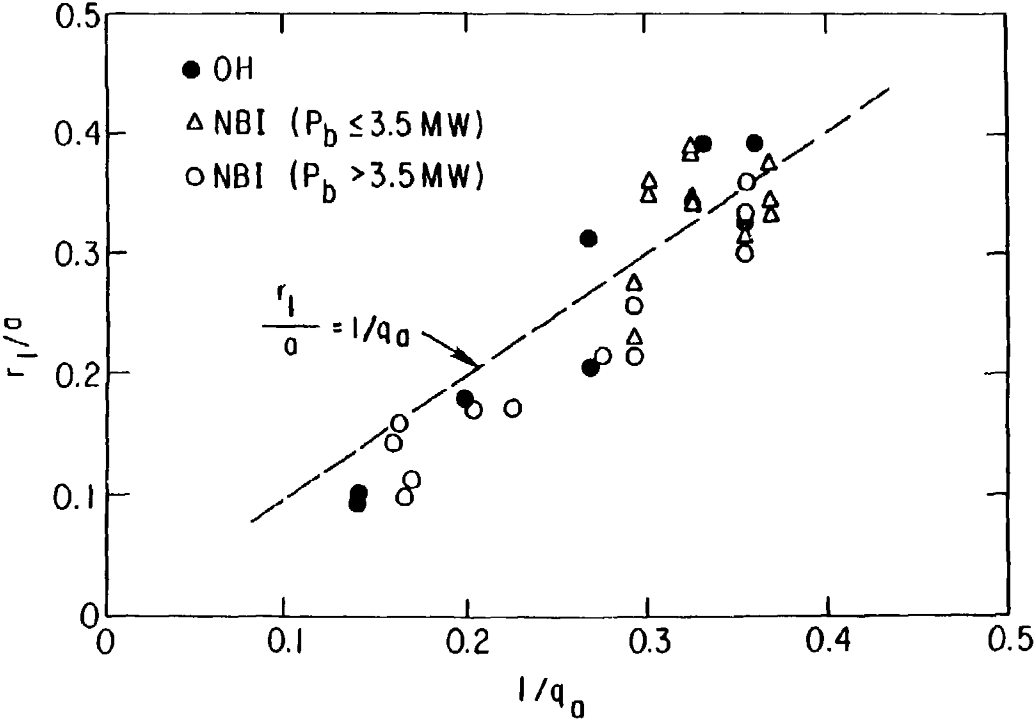

OH
NBI ($P_b \leq 3.5$ MW)
NBI ($P_b > 3.5$ MW)
$\frac{r_1}{a} = 1/q_a$
r_1/a
$1/q_a$
0
0.1
0.2
0.3
0.4
0.5

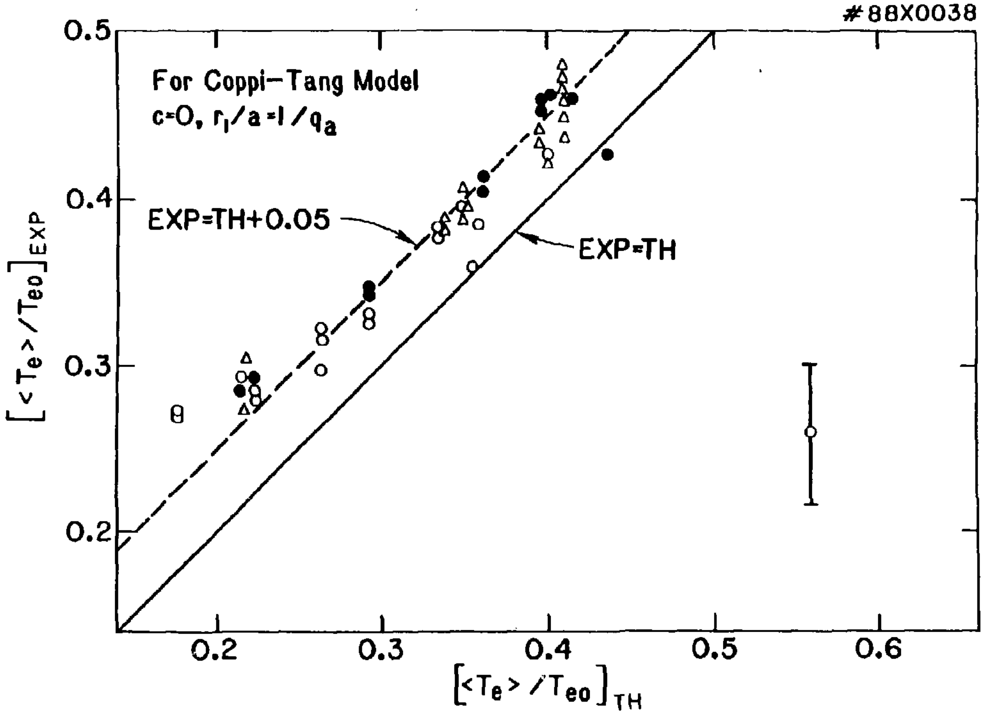
#88X0038
For Coppi-Tang Model
c=0, r1/a=1/qa
EXP=TH+0.05
EXP=TH
0.5
0.4
0.3
0.2
0.6
[<Te>/Teo]EXP
[<Te>/Teo]TH

Fig. 3a

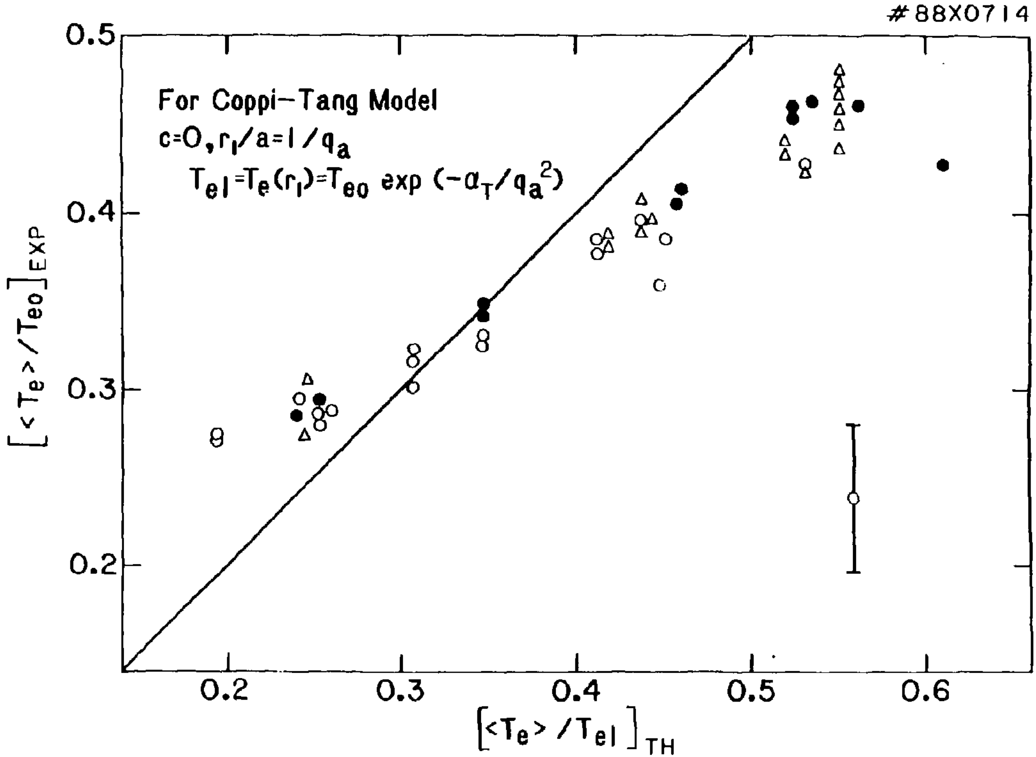

#88X0714
For Coppi-Tang Model
c=O, r_I/a=1/q_a
T_eI=T_e(r_I)=T_eo exp (-α_T/q_a^2)
[<T_e>/T_eo]_EXP
[<T_e>/T_eI]_TH
0.5
0.4
0.3
0.2
0.2
0.3
0.4
0.5
0.6

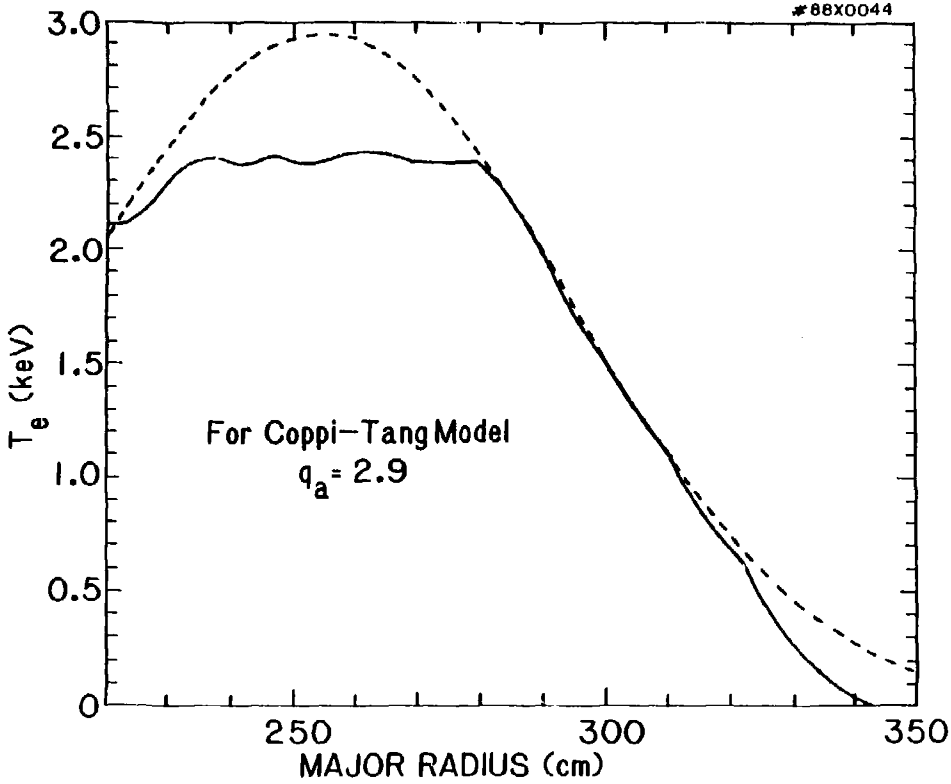
#88X0044
3.0
2.5
2.0
1.5
1.0
0.5
0
T_e (keV)
For Coppi–Tang Model
q_a = 2.9
250
300
350
MAJOR RADIUS (cm)

Fig. 4a

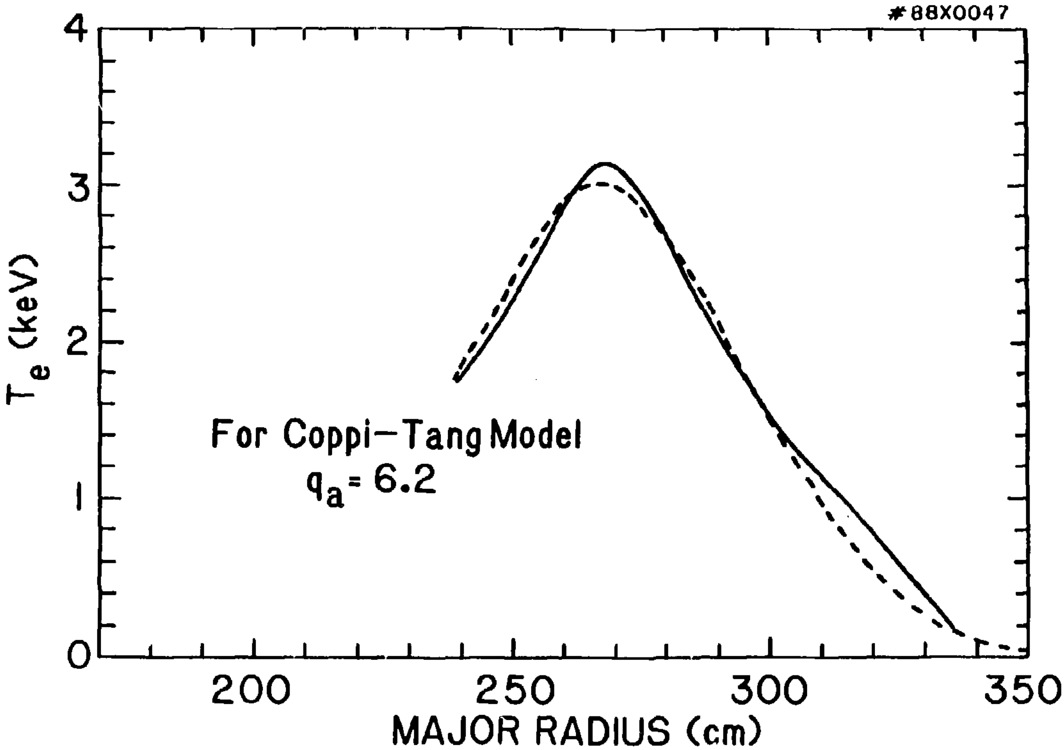

#88X0047
4
3
2
1
0
T_e (keV)
For Coppi–Tang Model
q_a = 6.2
200
250
300
350
MAJOR RADIUS (cm)

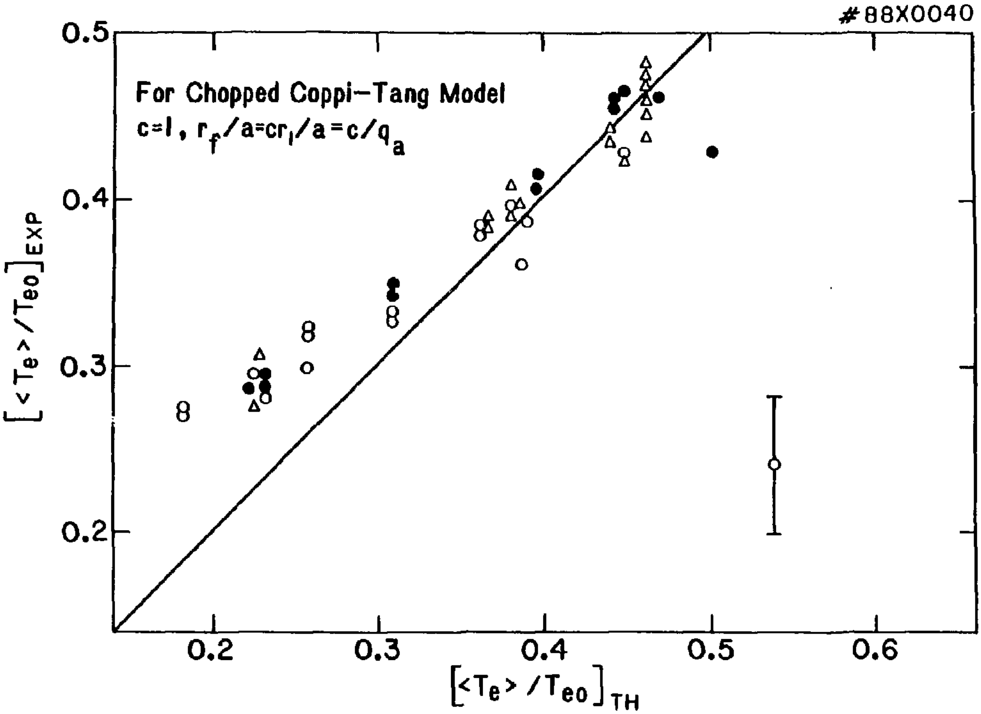
#88X0040
For Chopped Coppi–Tang Model
c=1, r_f/a=cr_1/a=c/q_a
[<Te>/Teo]_EXP
[<Te>/Teo]_TH
0.2
0.3
0.4
0.5
0.6

Fig. 5

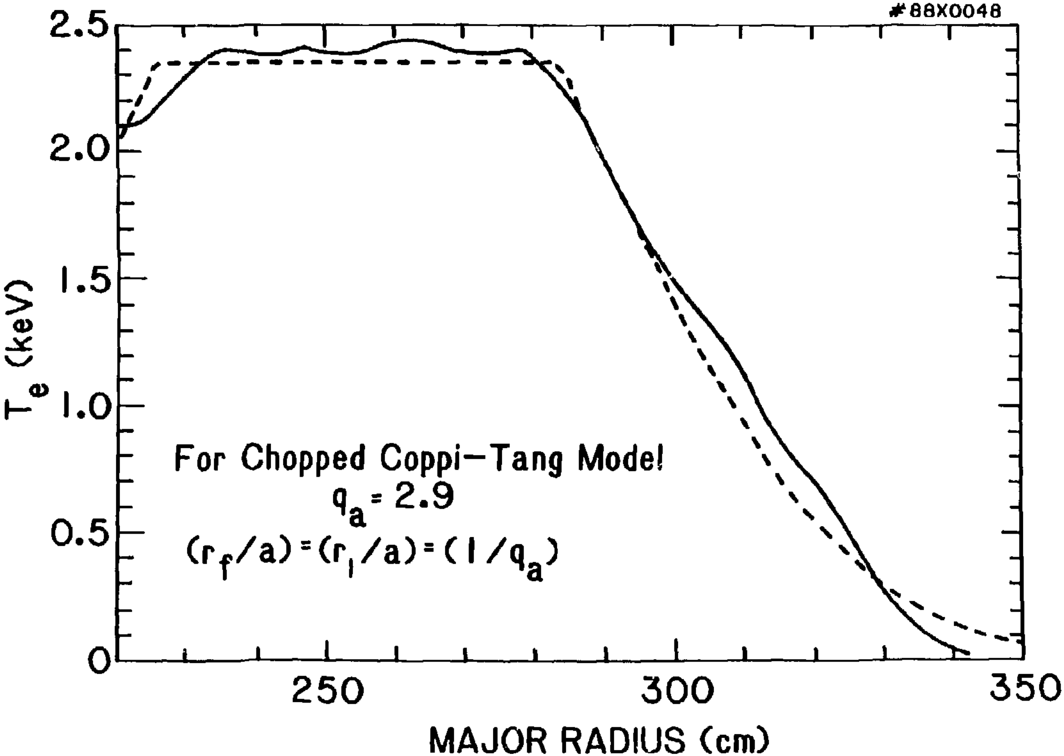
#88X0048
2.5
2.0
1.5
1.0
0.5
0
T_e (keV)
250
300
350
MAJOR RADIUS (cm)
For Chopped Coppi–Tang Model
$q_a = 2.9$
$(r_f/a) = (r_1/a) = (1/q_a)$

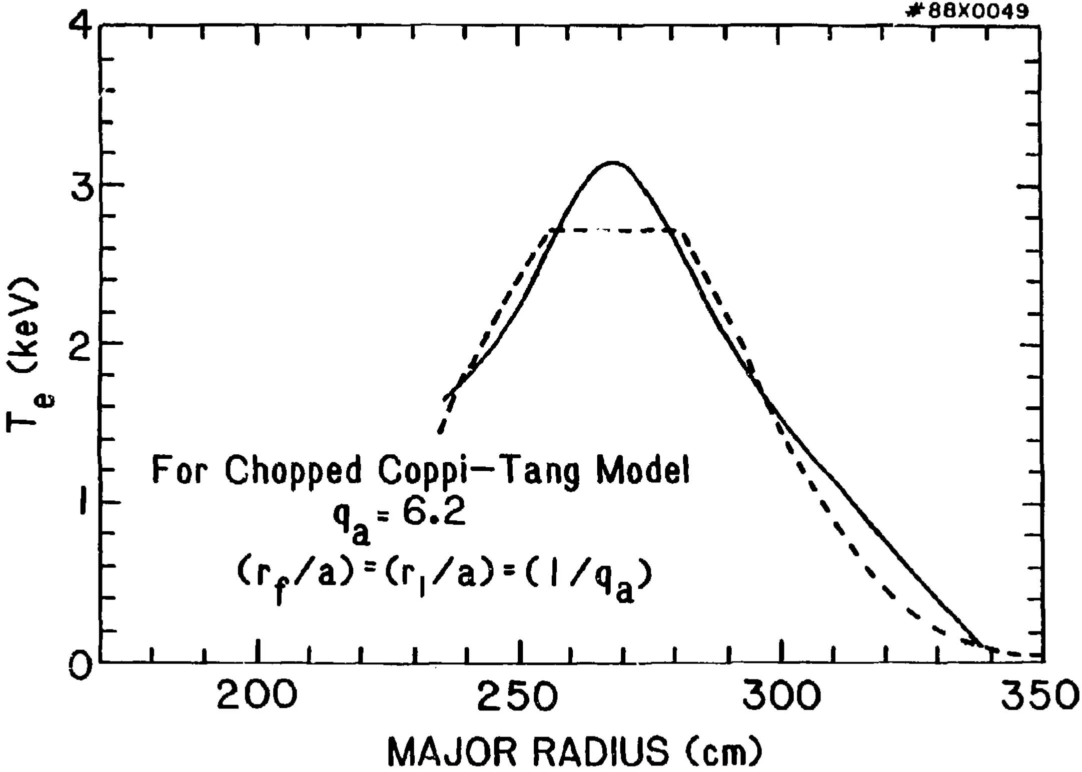
#88X0049
T_e (keV)
0
1
2
3
4
200
250
300
350
MAJOR RADIUS (cm)
For Chopped Coppi–Tang Model
$q_a = 6.2$
$(r_f/a) = (r_1/a) = (1/q_a)$

Fig. 6b

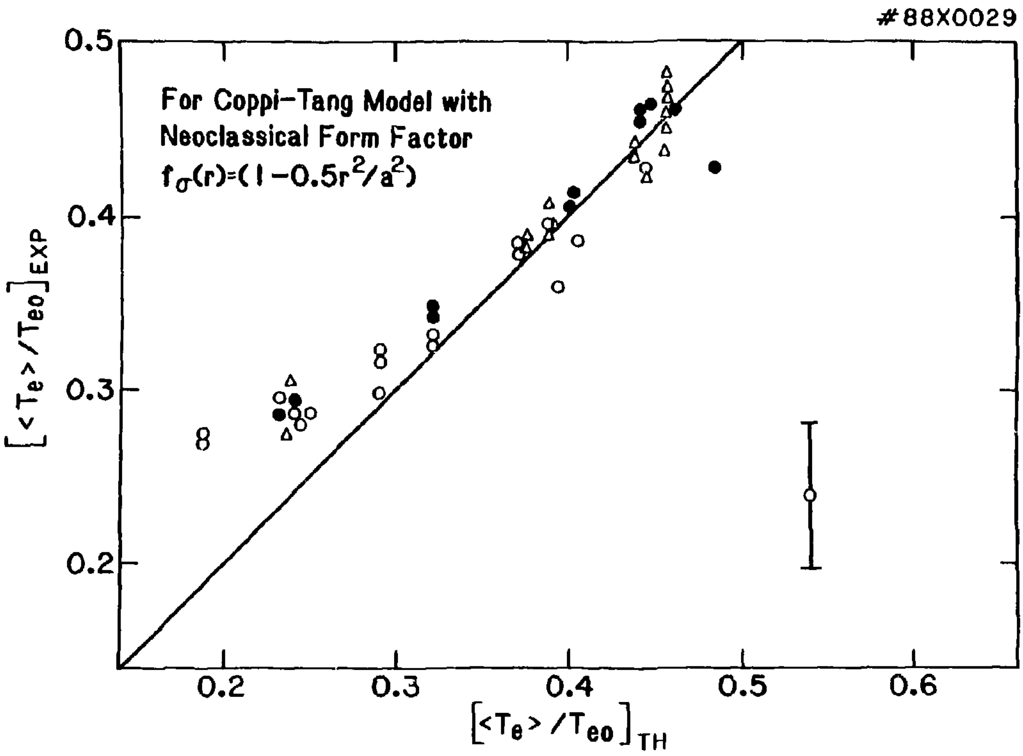
#88X0029
For Coppi-Tang Model with
Neoclassical Form Factor
$f_\sigma(r)=(1-0.5r^2/a^2)$
0.5
0.4
0.3
0.2
0.6
$[\langle T_e \rangle / T_{eo}]_{EXP}$
$[\langle T_e \rangle / T_{eo}]_{TH}$

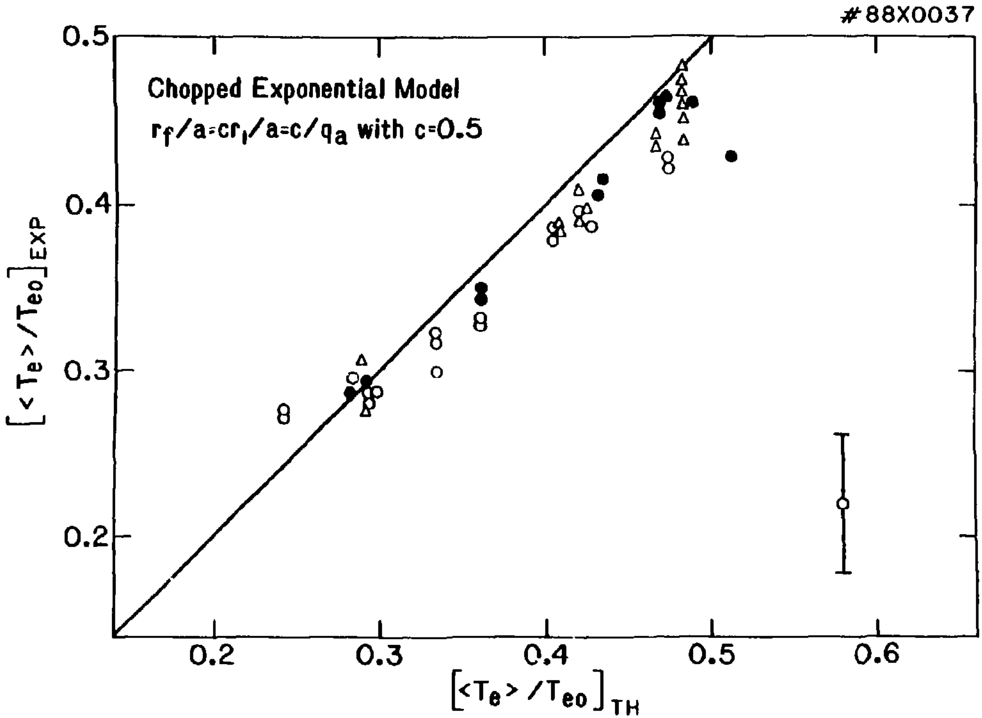
#88X0037
Chopped Exponential Model
$r_f/a=cr_l/a=c/q_a$ with c=0.5
0.5
0.4
0.3
0.2
$[\langle T_e \rangle / T_{eo}]_{EXP}$
0.2
0.3
0.4
0.5
0.6
$[\langle T_e \rangle / T_{eo}]_{TH}$

Fig. 8

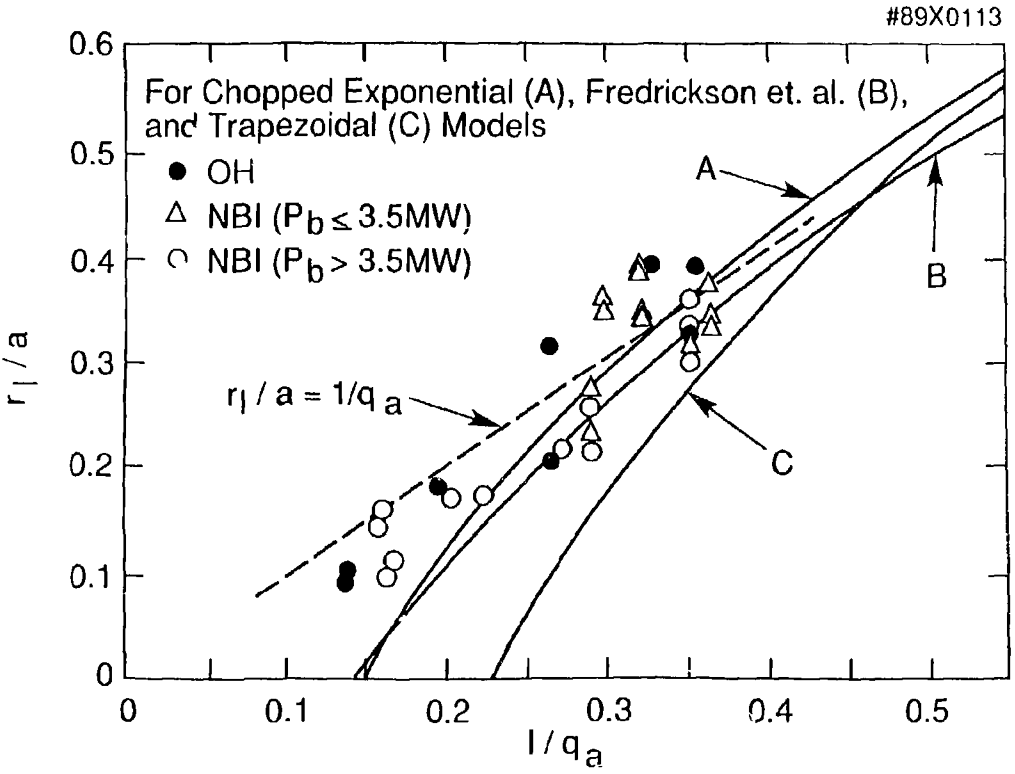

#89X0113
For Chopped Exponential (A), Fredrickson et. al. (B), and Trapezoidal (C) Models
OH
NBI ($P_b \le 3.5$MW)
NBI ($P_b > 3.5$MW)
A
B
C
$r_l / a = 1/q_a$
r_l / a
$1 / q_a$
0.6
0.5
0.4
0.3
0.2
0.1
0
0.1
0.2
0.3
0.4
0.5

#89X0114

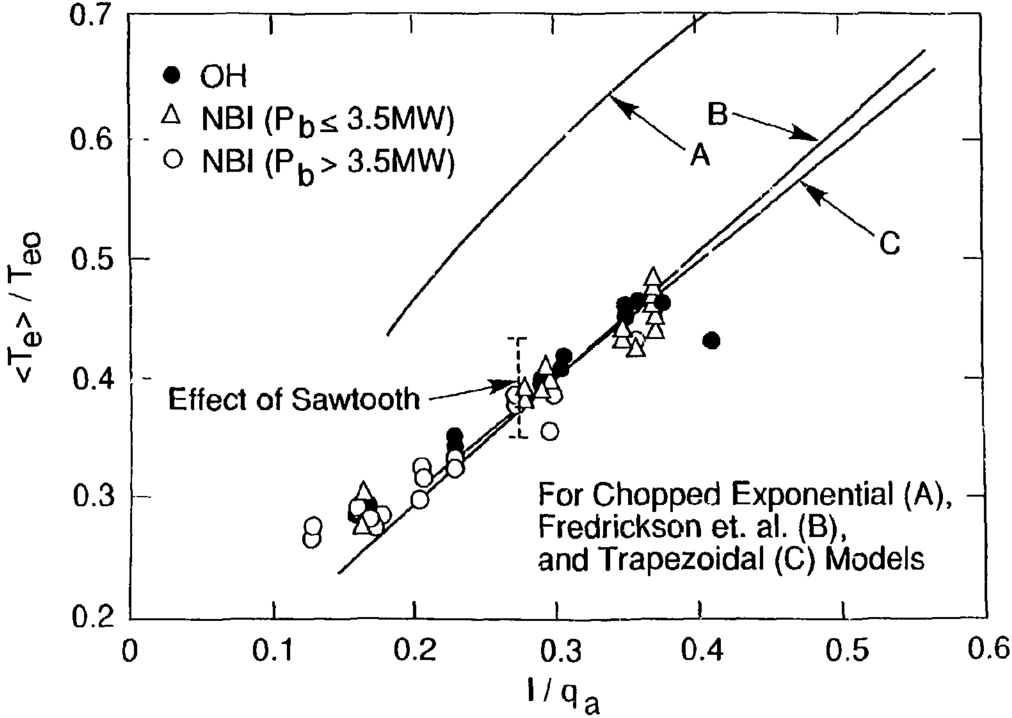

Fig. 10

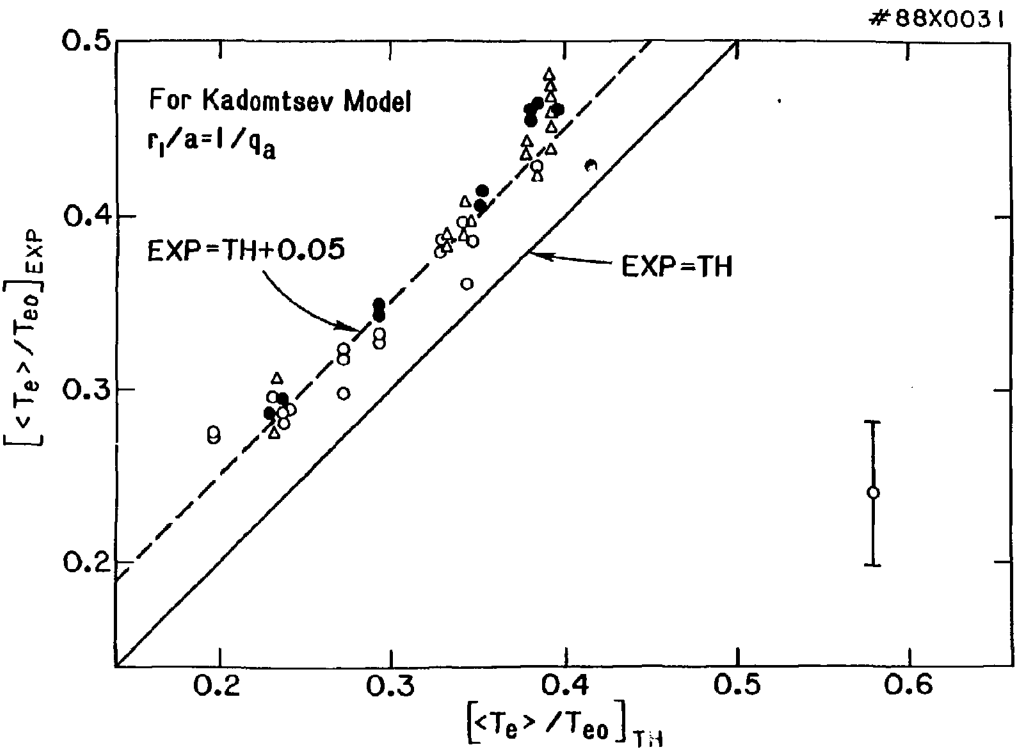

#88X0031
For Kadomtsev Model
$r_1/a = 1/q_a$
EXP=TH+0.05
EXP=TH
0.5
0.4
0.3
0.2
0.2
0.3
0.4
0.5
0.6
$[\langle T_e \rangle / T_{eo}]_{EXP}$
$[\langle T_e \rangle / T_{eo}]_{TH}$

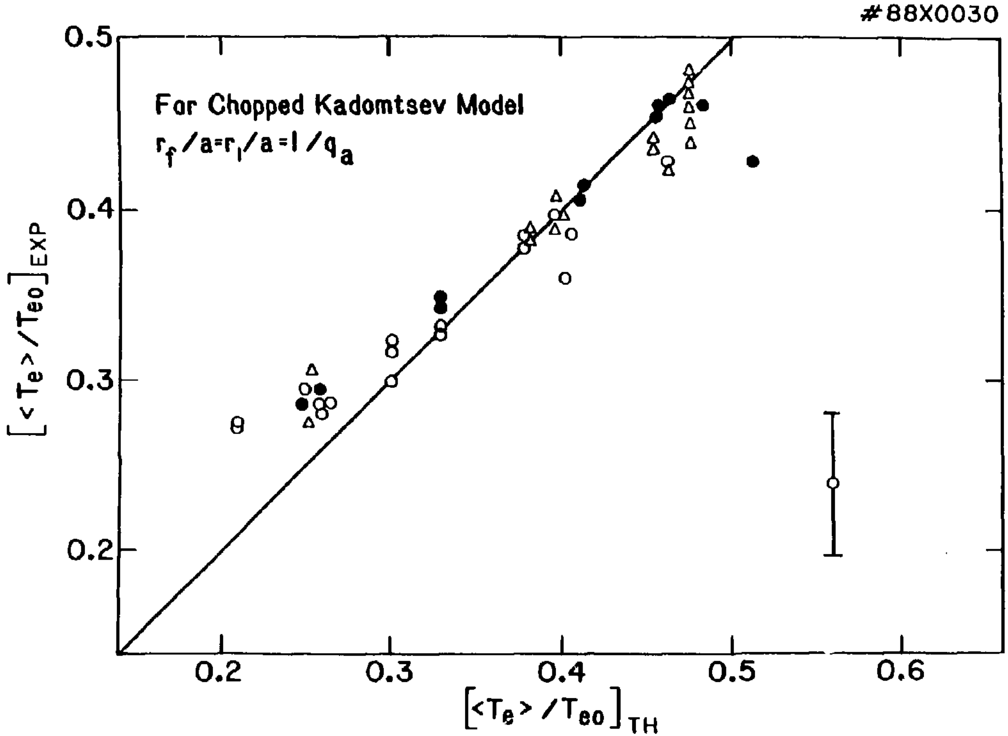

#88X0030
For Chopped Kadomtsev Model
$r_f/a = r_1/a = 1/q_a$
0.5
0.4
0.3
0.2
0.2
0.3
0.4
0.5
0.6
$[\langle T_e \rangle / T_{e0}]_{EXP}$
$[\langle T_e \rangle / T_{e0}]_{TH}$

Fig. 11b

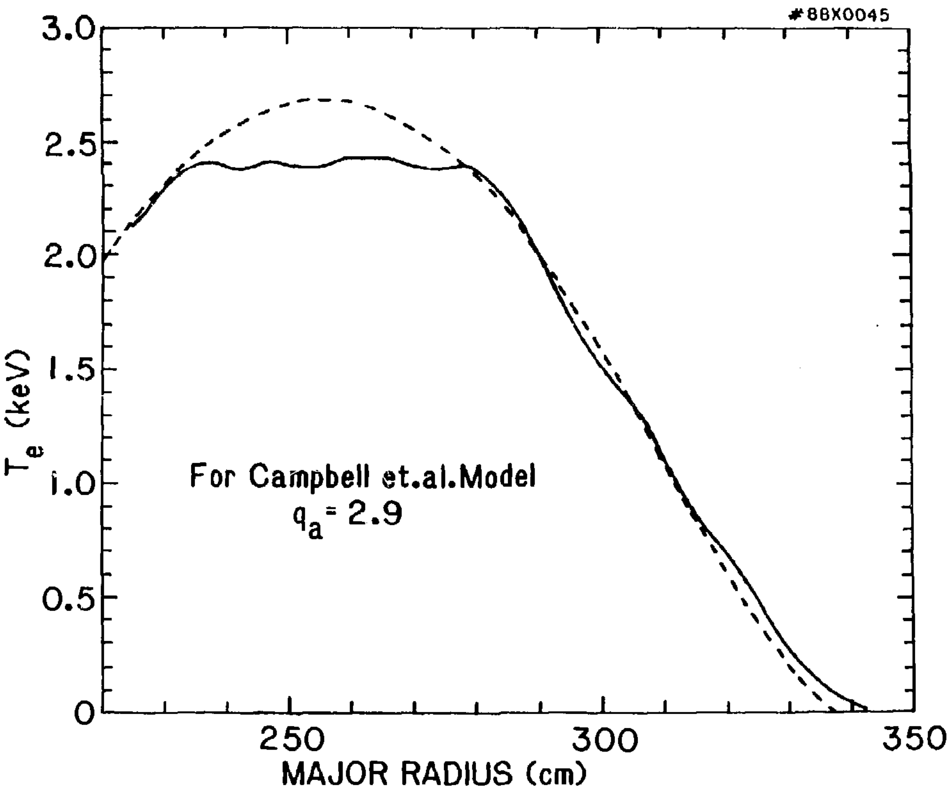

#88X0045
3.0
2.5
2.0
1.5
1.0
0.5
0
T_e (keV)
For Campbell et.al.Model
q_a = 2.9
250
300
350
MAJOR RADIUS (cm)

#88X0046

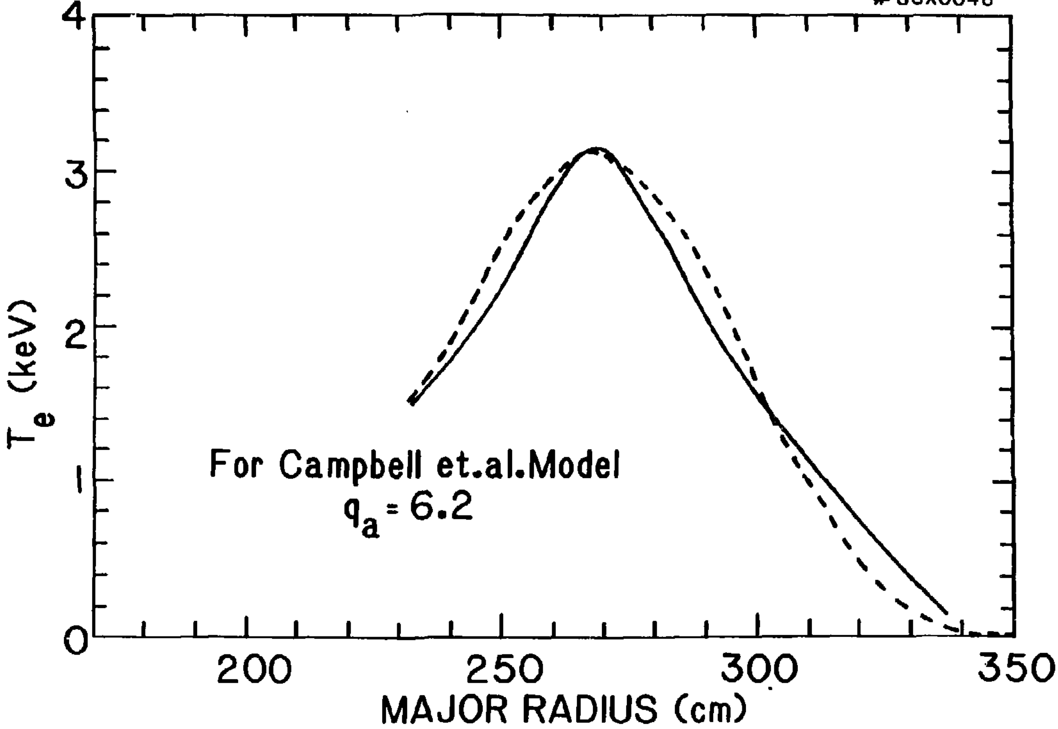

Fig. 12b

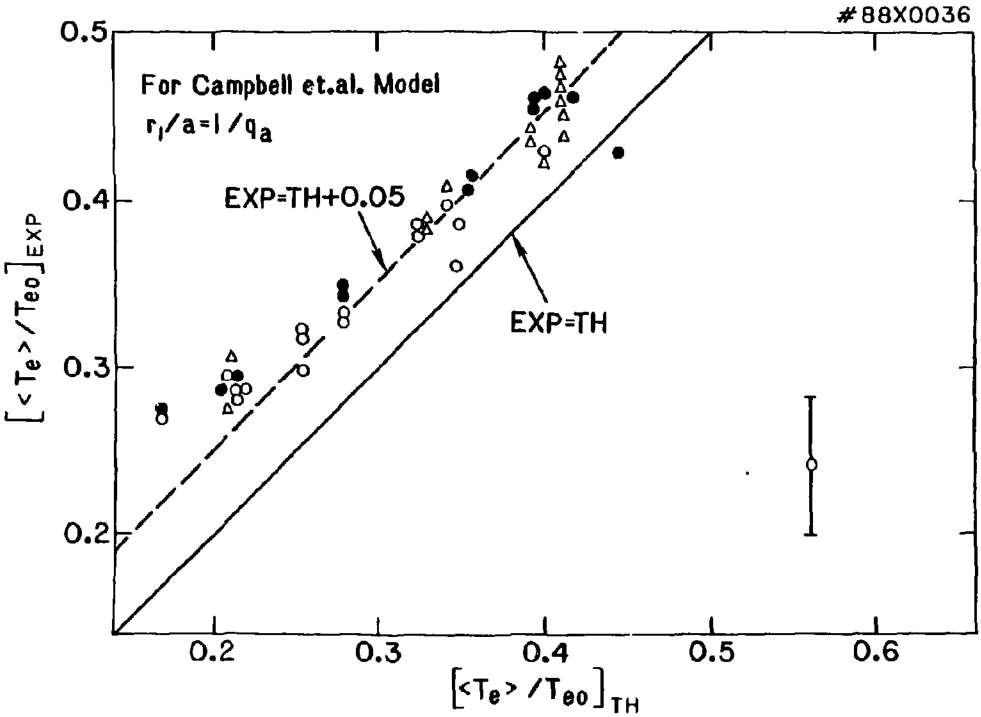
#88X0036
For Campbell et.al. Model
$r_1/a=1/q_a$
EXP=TH+0.05
EXP=TH
$[\langle T_e\rangle/T_{eo}]_{EXP}$
$[\langle T_e\rangle/T_{eo}]_{TH}$
0.2
0.3
0.4
0.5
0.6

#88X0035

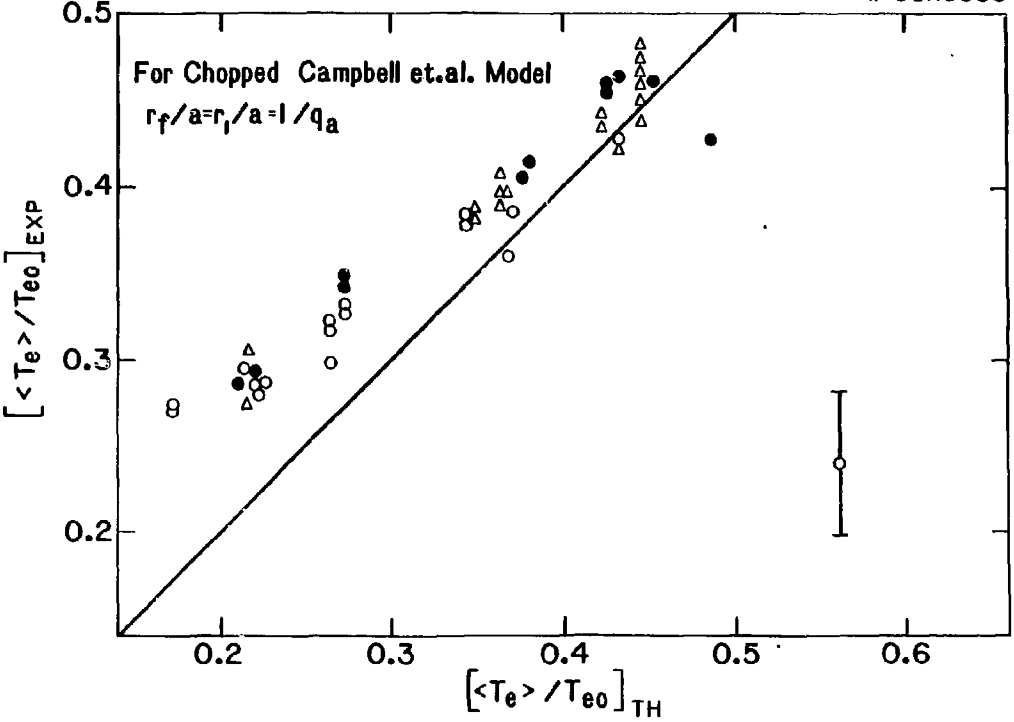

Fig. 13b

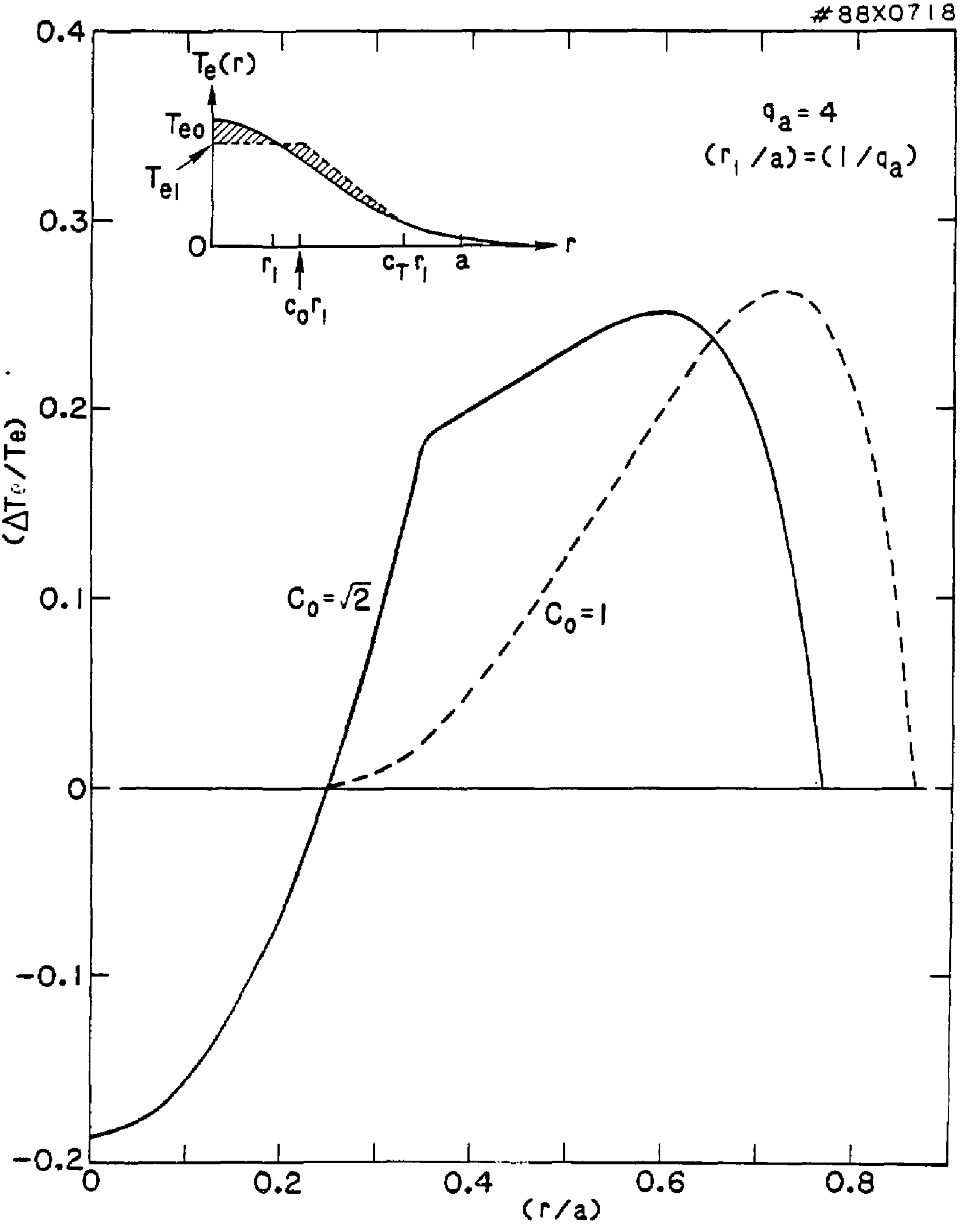
#88X0718
$T_e(r)$
T_{e0}
T_{e1}
O
r_1
$c_0 r_1$
$c_T r_1$
a
r
$q_a = 4$
$(r_1/a) = (1/q_a)$
$C_0 = \sqrt{2}$
$C_0 = 1$
$(\Delta Te/Te)$
(r/a)
0.4
0.3
0.2
0.1
0
-0.1
-0.2
0
0.2
0.4
0.6
0.8

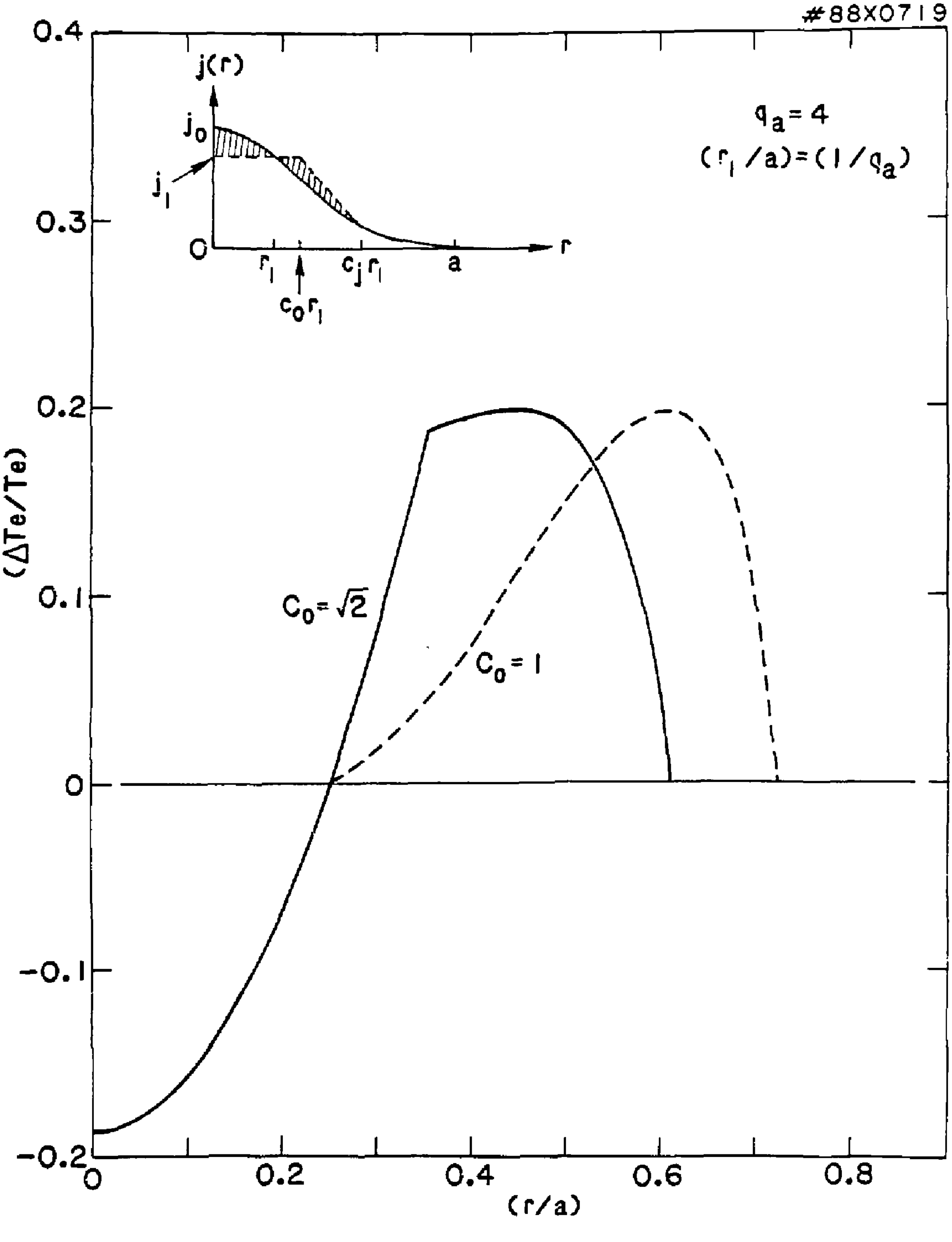
#88X0719
0.4
0.3
0.2
0.1
0
-0.1
-0.2
(ΔTe/Te)
0
0.2
0.4
0.6
0.8
(r/a)
j(r)
j_0
j_1
0
r_1
$c_0 r_1$
$c_j r_1$
a
r
$q_a = 4$
$(r_1/a) = (1/q_a)$
$C_0 = \sqrt{2}$
$C_0 = 1$

Fig. 14b

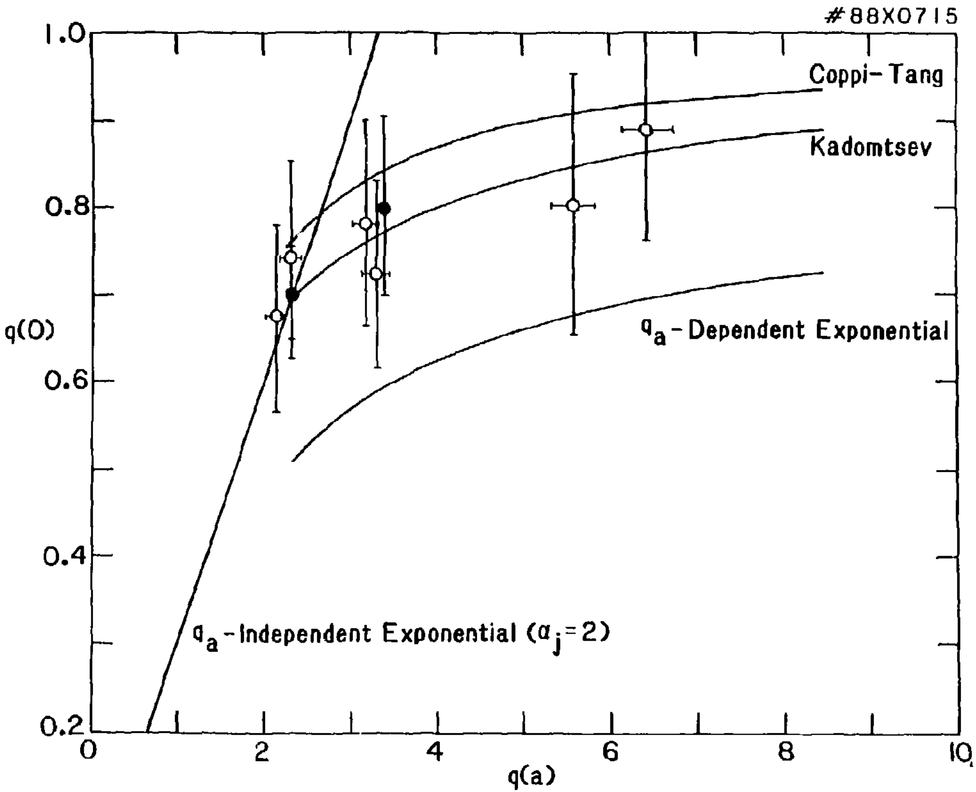
#88X0715
1.0
0.8
0.6
0.4
0.2
q(0)
0
2
4
6
8
10
q(a)
Coppi-Tang
Kadomtsev
q_a - Dependent Exponential
q_a - Independent Exponential ($\alpha_j = 2$)

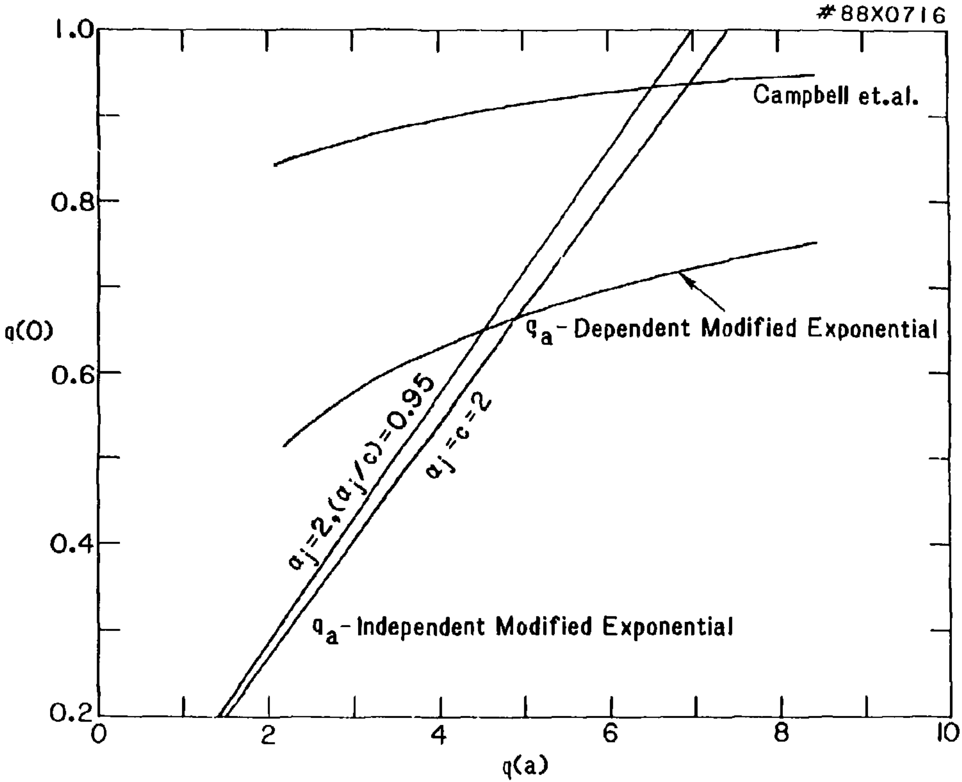
#88X0716
1.0
0.8
0.6
0.4
0.2
0
2
4
6
8
10
q(0)
q(a)
Campbell et.al.
qa - Dependent Modified Exponential
aj=2,(aj/c)=0.95
aj=c=2
qa - Independent Modified Exponential

Fig. 15b

EXTERNAL DISTRIBUTION IN ADDITION TO UC-420

Dr. Frank J. Paoloni, Univ of Wollongong, AUSTRALIA
Prof. M.H. Brennan, Univ Sydney, AUSTRALIA
Plasma Research Lab., Australian Nat. Univ., AUSTRALIA
Prof. I.R. Jones, Flinders Univ., AUSTRALIA
Prof. F. Cap, Inst Theo Phys, AUSTRIA
Prof. M. Heindler, Instut fur Theoretische Physik, AUSTRIA
M. Goossens, Astronomisch Instituut, BELGIUM
Ecole Royale Militaire, Lab de Phys Plasmas, BELGIUM
Commission-European, Dg-XII Fusion Prog, BELGIUM
Prof. R. Boucique, Rijksuniversiteit Gent, BELGIUM
Dr. P.H. Sakanaka, Instituto Fisica, BRAZIL
Instituto De Pesquisas Espaciasi-INPE, BRAZIL
Documents Office, Atomic Energy of Canada Limited, CANADA
Dr. M.P. Bachynski, MPB Technologies, Inc., CANADA
Dr. H.M. Skarsgard, University of Saskatchewan, CANADA
Dr. H. Barnard, University of British Columbia, CANADA
Prof. J. Teichmann, Univ. of Montreal, CANADA
S.R. Sreenivasan, University of Calgary, CANADA
M. Johnston, INRS-Energie, CANADA
...nadien de fusion magnetique, CANADA
CANADA
CZECHOSLOVAKIA
ENGLAND
The Librarian, Rutherford Appleton Laboratory, ENGLAND
Mrs. S.A. Hutchinson, JET Library, ENGLAND
C. Mouttet, Lab. de Physique des Milieux Ionises, FRANCE
J. Radet, CEN/CADARACHE - Bat 506, FRANCE
Ms. C. Rinni, Librarian, Univ. of Ioannina, GREECE
Dr. Tom Mual, Academy Bibliographic Ser., HONG KONG
Preprint Library, Hungarian Academy of Sciences, HUNGARY
Dr. B. Das Gupta, Saha Inst of Nucl. Phys., INDIA
Dr. P. Kaw, Institute for Plasma Research, INDIA
Dr. Philip Rosenau, Israel Inst. of Tech, ISRAEL
Librarian, Int'l Ctr Theo Phys, ITALY
Prof. G. Rostagni, Istituto Gas Ionizzati Del CNR, ITALY
Miss Clelia De Palo, Assoc EURATOM-ENEA, ITALY
Dr. G. Grosso, Istituto di Fisica del Plasma, ITALY
Dr. H. Yamato Toshiba Res & Dev, JAPAN
Prof. I. Kawakami, Atomic Energy Res. Institute, JAPAN
Prof. Kyoji Nishikawa, Univ of Hiroshima, JAPAN
Director, Dept. Large Tokamak Res. JAERI, JAPAN
Prof. Satoshi Itoh, Kyushu University, JAPAN
Research Info Center, Nagoya University, JAPAN
Prof. S. Tanaka, Kyoto University, JAPAN
Library, Kyoto University, JAPAN
Prof. Nobuyuki Inoue, University of Tokyo, JAPAN
S. Mori, JAERI, JAPAN
H. Jeong, Librarian, Korea Advanced Energy Res Inst, ...
Prof. D.I. Choi, The Korea Adv. Inst of Sci & Tech, K...
Prof. B.S. Liley, University of Waikato, NEW ZEALAND
Institute of Plasma Physics, PEOPLE'S REPUBLIC OF CHI...
Librarian, Institute of Phys., PEOPLE'S REPUBLIC OF C...
Library, Tsing Hua University, PEOPLE'S REPUBLIC OF C...
Z. Li, Southwest Inst. Physics, PEOPLE'S REPUBLIC OF ...
Prof. J.A.C. Cabral, Inst Superior Tecnico, PORTUGAL
Dr. Octavian Petrus, AL I CUZA University, ROMANIA
Dr. Jam de Villiers, Fusion Studies, AEC, SO AFRICA
Prof. M.A. Hellberg, University of Natal, SO AFRICA
C.I.E.M.A.T., Fusion Div. Library, SPAIN
Dr. Lennart Stenflo, University of UMEA, SWEDEN
Library, Royal Institute of Tech, SWEDEN
Prof. Hans Wilhelmson, Chalmers Univ of Tech, SWEDEN
Centre Phys des Plasmas, Ecole Polytech Fed, SWITZERL...
Bibliotheek, Fom-Inst Voor Plasma-Fysica, THE NETHERL...
Metin Durgut, Middle East Technical University, TURKE...
Dr. D.D. Ryutov, Siberian Acad Sci, USSR
Dr. G.A. Eliseev, Kurchatov Institute, USSR
Dr. V.A. Glukhikh, Inst Electrophysical Apparatus, US...
Prof. O.S. Padichenko, Inst. of Phys. & Tech. USSR
Dr. L.M. Kovrizhnykh, Institute of Gen. Physics, USS...
Nuclear Res. Establishment, Julich Ltd., W. GERMANY
Bibliothek, Inst. Fur Plasmaforschung, W. GERMANY
Dr. K. Schindler, Ruhr-Universitat Bochum, W. GERMANY
ASDEX Reading Rm, c/o Wagner, IPP/Max-Planck, W. GER...
Librarian, Max-Planck Institut, W. GERMANY
Prof. R.K. Janev, Inst of Phys, YUGOSLAVIA